Brain-Computer Interface for Lower-Limb Neurorehabilitation: From Signal Analysis to Practical Applications

Cristian Felipe Blanco Díaz

Postgraduate Program in Electrical Engineering
Federal University of Espirito Santo
Vitória, Brazil
2023

Brain-Computer Interface for Lower-Limb Neurorehabilitation: From Signal Analysis to Practical Applications

Cristian Felipe Blanco Díaz

Dissertation submitted for the Postgraduate Program in Electrical Engineering, Federal University of Espirito Santo as a preliminar requirement to obtain:

Master's Degree in Electrical Engineering

Under the guidance of:
Prof. Teodiano Bastos-Filho, **PhD**
Denis Delisle-Rodríguez, **PhD**
Alberto Ferreira de Souza, **PhD**

Federal University of Espirito Santo
Postgraduate Program in Electrical Engineering
Vitória, Brazil
2023

Examined by

Prof. PhD. Teodiano Bastos-Filho
Supervisor
Federal University of Espirito Santo, Vitória, Brazil

PhD. Denis Delisle-Rodriguez
Co-supervisor
Edmond and Lily Safra International Institute of Neurosciences, Macaíba, Brazil

---

PhD. Alberto Ferreira de Souza
Co-supervisor
Federal University of Espirito Santo, Vitória, Brazil

PhD. Andrés Felipe Ruiz Olaya
Jury
Antonio Nariño University, Bogotá, Colombia

PhD. Rafhael Milanezi de Andrade
Jury
Federal University of Espirito Santo, Vitória, Brazil

Vitória
2023

I dedicate this achievement to all those who have believed in me, even when I doubted my own abilities. Science, like a curious flame, illuminates a path to knowledge but often reveals new paths, each more intriguing than the last. I thank those who supported me on this journey and hope that these pages will inspire future researchers to embrace the challenges of discovery and resolution, even when the path becomes enigmatic and unknown.

*"Como no va a lucir sus alas con orgullo, si le costaron tantas tempestades"-**Joel Montero***

Acknowledgment

Initially, I want to thank God, life, and destiny for allowing me to be where I am, for giving me the opportunity to start and finish this master's degree successfully, along with all the blessings it brings with it.

To my mother, for being the driving force behind my efforts, and for giving me her support in all the decisions I have made, and above all, because she has taught me that with persistence and perseverance, you can achieve your goals. To my grandmother for her love, blessings, and wise advice, which allowed me to be constant in my path. Alexander, for representing support in the father figure and unconditional support in the last few years. To my grandfather, because after 14 years in heaven, he continues to give acts of presence. To my aunt Liana, my uncle Edwin, my cousins Marcela, Johana, Valentina, Samantha, Sonia, Nicole, Isaias and other members who continue to trust that I can achieve impressive things. To my almost brother Andrés for his constant support and presence over the last years.

To the family I was able to form during my stay in Brazil. To Ximena for being my partner in different "fofitos" moments. To the good "cara" and work colleague Cristian David, and to the other people who made this time an unforgettable experience: Brayan, Mafe, Sophi, Arthur, Yoshi, Angela, Laura, Camilo, Rosita, Juan Camilo, Marcela, Hamilton and others.

To my supervisor, Professor Teodiano Bastos, who gave me the vote of confidence to work with him, supported me in the face of different difficulties and helped me grow. Professor Denis Delisle, my co-supervisor, for the knowledge transmitted for my personal and professional growth during the development of this and other projects. To my co-supervisor, Professor Alberto de Souza, for his trust and support during my master's degree.

To professors Andrés Ruiz and Sebastián Jaramillo for always believing in me and for their wise advice that have allowed me to empower myself even more. To professor Christian and other members of the Universidad Antonio Nariño, who helped with my education.

To my colleagues and friends in Colombia, whom I have "saudades" for reliving moments of joy: Valery, Caraballo, Erickson, Gustavo, Ariza, Cura and B18.

To the members of the Laboratory of Robotics Assistive Technology (LRTA) for working together on different projects, as well as sharing different moments. Also, to the other mem-

bers of UFES who were there at different times, such as the members of LabGuará, Professor Rafhael, and members of LCAD.

To the Instituto Santos Dumont and all its staff for the opportunity to make me feel welcome during my stay in Natal, especially to Lab13 where everything works with "Imagination".

I would like to thank the Fundação de Amparo à Pesquisa e Inovação do Espírito Santo (FAPES) and the Instituto de Inteligencia Computacional Aplicada - I^{2}CA for the support and resources to successfully complete this master's degree.

Finally, I would like to emphasize that it was not an easy road, so I would like to thank the people who crossed paths with me at some point and somehow made me feel supported and helped.

Abstract

In recent years, the development of Brain-Computer Interfaces (BCIs) or Brain-Machine Intarfaces (BMIs) with Electroencephalography (EEG) has gained recognition in the scientific community for implementing robotic systems for rehabilitation. For instance, Motorized Mini Exercise Bikes (MMEBs) have been used for passive assistance with control driven by Motor Imagery (MI). However, these BCIs face challenges, such as long calibrations and low customization in applications. In addition, intentionality detection with EEG signals during pedaling tasks has not been fully explored.

This dissertation aims to use different strategies on EEG signals for the detection of pedaling tasks using several algorithms. In addition, these methodologies approaches to implement real-time neurorehabilitation BCIs. For this, protocols with active pedaling, passive pedaling, and MI tasks were executed, and different signal processing methodologies were addressed. Machine and deep learning techniques were used here to classify EEG signals with accuracies close to 0.95 for MI, and 0.80 for active pedaling. Riemannian geometry-based methods were also used to identify MI tasks after passive pedaling at three different speeds (30, 45, and 60 rpm) with accuracies close to 0.78.

Additionally, a BCI was designed with visual neurofeedback, passive pedaling assistance, and MI, which was evaluated in the online phase, achieving an accuracy of approximately 0.80, and providing a feedback to the subject, aiming to encourage modulations. Subsequently, it was possible to observe the cortical response in the parieto-central cortex of the brain during the session. The results allow concluding that the implemented methodologies are feasible and accurate for the design of robotic lower limb BCIs that allow more personalized physical and neural neurorehabilitation and better human-machine interaction, which could help in the restoration of skills of people with neuromotor disabilities.

The results presented here open the door to continue exploring brain information during the development of lower-limb tasks that may allow technological innovation in BCI systems for rehabilitation. Additionally, the proposed system can be used in therapeutic interventions for people with neuromotor impairments, such as post-stroke or spinal cord injury populations.

Resumo

Nos últimos anos, o desenvolvimento de Interfaces Cérebro-Computador (ICC) com Eletroencefalografia (EEG) ganhou reconhecimento na comunidade científica para a implementação de sistemas de reabilitação robótica. Por exemplo, os Monociclos Estáticos Motorizados (MEMs) têm sido usadas para assistência passiva, com controle acionado pela Imagética Motora (IM). No entanto, essas ICCs enfrentam desafios como longo tempo de calibração, baixa personalização em aplicativos. Ademais, a detecção de intencionalidade com sinais de EEG durante tarefas de pedalada ainda não foi totalmente explorada.

Esta dissertação tem como objetivo utilizar diferentes estratégias algorítmicas em sinais de EEG para a detecção de tarefas de pedalada, utilizando várias abordagens algorítmicas para implementar ICCs de neurorreabilitação em tempo real. Para isso, foram executados protocolos com tarefas de pedalada ativa, pedalada passiva e MI, onde foram abordadas diferentes metodologias de processamento de sinais. Foram utilizadas técnicas de aprendizado de máquina e aprendizado profundo para classificar sinais de EEG com precisão próxima a 0.95 para MI e 0.80 para pedalada passiva. Métodos baseados em geometria Riemanniana também foram utilizados para identificar tarefas de IM após o recebimento de pedaladas passivas em três velocidades diferentes (30, 45 e 60 rpm) com precisão próxima a 0.78.

Além disso, foi projetada uma ICC com neurofeedback visual, assistência passiva ao pedal e IM, que foi avaliada na fase on-line, alcançando uma precisão de aproximadamente 0.80 e fornecendo um feedback ao o indivíduo, com o objetivo de incentivar modulações. Posteriormente, foi possível observar a resposta cortical no córtex parieto-central do cérebro durante a sessão. Os resultados nos permitem concluir que as metodologias implementadas são viáveis e precisas para o projeto de ICCs robóticas de membros inferiores. Ademas, elas permitem uma neurorreabilitação física e neural mais personalizada e uma melhor interação homem-máquina, o que poderia ajudar na restauração das habilidades de pessoas com deficiências neuromotoras.

Os resultados apresentados aqui deixam a porta aberta para continuar explorando as informações cerebrais durante o desenvolvimento de tarefas para membros inferiores, o que pode permitir a inovação tecnológica em sistemas de ICC para reabilitação. Além disso, propõe-se utilizar o sistema proposto em intervenções terapêuticas para pessoas com deficiência neuromotora, como pacientes pós-AVC ou com lesão da medula espinhal.

Resumen

En los últimos años, el desarrollo de Interfaces Cerebro-Máquina (ICC) con Electroencefalografía (EEG) ha ganado reconocimiento en la comunidad científica para implementar sistemas robóticos de rehabilitación. Por ejemplo, Minibicicletas Estáticas Motorizadas (MEMs) han sido utilizadas para asistencia pasiva, con control impulsado por Imaginación Motora (IM). No obstante, estas ICC enfrentan desafíos como calibraciones largas, baja personalización en las aplicaciones, además de que la detección de intencionalidad con señales de EEG durante tareas de pedaleo no ha sido totalmente profundizada.

Esta disertación tiene el objetivo de utilizar diferentes estrategias en señales EEG para la detección de tareas de pedaleo, utilizando varios enfoques algorítmicos para implementar ICCs de neurorrehabilitación en tiempo real. Para esto fueron ejecutados protocolos con tareas de pedaleo activo, pedaleo pasivo e IM, donde diferentes metodologías de procesamiento de señales fueron abordadas. Fueron utilizadas técnicas de Aprendizaje de Máquinas y Aprendizaje Profundo para clasificar señales EEG con exactitudes cercanas a 0.95 para IM y 0.80 para pedaleo pasivo. También fueron utilizados métodos basados en la geometría de Riemann para identificar tareas de IM después de recibir pedaleo pasivo en tres diferentes velocidades (30, 45, y 60 rpm) con exactitudes cercanas al 0.78.

Adicionalmente, fue diseñada una ICC con neuroretroalimentación visual, asistencia pasiva de pedaleo e IM, la cual fue evaluada en fase online logrando una precisión de aproximadamente 0.80 y aportando un feedback al sujeto con el objetivo de incentivar las modulaciones. Posteriormente, fue posible observar la respuesta cortical en la corteza parieto-central del cerebro durante la sesión. Los resultados permiten concluir que las metodologías implementadas son viables y precisas para el diseño de ICCs robóticas de miembros inferiores. Además, dichas metodologías permiten una neurorehabilitación física y neural más personalizada y una mejor interacción humano-máquina, las cuales podrían ayudar en la restauración de habilidades de personas en condiciones de discapacidad neuromotora.

Los resultados aquí presentados dejan la puerta abierta para continuar explorando la información cerebral durante el desarrollo de tareas de miembros inferiores que puede permitir la innovación tecnológica en los sistemas ICC para rehabilitación. Adicionalmente, se propone utilizar el sistema propuesto en intervenciones terapeúticas de personas con deficiencia neuromotora, como población post-ictus o con lesión de la médula espinal.

Contents

List of Figures

List of Tables

1 Introduction

1.1 Motivation

According to the last report of the World Health Organization (WHO), approximately 15.6% of the world's population has a disability, of which 6.3% are related to neuromotor disability [1]. Most neuromotor disabilities are caused by injuries to the neurological system, such as Stroke or Spinal Cord Injury (SCI), which damage the Central Nervous System (CNS) and Periferal Nervous System PNS [2]. On the one hand, a stroke is a neurological syndrome that causes death or, in survivors, may cause the loss of the upper and lower limbs' voluntary control, thereby increasing the difficulty in performing Activities of Daily Living (ADLs) such as walking, pedaling, and stability [2]. SCI refers to damage that affects the spinal cord, the bridge between the brain and the body's periphery, which can be caused by accidents, falls, sports injuries, or other traumatic circumstances [3]. Depending on the severity and location of the injury, the symptoms can range from loss of sensation and motor function to complete paralysis. Therefore, neuromotor rehabilitation is essential for movement restoration and the independence recovery in this population. For instance, a form of rehabilitation for post-stroke or SCI patients is neuroplasticity [4].

Neuroplasticity is a phenomenon in the nervous system that refers to its ability to reorganize and adapt through changes in the neural structure and synapses in response to experience, learning, and injury [4]. This dynamic capacity allows the brain to modify its function to recover its abilities after injury, as well as to adapt to new challenges and acquire new skills. Neuroplasticity can manifest itself through changes in the strength of connections, formation of new neural synapses, and reassignment of functions in brain areas, which can be induced through physical, cognitive, and other exercise therapies [4]. The literature suggests that it is possible that these populations can maintain neuroplasticity, allowing better recovery with physical rehabilitation therapies, and even recovery of part of the movements approximately 6 months after injury [5].

Among the traditional methods of physical rehabilitation for post-stroke people are mirror therapy [6, 7], exoskeletons [8, 9], treadmill training [10, 11] and the use of machines for cycling exercises, such as Motorized Mini Exercise Bikes (MMEBs) [12, 13, 14]. Mirror therapy is a noninvasive technique used in patients who suffer from the loss of one side of the body (hemiparesis), which consists of performing tasks of the functional limb with a mirror that reflects it as if it was the affected limb, intending to work the brain in re-learning the movement [7]. However, it is a therapy that often may not generate any progress, or

the patient recovers movement after a long time [6]. On the other hand, for lower limb rehabilitation, exoskeletons have been used for gait assistance or stability in people with neuromotor disabilities. However, these systems have a lot of complexity in infrastructure, design, and control, and are often quite expensive [13, 15]. Finally, MMEBs in recent years have been implemented for recovery of neuromotor functions in lower limb tasks [12, 13, 14], considering that the literature reports that therapies related to cycling activities can have the same results as walking activities, and additionally these therapies offer advantages related to passive lower limb support, portability, among others [13].

Human-Machine Interfaces (HMIs) have been used to decode user intentions and control robotic devices [16]. However, the challenge of the scientific community in this area is the detection of intentions by different types of sensors that are comfortable, portable, and accurate. Among the most widely used strategies reported in the literature for the design of rehabilitation systems, the Electroencephalography (EEG) technique allows the detection of mental activities, transforming them into commands that allow interaction with the environment; this is known as Brain computer Interfaces (BCIs). However, it should be noted that EEG signals have low signal-to-noise ratios (SNR), are time-varying, and are affected by external noise as well as physiological artifacts of the individual [17].

BCIs have also been implemented with robotic systems, where it is possible to highlight the use of brain information as a control signal for different devices such as exoskeletons and prostheses [16]. In patients with brain and/or spinal cord injuries, it is important that these devices focus on rehabilitating or assisting ADLs related to the lower limbs, such as walking, pedaling, and standing, such as for instance, the proposals by Luu *et al.* and Ko *et al.* for the control of lower-limb robotic assistance devices for gait rehabilitation with EEG-initiated activation [18, 19]. However, it has also been identified that gait-related therapies may require minimal movement capability, which may limit BCI use [15]. The feasibility of MMEB has been envisioned because the patient can remain in a static position while passive assistance is performed with robotic devices, which induces lower-limb exercise [13].

Thus, BCIs have been developed in recent years to measure the user's brain signals and translate their intention to activate systems that provide cycling movements, such as MMEBs. For example, Romero *et al.* developed a low-cost system for detecting lower-limb MI and MMEB activation for post-stroke rehabilitation [13]. Cardoso *et al.* found interesting cortical information produced by the MI of pedaling tasks, along with connectivity, that could be used to command lower limb rehabilitation devices [20]. Nevertheless, these control strategies focus on on/off activations with constant speeds and high calibration times, which limit HMI and system usability [21]. This issue leaves a gap for further research on passive pedal-based BCIs, with the aim of improving intentionality detection, recognition models, and personalized rehabilitation applications.

Nevertheless, the above strategy could allow the application of the concept of cognitive tasks with passive movement, which would induce the use of brain regions that could be affected after a stroke or SCI. In addition to motor rehabilitation, neuroplasticity can be generated

(neurorehabilitation) [22]. A recently explored neurorehabilitation strategy is Neurofeedback (NFB) [23]. NFB is a technique that teaches individuals to self-regulate their brain activity using real-time measurements [23]. NFB can be visually indicated on a screen through instructions that induce the patient to modulate their brain signals with a target. The literature shows promising results obtained with this methodology when combined with BCIs in the rehabilitation of post-stroke patients [24]. In this context, it is important to highlight that NFB scanning combined with lower-limb assistive devices is not well known in the literature [25, 26].

1.2 Objectives

The main objective of this Master Dissertation is to propose a BCI based on pedaling tasks for conveying commands to a lower limb passive assistive device, in order to provide neurorehabilitation to patients with neuromotor disabilities. Several challenges define the following specific objectives:

- Design a system that allows the development of an experimental protocol for EEG acquisition during the development of pedaling tasks (Actual Movement – AM, and Motor Imagery – MI).
- Implement the protocol to experiments with healthy subjects using passive and active pedaling (using the MMEB).
- Develop algorithms of data processing for user's MI recognition through EEG.
- Design a control strategy that allows the interaction between the MMEB and the user based on the progressive intention of the subject.
- Validate the control strategy during pedaling by using real data.

1.3 Justification

According to WHO reports, stroke left permanently disabled approximately 5 million people worldwide in that year [27]. Stroke is a serious and disabling global health problem that has been increasing in the last few years [28]. On the other hand, between 250.000 and 500.000 people suffer from SCI every year [29]. In this context, the implementation of HMIs during rehabilitation and assistance therapies has demonstrated progressive advancement in the neuromotor restoration of individuals with disabilities [30]. For this purpose, BCIs have been useful because these systems allow a bridge between the subject and the environment without the need to incorporate the PNS, thus allowing their use by subjects with neuromotor disabilities [30, 13, 16]. EEG is commonly used to obtain this intentionality information

because of its noninvasive advantages and portability [31, 16]. However, there are still challenges in decoding these signals, owing to their low SNR, intersubject variability, influence of physiological artifacts, and random environmental noise [31, 32].

Despite technological advances in rehabilitation engineering, adequate HMI is necessary with respect to the tasks to be performed in this manner [16, 31, 13, 33]. For instance, interventions using MMEB-based BCIs that work with on/off control through MI with adequate accuracy detection have been reported in the literature [13]. However, there is still an open challenge in the implementation of different algorithms that allow proper identification of this type of movement, which could improve the control commands of this type of device.

Different algorithms have been reported in the literature to recognize the cortical activity produced by lower-limb movements or MI. For example, classification algorithms have been used with EEG to recognize different states using the lower limbs, such as sit vs. stand [34], idle vs. ankle dorsiflexion [35], go vs. stop, and walking speeds [36]. However, these studies only classified a small discrete number of states, which could limit the usability of BCIs.

One way to generate more personalized control strategies corresponds to motion estimation. In recent years, kinematic estimation algorithms for upper and lower limb tasks have gained recognition. For example Luu *et al.*, Nakagome *et al.* and Tortora *et al.* have developed techniques based on Kalman Filters (KF), Machine Learning (ML) and Deep Learning (DL) to estimate the position of joints during gait [18, 37, 38, 39]. This allows interaction with rehabilitation techniques, such as virtual reality games, to incentivate individuals during therapy. This is a motivator for deepening the use of these computational techniques in different lower-limb cyclic tasks, such as pedaling.

BCIs incorporating mental tasks combined with passive lower-limb movements have been used for the rehabilitation of post-stroke individuals, where MI recognition algorithms were implemented to activate and deactivate an MMEB. Nonetheless, these strategies only allow the intentional detection of MI using constant speeds and in a fixed period of time [21, 13, 20]. Therefore, the exploration of strategies that allow the identification of more personalized tasks through EEG is necessary, and has not yet been deepened in the literature. To address this, tasks can be accomplished by implementing protocols with variable-sized time windows along with exploration of different velocities during passive pedal assistance.

NFB has been explored in recent years because it promotes brain regulation and thus reorganizes synaptic configurations [24]. This could lead to the restoration of neural activity lost during the development of a neurological disease. However, to the best of the author's knowledge, NFB-based techniques using lower-limb assist devices have not been addressed yet [25, 26].

Considering the open challenge for the scientific community that is focused on the design of alternative strategies for neuromotor rehabilitation of people with disabilities, this work focuses on addressing different strategies of EEG signal analysis that extend the current knowledge about brain behavior during motor execution (Actual Movement-AM) and Motor Imagery (MI) of pedaling tasks. The findings of this research allow for the design of alter-

natives for the control of external devices involving EEG together with lower limb cyclic movements, which were implemented in the design of a visual NFB-based BCI during the execution of passive movement tasks. The results will deepen the medical and therapeutic applications of BCIs for the neurorehabilitation of people with disabilities, such as those affected by stroke or SCI.

Another important aspect of this Master Dissertation is that it is part of the objective of the Laboratory of Robotics and Assistive Technology (LRTA) of the Federal University of Espirito Santo (UFES) to build technological strategies that allow the motor rehabilitation of people with disabilities. Some of the previous approaches developed by the LRTA team at UFES to lower limb rehabilitation with pedaling tasks have been addressed by with post-stroke patients, so the results of this research can be used to improve the current systems, and thus, a more personalized and progressive rehabilitation.

1.4 Publications

In the time frame of this disertation, about 18 journals papers (J), 18 conference works (C) and 2 book chapters were either published, accepted, under review or are under preparation. These works also include the collaboration with other researchers and international groups. The contributions are divided into the ones that contributed directly in this research (marked as T) and the ones from collaborations and parallel researches (marked as P).

1.4.1 Journal Articles

- **[J1-T] Blanco-Díaz, C. F.**, Guerrero-Mendez, C. D., Delisle-Rodriguez, D., de Souza, A. F., Badue, C., and Bastos-Filho, T. F. (2023). Lower-limb kinematic reconstruction during pedaling tasks from EEG signals using Unscented Kalman filter. *Computer Methods in Biomechanics and Biomedical Engineering*, 1-11.

- **[J2-T]** Luiz Henrique Bertucci Borges, **Cristian Felipe Blanco-Díaz**, Bruno Henrique e Silva Bezerra, Caroline Cunha do Espirito Santo, Teodiano Bastos-Filho, Denis Delisle-Rodriguez, and André Felipe Oliveira de Azevedo Dantas. *Multichannel Functional Electrostimulation Integrated to a Human-Machine Interface for Lower Limb Rehabilitation. IEEE Transactions on Neural Systems and Rehabilitation Engineering.* (submitted in 08-2023).

- **[J3-P]** Gonzalez-Cely, A.X.,**Blanco-Díaz, C.F.**,Rodríguez-Díaz, C.A.,Bastos-Filho, T.F.,Krishnan, S. Towards Wheelchair Operation with Neck Movements using POF-based Sensors and Machine Learning. Optical Fiber Technology. (submitted in 01-2023).

- [**J4-T**] Guerrero Mendez, C. D., **Blanco-Díaz, C. F.**, Ruiz Olaya, A. F., Lopez-Delis, A., Jaramillo Isaza, S., Milanezi Andrade, R., ... and Bastos Filho, T. F. (2023). EEG Motor Imagery classification using Deep Learning approaches in naïve BCI users. *Biomedical Physics & Engineering Express.*

- [**J5-T**] **Blanco-Díaz, C. F**., Guerrero-Méndez, C. D., and Ruiz-Olaya, A. F. (2023). Enhancing P300 Detection Using a Band-Selective Filter Bank for a Visual P300 Speller. IRBM, 44(3), 100751.

- [**J6-T**] **Blanco-Díaz, C. F**., Guerrero-Méndez, C. D., Bastos-Filho, T., Jaramillo-Isaza, S., & Ruiz-Olaya, A. F. (2022). Effects of the concentration level, eye fatigue and coffee consumption on the performance of a BCI system based on visual ERP-P300. Journal of Neuroscience Methods, 382, 109722.

- [**J7-P**] González-Cely, A.X., **Blanco-Diaz, C.F.**, Bastos-Filho T. & Camilo A.R. Díaz. Real-time posture monitoring classification for wheelchair users preventing the generation of pressure ulcers. *IEEE Transaction on Human Machine Systems*. (submitted in 05-2023).

- [**J8-T**] **C.F. Blanco-Díaz**, C.D. Guerrero-Méndez, Denis Delisle-Rodriguez, Sebastián Jaramillo-Isaza, Andrés Felipe Ruiz-Olaya, Anselmo Frizera, Alberto Souza & Teodiano Bastos-Filho. Evaluation of Temporal, Spatial and Spectral Filtering in CSP-based Methods for Decoding Pedaling-Based Motor Tasks Using EEG signals. *Journal of Biomedical Physics & Engineering Express.*(submitted in 04-2023).

- [**J9-T**] Cristian D. Guerrero-Mendez, **Cristian F. Blanco-Diaz**, Teodiano F. Bastos-Filho, Sebastian Jaramillo-Isaza and Andres F. Ruiz-Olaya. On the Use of Power-Based Connectivity between EEG and sEMG Signals to Classify Three Different Weights During a Reach-to-Grasp Movement. *Research on Biomedical Engineering*. (submitted in 02-2023).

- [**J10-T**] C.D. Guerrero-Mendez, **C.F. Blanco-Diaz**, H. Rivera-Flor, A.F. de Souza, S. Jaramillo-Isaza, A.F. Ruiz-Olaya, and T.F. Bastos-Filho. Coupling Effects of Cross-Corticomuscular Association During Object Manipulation Tasks on Different Haptic Sensation. *Neurosci*. (Accepted in 07-2023).

- [**J11-T**] **Blanco-Díaz, C. F.**, Guerrero Mendez, C. D., Milanezi Andrade, R., Badue, C., D., de Souza, A. F., Delisle-Rodriguez, D. and Bastos-Filho, T. F. Decoding Lower-Limb kinematic Trajectory During Pedaling Tasks Using Deep Learning Approaches. *Biomedical Signal Processing and Control*. (submitted in 08-2023).

- [**J12-P**] Cristian D. Guerrero-Mendez, Alberto Lopez-Delis , **Cristian F. Blanco-Diaz**, Teodiano F. Bastos-Filho, Sebastian Jaramillo-Isaza and Andres F. Ruiz-Olaya.

Continuous Reach-to-Grasp Motion Recognition Based on Extreme Machine Learning Algorithm Using sEMG Signals. (under preparation process).

- **[J13-T] Cristian F. Blanco-Diaz**, Ericka Raiane da Silva, Caroline Cunha do Espirito Santo, Teodiano Bastos-Filho, Denis Delisle-Rodriguez. BCI based visual neurofeedback during the use of robotic-assisted treadmill walking for rehabilitation. (under prereration process).

- **[J14-T] Cristian F. Blanco-Diaz**, Aura Ximena González-Cely, Cristian David Guerrero-Méndez, Denis Delisle-Rodriguez, Teodiano Bastos-Filho. BCI based on Motorized Mini Exercise Bikes and visual neurofeedback for lower-limb rehabilitation. (under prereration process).

- **[J15-T] Cristian F. Blanco-Diaz**, Cristian David Guerrero-Méndez, Aura Ximena González-Cely, Denis Delisle-Rodriguez and Teodiano Bastos-Filho. Intent-based decoding of continuous pedaling motion using EEG signals. (under preparation process).

- **[J16-T] Cristian F. Blanco-Diaz**, Aura Ximena González-Cely, Cristian David Guerrero-Méndez, Denis Delisle-Rodriguez, Teodiano Bastos-Filho. Motor Imagery task recognition of pedaling at three different velocities with passive assistance and Riemann Geometry. (under preparation process).

- **[J17-P]** CD. Guerrero-Mendez, **CF. Blanco-Diaz**, H. Rivera Flor, C. Badue, D. Delisle-Rodriguez, AF. De Souza, TF. Bastos-Filho. Neural Network Incremental Training to Discriminate Motor Imagery Patterns of Complex Upper Limb Tasks. (under preparation process).

- **[J18-P]** González-Cely, A.X., **Blanco-Diaz, C.F.**, Camilo A.R. Díaz, Bastos-Filho T. Roborueda: Python-based GUI to control a wheelchair and monitor user posture *Software X*. (submitted in 07-2023).

1.4.2 Conference papers

- **[C1-T] C.F. Blanco-Díaz**, A.X. González-Cely, C.D. Guerrero-Méndez, A.F. De Souza, D.Delisle-Rodriguez, T.F.Bastos-Filho. Machine Learning Classification of Pedaling Phases Using sEMG Signals: Towards Adaptive Control-based Muscle-Machine Interfaces. *IX neuroengineering symposium*. (submitted in May 2023).

- **[C2-T] C.F. Blanco-Diaz**, A.X. Gonzalez-Cely, M. Callejas-Cuervo, A.F. De Souza, D. Delisle-Rodriguez, T.F. Bastos-Filho. Characterization of a Motorized Mini Exercise Bike: Towards the Adaptive Control of a Lower-Limb Rehabilitation System Based on Pedaling. *IX neuroengineering symposium*. (submitted in May 2023).

- **[C3-T]** Cristian David Guerrero-Mendez, **Cristian Felipe Blanco-Díaz**, Rafhael Milanezi de Andrade, Claudine Badue, Alberto Ferreira De Souza, Teodiano Freire Bastos-Filho. Decoding Knee Joint Angles During Gait Using Electroencephalography Signals and Convolutional Neural Networks. *IX neuroengineering symposium.* (submitted in May 2023).

- **[C4-T]** A.X. González-Cely, **C.F. Blanco-Diaz**, D. Delisle-Rodriguez, T.F. Bastos-Filho. Decoding Lower-Limb Motion with Pedaling-Based HMIs Using EEG and sEMG for Rehabilitation Purposes. *IX neuroengineering symposium.* (submitted in May 2023)

- **[C5-T]** **Cristian F. Blanco-Diaz**, Cristian D. Guerrero-Mendez, Denis Delisle-Rodriguez, Teodiano F. Bastos-Filho, Andres F. Ruiz-Olaya and Sebastian Jaramillo-Isaza. Detection of Pedaling Tasks through EEG Using Extreme Learning Machine for Lower-Limb Rehabilitation Brain-Computer Interfaces. *IEEE Colombian Conference on Applications of Computational Intelligence – ColCACI.*

- **[C6-P]** González-Cely, A.X., **Blanco-Diaz, C.F.**, Camilo A.R. Díaz & Bastos-Filho T. Real-Time Wheelchair Controller Based on POF-Based Pressure Sensors. *2023 IEEE Latin American Electron Devices Conference (LAEDC).*

- **[C7-P]** Cristian D. Guerrero-Mendez, **Cristian F. Blanco-Diaz**, Denis Delisle-Rodriguez, Andres F. Ruiz-Olaya, Teodiano F. Bastos-Filho and Sebastian Jaramillo-Isaza. Analysis of EEG Rhythms During Four-Direction First-Person Reach-to-Grasp Kinesthetic Motor Imagery Tasks from the Same Limb. *IEEE Colombian Biocas workshop 2023.*

- **[C8-T]** C.D. Guerrero-Méndez, **C.F. Blanco-Díaz**, A.Lopez-Delis, T. Bastos-Filho and R.M.Andrade. Decoding sEMG Under Non-Ideal Conditions Toward Robust Muscle-Machine Interface Control. *International Conference on Intelligent Robots and Systems.*

- **[C9-T]** **Cristian Felipe Blanco-Díaz**, Cristian D. Guerrero-Mendez, Denis Delisle-Rodriguez & Teodiano F. Bastos-Filho. Protocolo de Medida de EEG, sEMG y Cinemática hacia el control de un sistema de rehabilitación de miembro inferior post-AVC. *XII Ibero-American Congress of Support Technologies to Disability.*

- **[C10-T]** Cristian D. Guerrero-Mendez, **Cristian Felipe Blanco-Díaz**, Denis Delisle-Rodriguez & Teodiano F. Bastos-Filho. Avances y Retos Computacionales para Interfaz Cerebro-Computador basado en Imaginación Motora. *XII Ibero-American Congress of Support Technologies to Disability.*

- **[C11-P]** S. Jaramillo-Isaza, C.D. Guerrero-Mendez, L.V. Montealegre, **C.F. Blanco-Diaz**, T.F. Bastos-Filho & A.F. Ruiz-Olaya. Estimation of pathological gait asym-

metry of lower-limb prosthetic users at high and low walking speeds. In *IX Latin American Congress on Biomedical Engineering*.

- **[C12-P]** Guerrero-Méndez, C. D., **Blanco-Díaz, C. F** & Bastos-Filho, T. Wavelet coherence corticomuscular analysis during tasks involved in object manipulation. In *IX Latin American Congress on Biomedical Engineering*.

- **[C13-P]** A.F. Ruiz-Olaya, **C.F. Blanco-Diaz**, C.D. Guerrero-Mendez, T.F. Bastos-Filho & S. Jaramillo-Isaza. Enhancing classification of grasping tasks using hybrid EEG-sEMG features. In *IX Latin American Congress on Biomedical Engineering*.

- **[C14-T]** **Blanco-Díaz, C. F**., Guerrero-Méndez, C. D., & Bastos-Filho, T. Single Trial P300 Detection Using Dimensionality Reduction and Extreme Learning Machine. In *IX Latin American Congress on Biomedical Engineering*.

- **[C15-T]** A.X. González-Cely, **C.F. Blanco-Díaz**, C.D. Guerrero-Méndez, D.Delisle-Rodriguez, T.F.Bastos-Filho. One-handed open/close motor imagery classification including passive assistance and a robotic glove. *IEEE Colombian Caribbean Conference)*. (submitted in 08-2023).

- **[C16-T]** **C.F. Blanco-Díaz**, A.X. González-Cely, C.D. Guerrero-Méndez, F. Vaz de Souza, D.Delisle-Rodriguez, T.F.Bastos-Filho. Effects of the passive movement produced by a robotic glove on the design of a MI-based BCI. *IEEE Colombian Caribbean Conference)*. (submitted in 08-2023).

- **[C17-T]** Cristian Guerrero-Mendez, **Cristian Felipe Blanco-Diaz**, Rafhael Andrade, Denis Delisle-Rodriguez, Bastos-Filho, Teodiano. Proposta de desenvolvimento de um controlador para um exoesqueleto robótico usando decodificação de imagética motora. in *VIII Simpósio de Neuroengenharia Instituto Santos Dumont*.

- **[C18-T]** **Cristian Felipe Blanco-Diaz**, Cristian Guerrero-Mendez, Denis Delisle-Rodriguez, Bastos-Filho, Teodiano. Proposta de desenvolvimento de um protótipo de interface humano-máquina híbrida para reabilitação de membros inferiores. in *VIII Simpósio de Neuroengenharia Instituto Santos Dumont*.

1.4.3 Book Chapter

- **[B1-T]** C.D.Guerrero-Mendez, **C.F Blanco-Díaz**, T. Bastos-Filho, A.F.Ruiz-Olaya & S. Jaramillo- Isaza. Artificial Intelligence applied to Neuromotor Rehabilitation Engineering: Advances and challenges. in *Computational Approaches in Biomaterials, Bioinformatics and Biomedical Engineering Applications*. Ed: CRC Press, Taylor and Francis Group, USA. (Accepted in 01-2023).

- **[B2-T] C.F Blanco-Díaz**, C.D.Guerrero-Mendez, A.D. Orjuela-Cañon, T. Bastos-Filho, A.F.Ruiz-Olaya & S. Jaramillo- Isaza. The brain response to coffee consumption: electroencephalogram (EEG) changes and implications. in *Coffee in Health and Disease Prevention 2ed.*. Ed: Academic Press-Elsevier. (Accepted in 07-2023)

1.5 Organization of this dissertation

This dissertation is divided into six chapters as follows. Chapter 1 presents the motivation and introduction aspects. Chapter 2 provides the theorical background and some knowledge to understand the methodology implemented in the following chapters, as well as a contextualization of the state of the art to support and discuss the results of this research. Chapter 3 presents the materials and methods used to build the proposed BCI. Additionally, algorithmic methods for the recognition of lower limb tasks, either executed or imagined, through EEG signals are presented. Chapter 4 presents the most important results obtained during the development of this research, which are discussed in the following chapter. Chapter 5 includes the discussion of the results obtained, as well as the comparison with some related works reported in the literature. Based on this, potential applications and identified limitations are mentioned. Finally, conclusions and future work are presented in Chapter 6.

2 Theorical Background

2.1 Rehabilitation Principles

Considering the alarming statistics provided by international organizations regarding neuromotor disabilities, it is important to search for strategies for the restoration of neuromotor, cognitive, psychological, and social functionality [40]. Rehabilitation plays an important role in improving the quality of life of people with impairments in the performance of Activities of Daily Living (ADLs) [41].

Rehabilitation is a multidisciplinary therapy designed to help people who have experienced an injury, illness, or disability to recover or improve their physical, cognitive, and/or emotional function [40]. The goal of rehabilitation is to maximize individuals' independence, helping them reintegrate into their social environment in an appropriate manner. Therefore, motor rehabilitation involves a set of mechanisms, activities, and protocols that improve or recover neuromotor functions of the body, such as mobility, stability, and manipulation of the environment [41]. However, the effectiveness of a patient's rehabilitation depends on different factors, according to the integral needs and capabilities of each individual. Therefore, designing a rehabilitation plan with appropriate strategies and equipment becomes a challenge for the community in this area [40]. Some of the current challenges and principles of neuromotor rehabilitation are summarized in Table **2-1** [40, 42, 43].

2.2 Signals used in rehabilitation: an overview

As mentioned in Section 2.1, for the design and implementation of HMIs in the field of rehabilitation and neuromotor assistance, it is important to consider functional characteristics such as range of motion, muscle strength, and perception of the individual. By contrast, a signal is defined as a form of energy or information that is transmitted, propagated, or modified to convey a message or perform a specific function [44]. For this reason, different types of signals generated or obtained by the human body have been used as a second way to obtain information about the patient's intention, and thus execute some interaction with the environment [45], such as Electroencephalography (EEG), surface electromyography (sEMG), and inertial measurements, among others.

Table 2-1: Currents challenges and principles in neuromotor rehabilitation.

	Challenges	**Principles**
Range of motion	Several factors, such as pain, inflammation, and joint hypomobility, can limit range of motion. In addition, lack of muscle flexibility and weakness may also contribute to these limitations	Rehabilitation programs that emphasize early movement, assisted and unassisted weight lifting are successful in restoring mobility
Flexibility	Contractures are permanent muscle shortening that occur due to lack of stretching and movement in the joints.	Flexibility deficits are best treated through the use of various stretching techniques utilizing static, dynamic and proprioceptive neuromuscular facilitation stretching
Muscular strength	Lack of use and lack of physical activity can lead to muscle atrophy in people with neuromotor disabilities. Muscle atrophy results in decreased muscle strength and mass, limiting the ability to generate adequate force.	Funtional Electrical Stimulation (FES) involves the application of mild electrical currents to muscles to stimulate muscle contraction. This technique can be used in rehabilitation to activate muscles affected by atrophy and promote their development. Neuromuscular Electrical Stimulation (NMES) can be combined with active or passive exercises to maximize the benefits.
Propioception and neuromuscular control	Alterations in muscle activation and control can cause imbalances between agonist and antagonist muscle groups. These imbalances can affect flexibility and limit range of motion in certain joints.	Rehabilitation can use biofeedback devices to improve neuromuscular control and proprioception. These devices provide real-time information on therapeutic activity, stability or joint position, allowing the person to have visual or auditory feedback on their own performance. This helps to improve perception and awareness of movements, thus promoting better recovery.
Functional progression	Each person may have a unique pace and level of progress, and it is essential to tailor functional progressions to the specific capabilities and needs of each individual.	In some cases, adaptations or modifications to rehabilitation exercises may be necessary to suit individual needs. This may involve adjusting technique, using aids or assistive devices, or changing the way certain movements are performed to facilitate participation and progression.
Patient perception	Neuromotor disabilities can affect spatial perception, which can make it difficult to understand position and the relationship between the body and the environment.	HMIs can enable patients to control prosthetic or assistive devices, improving their perception and control, allowing them to interact directly with the environment in a more natural and effective way.

2.2.1 Electroencephalography (EEG)

The interaction and communication of neurons results in electrical activity in the brain. These electrical signals, also known as brain waves, provide information about brain function and activity under different mental states and conditions [46]. EEG is a non-invasive technique for recording and measuring the electrical activity of the brain through electrodes placed on the scalp [47]. Generally, an EEG test consists of a cap of strategically placed electrodes (see Figure 2.1(a)) that captures brain signals and amplifies them for recording [47]. Strategic electrode placement is usually performed using the international 10-20 system (see Figure 2.1(b)), which was developed as a guideline to ensure accurate and consistent electrode placement on the scalp, thereby allowing for a more reliable comparison of EEG results between different patients and studies [48, 49].

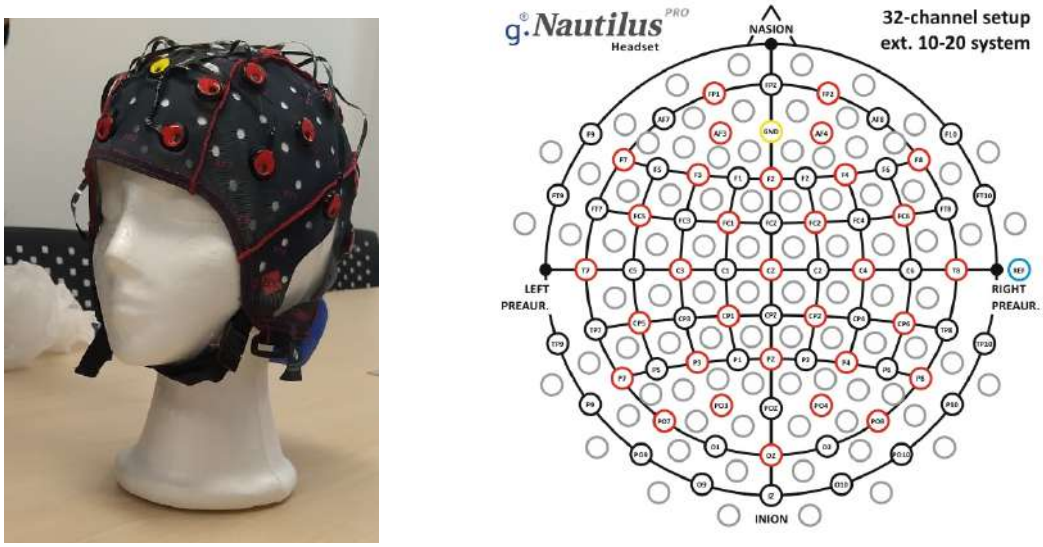

(a) (b)

Figure 2-1: (a) Cap with electrodes for EEG acquisition. (b) International 10-20 system for EEG acquisition. Image taken and modified from [49,50].

EEG shows different brain wave patterns that vary according to an individual's physiological conditions and mental state. For instance, brain waves can be classified into different frequency bands, which are presented in Table **2-2** [46, 47, 50].

Table 2-2: Classification of EEG waves according to frequency bands

EEG wave	Frequency (Hz)	Principle
Delta (δ)	0.1 - 4	It is the wave with the highest amplitude but slowest of all, and normally appears in deep sleep states.
Theta (Θ)	4 - 8	It manifests itself mainly in phases of deep meditation and is related to the production of serotonin and relaxation. It has also been associated with lower limb activities in recent years.
Alpha (α)	8 - 13	It manifests mostly in adults in a relaxed or concentrated state, eyes closed, and is recorded mainly in the occipital and parietal lobes.
Beta (β)	13 - 30	It manifests in states of actions and imagination, related to the senses, memory, decision making and problem solving, registered in the frontal and parietal lobes.
Gamma (γ)	30-100	It is related to perception and consciousness, high brain activity in alert states.

Considering brain wave patterns, it is possible to develop strategies for the identification of intentionality of individuals and create rehabilitation strategies focused on HMIs, such as BCIs or BMIs [51]. In this phase, EEG signals can be divided into two groups based on the paradigm and brain waves of interest:

- **Exogenous EEG Signal:** This type of EEG signal is generated independently of external stimulation and may be freely regulated by the individual, which is helpful for patients with neurological problems because it allows for more natural and spontaneous interactions [51]. However, this type of signal often requires longer training time. Among the most widely used paradigms in rehabilitation are those based on sensorimotor rhythms and slow cortical potentials, which are associated with Motor Imagery (IM) or Actual Movement (AM) due to the generation of Event-Related Desynchronization/Synchronization (ERD/ERS) [31, 32, 52, 53].

- **Endogenous EEG Signal:** This type of EEG signal is produced in response to external inputs such as visual or auditory cues. External stimuli, such as flashing LEDs and music, can influence brain activity. However, to evoke patterns, it is necessary for the subject to concentrate on external stimuli, which limits their applications. Among the most widely used paradigms in rehabilitation are Event Related Potentials (ERPs), such as the P300, and Evoked Potentials, such as the Steady State Visual Evoked Potentials (SSVEP) [50, 54, 55, 56, 17].

In summary, EEG signals are proposed to be a suitable sensing system to detect the intentions of individuals using brain information [51], so they have been shown to be useful for the

creation of BCIs/BMIs applied to rehabilitation, which will be discussed in Section 2.3.

2.2.2 Surface Electromyography (sEMG)

Similar to EEG, Electromyography is a technique used to measure and record muscle electrical activity. It is used to evaluate the behavior of muscle fibers by detecting the electrical impulses generated during muscle contraction (action potentials) [57]. During EMG acquisition, it is necessary to strategically place electrodes, where the most used technique corresponds to sEMG because of its non-invasive characteristics. The sEMG is detected by electrodes placed on the skin and recorded as a graphic trace in an electromyogram [58].
In the electromyogram, it is possible to observe patterns and characteristics of action potentials, such as amplitude, duration, waveform, and frequency of action potentials [58]. These patterns can provide valuable information about muscle function and health as well as possible neuromuscular disorders or injuries. In this context, technological advancements in the areas of signal processing have allowed the development of another approach, myoelectric control [57].
Myoelectric control refers to the use of electrical signals generated by muscle activity to control electronic devices or prostheses [59]. Once myoelectric signals are acquired, algorithms and signal processing techniques are used to analyze and extract relevant information. This information is used to translate electrical signals into commands that control the devices [59]. Myoelectric control has provided significant opportunities to improve the quality of life for people with neuromuscular disorders. Through this technology, it has been possible to design HMIs in which people can regain some level of independence and functional ability by using residual muscle activity to control robotic devices with greater precision and naturalness [58].

2.2.3 Other signals used in rehabilitation

Other types of signals have been used for the design of rehabilitation and assistive devices, among which inertial sensors, computer vision, and fiber-optic-based sensors are among the most prominent.

- **Inertial Sensors:** Inertial sensors are electronic devices that combine accelerometers and gyroscopes to measure and record the acceleration, angular velocity, and orientation of an object in a three-dimensional space, providing information about the movements and position changes of the object to which they are attached [60]. In rehabilitation and assistive engineering, inertial sensors are used to monitor and analyze the biomechanics of the body during the execution of movements through real-time capture, which facilitates the design of personalized interventions and evaluation of progress in the treatment of neuromotor disorders. Additionally, this technology en-

ables the development of assistive devices, such as exoskeletons and prostheses, with improved detection capabilities and adaptation to user needs [60, 61].

- **Computational vision:** Considering images as two-dimensional signals, computer vision has been widely used in rehabilitation and assistive engineering to provide alternatives for improving the quality of life of people with disabilities. Through the analysis and processing of images or videos, computer vision systems can detect and track body movements, identify gestures and facial expressions, and evaluate posture and biomechanics [62, 63, 64, 65]. These advances have enabled the development of assistive technologies such as gaze- or motion-controlled prostheses, rehabilitation systems with real-time visual feedback, and navigation devices for the visually impaired [66, 65]. Computer vision has also been used to track body movements to detect neuromotor disorders.

- **Fiber optic sensors:** Fiber optic sensors are an emerging technology in rehabilitation and assistive engineering because of their numerous advantages and benefits for monitoring and improving the motor function and quality of life of people with disabilities [67]. These sensors offer high precision and sensitivity in the measurement of variables such as posture and body forces, so they have been used in different assistive device contexts, for instance, posture control and monitoring during the use of powered-electric wheelchairs [68].

2.3 Human-Machine Interface

A Human-Machine Interface (HMI) is a communication and control system that allows humans to interact with machines or electronic devices through different modalities, such as body-generated signals, voice, or movement commands [69]. In the field of rehabilitation and assistance, HMIs have been implemented as a bridge between people and devices to restore the physical, psychological, and social capabilities of people with disabilities [16]. In other words, these interfaces can enable people with disabilities to control prostheses, assistive devices, and virtual reality systems through muscle signals, brain signals, or other forms of interaction [16, 70]. The concept of an HMI can be seen in Figure **2-2**, where it can be observed this signal-based HMIs are composed of different sets of complex steps and processes that still present challenges to the scientific community [16].

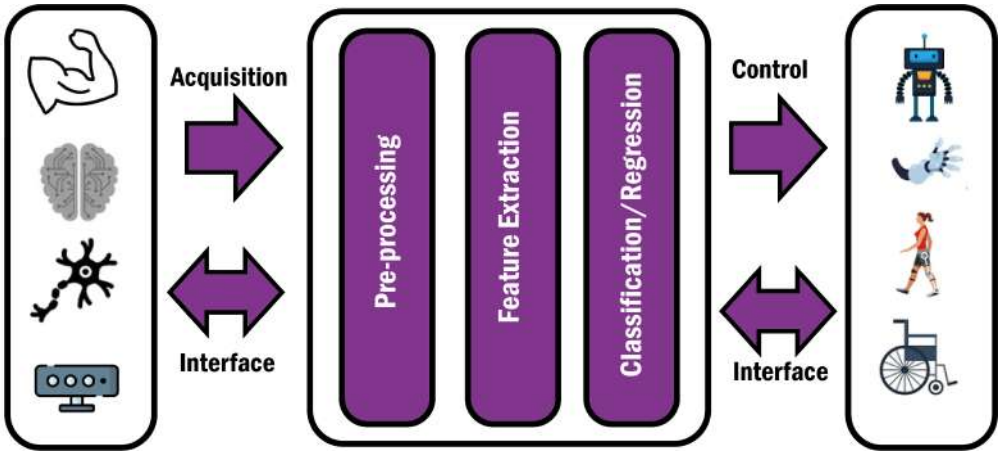

Figure 2-2: HMIs are based on human intention (EEG, sEMG, kinematics, among others), and include processing, feature extraction, classification/regression stages, and finally control commands for various assistive, rehabilitation or assistive devices.

It is noteworthy that HMIs provide opportunities for greater independence and functionality, as individuals can actively participate in their rehabilitation and perform daily activities with greater ease and precision, providing them with a better quality of life and greater social inclusion [70]. However, it is necessary to know the physical, functional, and neurological limitations of a person to design an HMI focused on assistance or rehabilitation. For example, previous studies have shown that patients with neuromotor impairment (such as post-stroke or SCI) have reduced electrical functionality in some parts of the body, which becomes a barrier for HMIs based on sEMG. Therefore, each signal has advantages and challenges in designing HMIs for rehabilitation and assistive devices, which are presented in Table **2-3** [69, 16].

Table 2-3: Advantages and limitations of different types of signals for user intent and application detection in HMIs

Type of Signal	Advantages	Limitations
EEG	* Access to brain information. * Multisensory information. * Non-invasive. * Not dependent on movement or muscle activity. * Potential for neurofeedback and therapy. * Portability.	* Low Signal to Noise Ratio (SNR). * Commonly affected by environmental or physiological conditions of the individual. * Non-stationary. * Intersubject variability. * Often require calibration.
sEMG	* Non-invasive. * High Precision. * Greater resistance to ambient noise. * Adaptability to different body parts and conditions.	* Muscle fatigue. * Electromyographic interfaces of nearby muscles. * May require learning and training. * Sensitivity to non-ideal conditions that may affect data collection.
Inertial sensors	* Size and weight. * High accuracy in dynamic measurements. * Low power consumption.	* May be affected in acquisition over prolonged periods of time. * Sensitivity to vibrations and shocks. * Information on velocities and accelerations but do not provide absolute position. * Periodic calibration.
Computational vision	* Perception of the environment. * Object detection and recognition. * Task automation.	* Complexity and computational resources. * Sensitivity to light and noise conditions . * Training and labeling requirements . * Limitations of complex environments (overlapping data).
Fiber optic sensors	* Immunity to electromagnetic fields. * High sensitivity. * Do not conduct electricity. * Resistance to hostile environments.	* Light dependence. * Non-stationary signals in dynamic conditions. * Alignment requirements.

As mentioned above, an HMI is composed of different stages that are responsible for converting the user's intention (measured by a sensor and transduced to a signal) into the task of a device, which can be a robotic assistive device [16]. These stages can be summarized as follows:

- **Acquisition:** Here, the sensors are positioned with the objective of acquiring information about the individual's intention (EEG, sEMG, movements, etc.). Depending on the type of signal, amplifiers and physical filters may be used. In addition, the sampling rate must be adjusted depending on the frequency band of the signals and the physical capacity of the electronic devices [69, 16].

- **Pre-processing:** It is necessary to implement strategies to eliminate noise present in the signals. Time window segmentation, frequency domain filters, and other filters, such as spatial reference filters, can be examples of signal pre-processing [71].

- **Feature extraction:** For the identification of intentionality through patterns in the signals, extraction techniques are applied to obtain the features that allow the discrimination of the user's intention in an adequate way [72].

- **Classification and regression:** Considering the problem faced or the objective of the HMI, control triggers can be established through discrete (classification) or continuous (regression) outputs. In this phase, algorithms based on artificial intelligence, such as machine learning or deep learning, are applied to identify patterns in signals obtained from the human body [73, 74].

- **Control:** Depending on the sensors and actuators, the output is translated into the action of a device that interacts with the environment. In the literature, a large number of robotic devices for rehabilitation and assistance have been reported, controlled by signals obtained from the human body, where the most common are exoskeletons, prostheses, electric wheelchairs, among others [75, 76].

- **Interface:** A very important factor in the design of an HMI is the construction of an adequate interface that allows a correct human-machine interaction, as well as the patient's feedback regarding the task performed [77].

2.3.1 Brain-Computer Interface

A Brain Computer Interface (BCI) is a system that functions as a communication channel between the brain and computers, so that the user's environment can be controlled in a way that is compatible with the user's intentions. BCIs have been widely used in rehabilitation engineering because these technologies allow interaction with the environment through signals resulting from mental tasks; therefore, physical mobility is not necessary to use the interface, which is useful for people with reduced mobility. However, considering some of the

disadvantages of acquisition systems, such as EEG (see Table **2-3**), it is necessary to design an interface that can be used by the target population; therefore, the type of paradigm to be used is important [51]. Considering the BCI proposed based on ERD/ERS in Section 3.1, cortical rhythms generated in Actual Movement (AM) and Motor Imagery (MI) tasks are discussed in this section.

2.3.1.1. Event Related Desynchronization/Synchronization

ERD/ERS are oscillatory cortical phenomena generated by a large group of neurons involved in activities related to cognitive processes in the Mu (μ) and Beta (β) bands [78]. These rhythms can be captured with EEG during the performance of limb motor tasks or even the imagination of limb movement [78, 32]. ERD refers to the temporal slowing in response to a stimulus or event. For example, when a subject performs a motor task related to the lower limbs, a decrease in the amplitude and frequency of the Mu band may be observed in the EEG in the central area of the cortex. In contrast, ERS refers to an increase in the cortical rhythm in response to an event. For example, this increase in electrical activity may be observed in the beta rhythm in parieto-central areas of the brain when a person is performing a task that requires increased cognitive or motor activation [78]. An example of these cortical responses is shown in Figure. **2-3**.

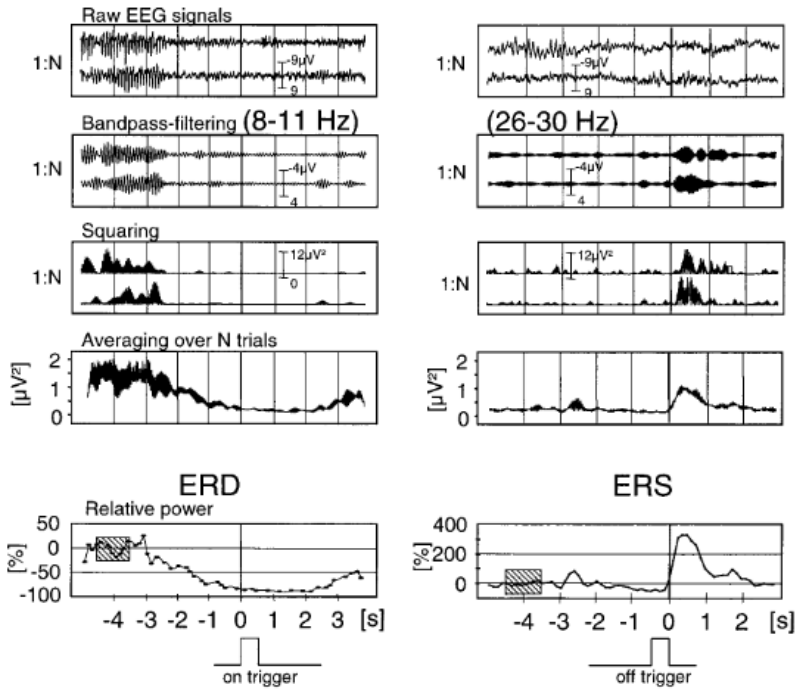

Figure 2-3: ERD/ERS principle of processing. Image taken from [119].

2.3.1.2. Preprocessing Techniques

As discussed above, EEG signals are of low amplitude and are usually influenced by external noise or artifacts produced by the physiological processes of each subject [17]. For this reason, different types of preprocessing are recommended for the design of BCIs. Among the most prominent in the literature are those based on signal filtering in the time, frequency, or spatial domains [79].

Time domain filters tend to reduce and/or eliminate noise related to event-related potentials, such as ocular artifacts [79]. One of the most commonly applied filters in the neuroscience world is the Common Average Filter (CAR), which consists of averaging the temporal information of the channels of interest in a region to eliminate the common noise present in the electrodes [80].

Frequency domain filters consist of filtering the signal with respect to the frequencies of interest, such as those shown in Table **2-1**, which allows the analysis of the signal content where it is possible to detect the paradigm. For example, a frequency filter between 8 and 13 Hz would allow the analysis of the signal in the Mu band, which is one of the most important bands during MI tasks [31].

On the other hand, spatial filtering allows discriminating information from channels of interest or with low noise content, which would allow for an improvement in task detection through EEG. Some of them consist of channel weighting, and more mathematically complex techniques such as Common Spatial Patterns (CSP), which will be contextualized below [79, 31, 32].

Other processing steps may include those related to the windowing. Windowing is a technique used in both signal analysis and real-time HMI, because it allows information to be obtained from a time segment [81]. Here, it is necessary to choose a suitable number of windows that allow the determination of a window that provides sufficient information to decode the task as well as an adequate response time in the BCI [81]. Each window can be considered as a trial or example (speaking in Machine Learning terms), in which different features can be extracted for the design of classification and/or regression strategies [81, 54].

2.3.1.3. Feature Extraction

Feature extraction in EEG signal processing is a fundamental process that involves identifying and quantifying the relevant and distinctive patterns present in brain signals [82]. These features are numerical values that represent the key attributes of the signals, such as the amplitude, frequency, symmetry, and variability. Feature extraction reduces the complexity of EEG data, highlights the most relevant information, and facilitates its analysis and understanding [82]. By selecting and quantifying specific features, it is possible to identify cortical rhythms, patterns associated with cognitive functions, or neurological abnormalities, and then apply classification or recognition techniques to interpret brain signals. Some feature extraction techniques for motor tasks are described below [31].

- **Amplitude:** In recent years, the feasibility of decoding continuous movements has been demonstrated through mathematically complex techniques, as well as the use of signal amplitude information in the delta band, which are slow signals that allow the prediction of positions and kinematic velocities through EEG signals [38, 83, 84].

- **Features in Time-domain:** Techniques based on the statistical behavior of signals in the time domain have also been used in the literature because of their low computational cost and because they can provide discriminant information of EEG signals considering mental tasks. Among these, it is possible to highlight the mean, median, variance, or Root Mean Square (RMS) [85].

- **Power Spectral Density:** Is a measure used to characterize the distribution of energy at different frequencies, which, in the context of EEG, is applied to study brain electrical activity in different frequency bands [86]. This technique provides information regarding the intensity of brain oscillations at each frequency, allowing the identification of characteristic patterns associated with different mental states and cognitive functions. The PSD is obtained by computing the frequency spectrum of the signal; then, a statistical process may be used, such as the integral of the signal at certain frequencies of interest, to obtain features and classify mental tasks, such as motor tasks [86]. An example of extracting the integral of the power spectral density and obtaining features through the discrete Fourier transform is presented in Algorithm 1.

- **%ERD:** Considering that the power in the Mu and Beta bands fluctuates in MI tasks, one of the metrics used in the literature corresponds to the %ERD, which marks the ratio between the power obtained from the baseline and the power obtained during MI. This is represented by Equation 2-1.

$$ERD(\%) = 100 * \frac{(P_{MI} - P_B)}{P_B}, \tag{2-1}$$

  where P_{MI} corresponds to the power during MI tasks, and P_B corresponds to the power during the baseline.

- **CSP:** Is an EEG signal processing technique that is widely used in BCIs and brain rhythm analysis applications [31]. This technique aims to identify spatial patterns that maximize the separation of the features associated with different mental states. CSP extracts an optimal linear combination of EEG channels, resulting in a series of characteristic spatial patterns that reflect the specific activation of brain areas involved in a specific task or condition [79]. These spatial patterns allow for improved discrimination between different mental states or actions. For example, in motor tasks, this

Algorithm 1 Feature Extraction based on PSD for EEG

Input: $S_A, S_E \in \mathbb{R}^{t \times s \times c}$ ▷ where S_A and S_E are the EEG signals for the training and testing set, respectively; t is the number of trials, c is the channels number, and s is the number of samples.

Output: F_A, and F_E ▷ where F_A and F_E are the feature matrices for training and testing

for each trial t_i in S_A and S_E **do**
  $F_{t_i} \leftarrow \text{fft}(s_i)$ ▷ Compute the DFT for the segment for all channels
  $PSD_{s_i} \leftarrow |F_{s_i}|^2$ ▷ Compute the power spectral density (PSD)
  $Power_{s_i} = \int_b PSD_{s_i} df$ ▷ b is the Frequency band of interest.
end for
$F_A = Power_A$
$F_E = Power_E$

Note: The choice of frequency bands depends on the specific analysis.

technique has been used to maximize signal features with higher variance and minimize those with lower variance [32]. Some algorithms for computing CSP-based methods are available in [87], where the concept of CSP to extract features from two motor tasks for classification is shown in Algorithm 2:

Other variations of the CSP have been presented with the aim of improving the identification rate of motor tasks using EEG signals, such as the Filter Bank CSP (FBCSP) or Filter Bank Common Spectral Spatial Patterns (FBCSSP). Further information on these methods is available in [88, 32, 87].

- **Riemann Geometry:** Is a method based on unsupervised operations such as temporal filtering and covariance estimation, which has been widely used in the literature for the detection of mental tasks such as MI [89, 21]. This method reduces common interference and enhances the variance ratio between EEG trials from different motor tasks. Some algorithms for computing Riemann Geometry-based methods are available in [89], where the concept of Riemannian Geometry for extracting EEG features in binary classification tasks can be seen in Algorithm 3.

2.3.1.4. Classification

Classification is a fundamental task in the field of Artificial Intelligence (AI), and consists of assigning objects, data, or examples to predefined categories or labels based on their characteristics or attributes [90]. Commonly, Machine Learning-based techniques have been used to classify tasks recognized through EEG, as described below [56].

- **LDA:** Linear Discriminant Analysis (LDA) is a ML technique for classification and dimension reduction in multivariate data. Its main objective is to find a linear combination of the original features that maximizes the separation between classes and

Algorithm 2 CSP for feature extraction and spatial filtering

Input: $S_A, S_E \in \mathbb{R}^{t \times s \times c}$ ▷ where S_A and S_E are the EEG signals for the training and testing set, respectively; t is the number of trials, c is the channels number, and s is the number of samples.
Output: F_A, and F_E ▷ where F_A and F_E are the feature matrices for training and testing

Let $\mathbf{S}_A$ and $\mathbf{S}_E$ ▷ Training and Testing Sets.
Separate the groups considering the labels of $\mathbf{S}_A$ (class 1 and class 2).
$C_1 = \mathbf{S}_{A_1}\mathbf{S}_{A_1}^T$ ▷ Computing the covariance matrix for the class 1.
$C_2 = \mathbf{S}_{A_2}\mathbf{S}_{A_2}^T$ ▷ Computing the covariance matrix for the class 2.
$J_{CSP} = (w\ C_1\ w^T)\ /\ (w\ C_2\ w^T)$
Extreme $J_{CSP(w)}$, i.e., maximize and minimize it, to obtain spatially filtered signals whose band power is maximally different between classes.
$X_A = wS_A$ ▷ Applying the spatial filtering for training set
$X_E = wS_E$ ▷ Applying the spatial filtering for testing set
$F^A = log(var(X_A))$ ▷ Computing the features based on logarithm of variance
$F^E = log(var(X_E))$

Note: ^{T} corresponds to the transpose.

Algorithm 3 Feature extraction based on Riemann Geometry

Input: $S_A, S_E \in \mathbb{R}^{t \times s \times c}$ ▷ where S_A and S_E are the EEG signals for the training and testing set, respectively; t is the number of trials, c is the channels number, and s is the number of samples.
Output: F_A, and F_E ▷ where F_A and F_E are the feature matrices for training and testing

Let $\mathbf{S}_A$ and $\mathbf{S}_E$ ▷ Training and Testing Sets.
$C_A = covariances(S_A)$ ▷ Computing the covariances matrices for the training set
$C_{ref} = mean\_covariances(C_A, 'riemann')$ ▷ Computing the covariance mean based on Riemann distance.
$C_E = covariances(S_E)$ ▷ Computing the covariances matrices for the testing set
$F_A = tangent\_space(C_A, C_{ref})^T$ ▷ Projection of the covariance matrices onto the reference matrix (training set).
$F_E = tangent\_space(C_E, C_{ref})^T$ ▷ Projection of the covariance matrices onto the reference matrix (testing set).

Note: ^{T} corresponds to the transpose.

minimizes the variability within each class. In this manner, LDA seeks to project the data into a new, lower-dimensional space while maintaining discrimination between classes.

- **SVM:** Support Vector Machine (SVM) is a supervised ML algorithm used for classification and regression. Its main objective is to find the optimal hyperplane that best separates the data into different classes, maximizing the margin between the closest samples in each class. In addition, SVM can be extended to work in higher-dimensional spaces using kernel functions to solve nonlinear classification problems.

- **KNN:** k-Nearest Neighbor (KNN) is a simple, non-parametric ML algorithm used for classification and regression. In KNN, predictions are based on the similarity between the data to be classified and their nearest " neighbors " in the feature space. The number of neighbors considered (k) determines the accuracy and robustness of the algorithm. KNN is effective for problems where the data have a clear neighborhood structure and can adapt well to different forms of data distribution. However, their performance can be affected by noisy data and high dimensionality.

- **LR:** Logistic Regression (LR) is a classification model used to solve binary problems, which is used for classification. It uses a logistic function to model the probability of belonging to one of the two classes as a function of the predictor variables.

2.3.1.5. Regression

One of the disadvantages of using classifiers in BCIs is that the outputs are discrete, which limits the use of continuous controllers, and thus may reduce the usability of the system [91]. In recent years, it has been possible to demonstrate the use of decoders, such as those based on Kalman Filters (KF) [91], Deep Learning (DL) [38], or ML regressors [83]. Some of these are defined as follows.

- **KF:** Is a recursive estimation technique used to estimate the state of a dynamic system based on noisy measurements and previous data [91]. Although it shares some concepts with regression, its main objective is to provide an optimal and accurate estimate of the system state in an environment with uncertainty and noise. For BCIs, the KF and its variations have been used as decoders of kinematic signals using brain information. It is important to note the use of the Unscented Kalman Filter (UKF), which has been one of the most widely used filters for decoding motor tasks, because this mathematical model considers the nonlinear relationship between the neural system and the movement [91, 92]. More information on this method is available in [91].

- **Regressors:** Regression is a statistical and ML technique used to predict continuous numerical values from a dataset. Different classifiers mentioned above can be used as

regressors, such as SVM, KNN, or LR, where in this case the target output variable is continuous and is not labelled as if it was a class [93].

2.3.1.6. Artificial Neural Networks (ANNs)

ANNs have emerged as attempts to emulate the functioning of biological neurons. This is done with the aim of developing a system that has high processing capacity and performs highly complex tasks from input signals. An artificial neuron, similar to a biological neuron, communicates with other neurons through synapses with a respective weight, which allows the generation of one or several outputs [54]. ANNs have been widely used in the context of BCIs for signal analysis because they allow the discrimination of more relevant information using more mathematically complex techniques, which means that detection algorithms can be more robust and accurate. [94]. However, for real-time applications, it should be noted that they tend to be computationally expensive, which is limited in some cases when considering the response times and computational resources. Some of the most widely used methods are the Multilayer Perceptron (MLP), Extreme Learning Machine (ELM), Convolutional Neural Network (CNN), and Long Short-Term Memory (LSTM) [94].

- **MLP:** Is a type of ANN consisting of multiple layers of neurons connected together, which is designed to solve complex classification and regression problems by learning nonlinear representations of data [95]. The MLP has an input layer that receives input data, one or more hidden layers that process and transform information, and an output layer that produces the final predictions or classifications. Each neuron in the MLP uses a nonlinear activation function to introduce nonlinearities into the model, allowing it to learn more complex relationships in data [54].

- **ELM:** Is a neural network family of Single Hidden Layer Feedback Neural Networks, that has been reported in the literature for motor tasks classification and regression [96]. It is composed of a single hidden layer with its respective activation function, where the objective is to train the network by modifying the weights of the neurons in the inner layer to such an extent that it allows the classification of a group of input variables [97]. The ELM has advantages over other types of classifiers because its training time is low.

- **CNN:** Is a type of ANN inspired by the human visual system that uses convolutional layers to extract relevant features from the data. It then employs clustering layers to reduce dimensionality and fully connected layers to perform classification or regressions [94]. CNNs have demonstrated outstanding performance in task classification using EEG signals [94].

- **LSTM:** Is a special type of Recurrent Neural Network (RNN) designed to process and model sequences of data, where LSTMs have a gated cell structure that allow

them to remember long-term information and avoid the problem of gradient fading [38]. These gates control the flow of information in the cell, allowing the LSTMs to retain and forget relevant information over time. This is because of its long-term memory capability. LSTMs have demonstrated an outstanding performance in task classification and regression using EEG signals [38].

2.3.1.7. Performance Metrics

Performance metrics are normally used to evaluate the performance and effectiveness of classifiers. For example, in the case of classifiers, performance metrics are based on confusion matrices between the predicted variables and the original variables, such as Accuracy (ACC), which is indicated in Equation 2-2.

$$ACC = \frac{TP + TN}{TP + FP + TN + FN}, \tag{2-2}$$

where TP is a true positive, TP is a true negative, FP is a false positive, and FN is a false negative. On the other hand, for regression-based continuous representations, the most commonly used metric is Pearson's Correlation Coefficient (PCC), which allows quantification of the prediction data versus the true data, normally when kinematic information is predicted. PCC takes values in the range of -1 to 1. A value of 1 indicates a perfect positive correlation, meaning that as one variable increases, the other increases in proportion. A value close to zero indicates a weak correlation, suggesting that there is no linear relationship between the two variables [83].
In the context of decoding, if the PCC between the independent variable and the dependent variable is close to 1 or -1, it suggests that there is a strong linear relationship between them, which may indicate that a linear regression model could work well in predicting the dependent variable as a function of the independent variable [83]. This metric is computed using 2-3.

$$PCC = \frac{1}{N-1} \sum_{i=1}^{N} \left(\frac{P_x^i - \mu^{P_x}}{\sigma^{P_x}} \right) \left(\frac{P_y^i - \mu^{P_y}}{\sigma^{P_y}} \right), \tag{2-3}$$

where P_x is the measured data, P_y is the estimated data for a total number of samples N, and μ_q and σ_q are the mean and standard deviation of q, respectively, with $q \in P_x, P_y$ [83].

2.4 HMI for Lower-Limb Rehabilitation and Assistance

Robotic devices are electromechanical systems that use different types of technologies and automation to perform physical tasks and/or assist humans in various activities [98]. Over

the years, these devices have been modified and adapted, thus having a wide variety of shapes and sizes from industrial robotic arms to portable exoskeletons and bionic prostheses [99].
In the context of rehabilitation and assistance, robots have proven to be useful in improving the functionality and quality of life of people with disabilities or physical limitations [99]. Among these, it is possible to highlight limb exoskeletons, assistive and postural devices for gait rehabilitation, electrically powered wheelchairs, and assistive devices for other types of movements, such as pedaling [99]. Several robotic devices for rehabilitation and assistance in lower limb rehabilitation are listed in Table **2-4**.

Table 2-4: Devices used for the rehabilitation and assistance of persons with lower limb neuromotor disabilities.

Name	**Tasks (Type)**	**Principle**	**Limitations**
Electrical powered wheelchair	Transport (Assistance)	They are equipped with motors that drive the wheels, allowing the user to control the wheelchair movements easily and comfortably. They can be equipped with sensors that allow monitoring of the person as well as the environment.[100]	* No rehabilitation. * Weight and size. * Difficulty in uneven terrain.
Lokomat	Walking (Rehabilitation)	It consists of a user-fitted robotic leg exoskeleton whose motors and sensors are synchronized with the patient's movement, enabling precise assistance and support during walking. This system combines robotic technology with assisted locomotion therapy to provide an intensive and effective form of rehabilitation for patients with neuromotor impairments [101].	* Cost. * Space requirements. * Requires patient adaptability. * Fatigue.

Continued on next page

ZeroG	Walking (Rehabilitation)	It is a suspension and body weight assistance system used in rehabilitation therapies, whose operation consists of providing a safe and effective way to perform exercises and functional activities while reducing the weight load on the patient's body. This system consists of an aerial track installed on the ceiling or on an elevated structure, on which a motorized trolley moves [102].	* Cost. * Space requirements. * Infrastructure. * Patient adaptability.
Prosthesis	Movement (Assistance)	Artificial devices designed to replace a missing limb, such as a leg or foot. These prostheses are designed to restore function and mobility lost due to amputation, allowing the performance of various physical activities such as standing or walking [103].	* Shelf life. * Adaptability of the person. * Functional limitations. * Physical and psychological changes in the person.
Motorized Mini Exercise Bike	Pedaling (rehabilitation)	Device used in rehabilitation to improve mobility and muscle strength of users. This compact and portable bicycle is equipped with an electric motor that provides automatic movement of the pedals, allowing the individual to perform pedaling exercises without exerting significant force (passive pedaling). In recent years it has emerged as an alternative for patients with mobility limitations or weakness in the lower extremities, as it allows them to participate in a gentle and controlled form of exercise. Additionally, it can be used at home or in rehabilitation centers [13].	* Limitation in exercises. * Lack of adjustable parameters. * Static position. * Little known in the literature.

Although advances in robotics for lower limb rehabilitation and assistance have been significant, it should be noted that commercial devices can be expensive and require complex physical structure, while MMEB-based therapies have proven to be viable for their ability to assist in cyclic movements and portability [13]. However, the exploration of this type of technologies with BCIs has not been fully explored, leaving a gap to continue deepening in control and neurorehabilitation methodologies. Some strategies, proposals and results will be discussed below.

3 Methodology

3.1 Robotic system

The development of lower-limb assistance addressed in this work is an adaptation of the commercial low-cost pedal-assisted MMEB used in previous research [104, 13]. This device proved to be robust in the implementation of BCI systems for lower limb rehabilitation, however, the default configuration of this MMEB is eight speeds, and the activation is discrete. Therefore, an external circuit for speed control was realized to enhance usability. The MMEB is shown in Figure 3.1(a).
The circuit was designed to control the velocity of the motor power supply to 100 VDC. A full-wave rectifier circuit was implemented using a 127 VAC power-line source. Subsequently, a filter configuration before a metal–oxide–semiconductor field-effect transistor (MOSFET) device was used to commute at high velocities while controlling the motor. Moreover, an optoisolator (MOC3021) was used to send control signals to the motor, which was powered at 5 VDC using a voltage regulator and pull-down connection. Figure 3.1(b) shows the circuit described above, where ESP32 is the device used to send the velocity control commands through Pulse Width Modulation (PWM) signals to the MMEB.

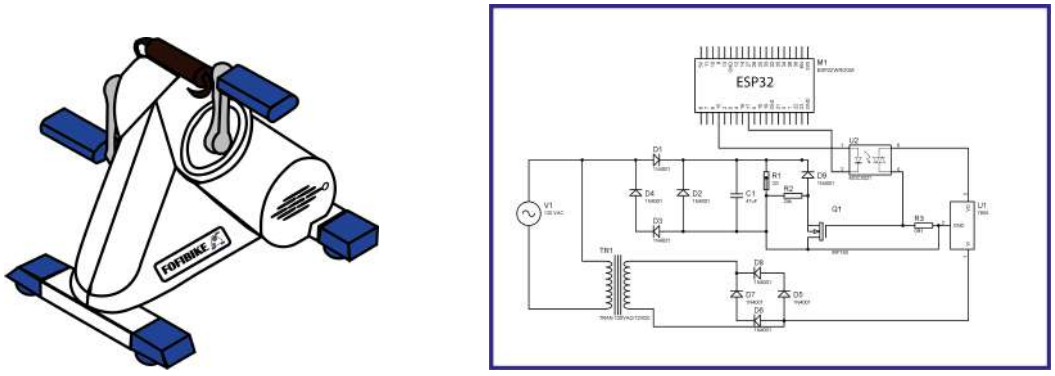

(a) (b)

Figure 3-1: (a) MMEB used and adapted for the development of this research. (b) Electronic instrumentation for power supply and velocity control of MMEB.

Subsequent to the realization of the circuit and initial checks, it was necessary to perform a characterization to determine the PWM ratio with respect to the final speed. Kinematic

characterization was performed based on camera and inertial motion recordings. A camera was placed in front of the MMEB to identify the reflective marker placed in the user [63], whereas a motion capture device based on inertial sensors (IMOCAP) was placed in the MMEB pedal [105, 106]. Then, for the motion data, signal integration was performed according to the acceleration to obtain the angular velocity. For the camera information, a grayscale filter was implemented to analyze the videos using the DL software for pose estimation DEEPLABCUT, where the positions of the interest points were obtained from both the image and angular velocity computation with the signal difference [107]. Figure **3-2** illustrates the previously explained methodology used for the MMEB calibration.

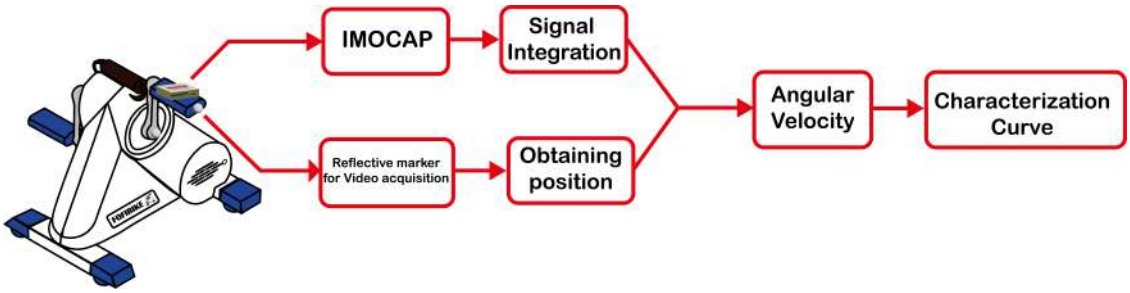

Figure 3-2: Methodology used in this work for MMEB characterization based on a motion capture system and a camera.

3.1.1 Error

To evaluate the behavior of MMEB with respect to the modification of Pulse Width Modulation (PWM) signals with IMOCAP and reflective markers, the Root Mean Square Error (RMSE) metric between the two signals was evaluated. Subsequently, curve fitting was performed between the PWM values and the computed angular velocity, where the hypothesis was that the system exhibits a linear behavior. Finally, the RMSE metric was again calculated during the acquisition of the protocol with and without the subject to observe if there was a difference in the passive pedaling as a consequence of the weight characterization, where a linearity value of $r = 0.9797$ was found, which allowed the estimation of the proportional rate of the MMEB and the input signal. With this procedure, it is possible to adjust continuous velocities in the MMEB, which will be useful in the protocol implementations.

3.2 EEG acquisition and protocols

During the development of this work, different protocols for EEG acquisition during pedaling-related tasks have been proposed. Mainly three protocols: The first includes active pedaling tasks, where pedaling tasks are generated voluntarily by the person. The second protocol involved the implementation of MMEB-generated passive pedaling tasks combined with MI

at different velocities. The third stage consisted of two main stages: passive pedaling, presentation of visual neurofeedback during MI and passive pedaling, and real-time BCI to classify MI and neuromodulation of the visual stimulus. The protocols are described in detail below.

3.2.1 EEG acquisition

EEG signals were recorded using an OpenBCI cap with eight electrodes placed on the scalp following the 10-20 international system, as shown in Figure **3-3**. Reference electrodes were placed on the left (A_1) and the right (A_2) earlobes, and conductive gel was applied to all electrodes to reduce impedance (< 20 kΩ). This choice of electrodes was made by considering the cortical response in the cerebral cortex during pedaling exercises, which has been reported in the literature: FC_1, FC_2, C_3, C_Z, C_4, CP_1, CP_2, and P_Z [21, 13, 20, 108]. EEG signals were recorded at a sampling rate of 250 Hz, and a notch filter was implemented at 60 Hz to reduce the power line artifact. Initially, impedances were verified using software provided by OpenBCI, whereas environments for stimulus acquisition and generation were designed using OpenVibe [109]. OpenVibe is compatible with the openBCI card, where it is possible to generate environments for the acquisition and processing of EEG signals through blocks with functions. Additionally, this execution environment is compatible with Python, which facilitates the operation of data and compilation of algorithms in real time [109].

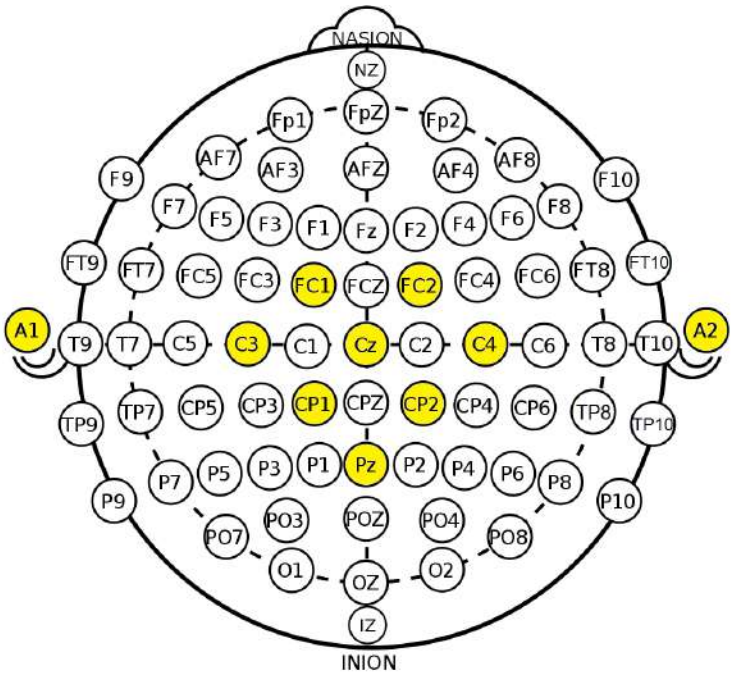

Figure 3-3: Electrodes used for EEG acquisition according to the 10-20 international system considering the parieto-central cortex and the reference electrodes (A_1 and A_2).

3.2.2 Experimental Design

For the experimental designs, it was necessary to use a noise-free isolated room, where the MMEB was used to perform pedaling tasks (passive or active). Everything related to indications or visual stimuli was presented on a 1280 × 768 screen located two meters away from the individual at a 60 Hz refresh rate. Additionally, all sessions were recorded using a high-speed camera at 60 fpm, which was positioned in the sagittal plane and synchronized with the open acquisition system for analysis related to kinematics [110]. The sEMG electrodes were placed on the vastus lateralis (VL) and Gastrocnemius Lateralis (GL) muscles [111], whose analyses were not included in this study. Graphical representations of the experimental design are shown in Figures 3.4(a) and 3.4(b).

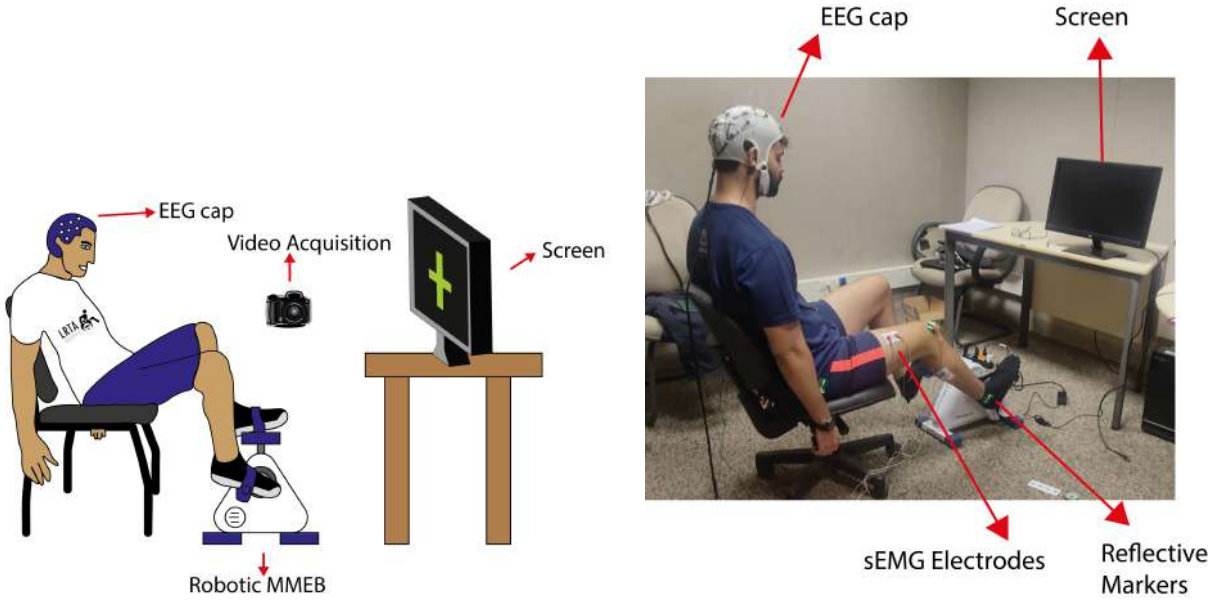

(a) (b)

Figure 3-4: Experimental environment for performing EEG acquisition protocols and pedaling tasks.

3.2.3 Acquisition protocols

3.2.3.1. Active pedaling

This protocol was intended to acquire EEG and kinematic information during the execution of active pedaling tasks, meaning that the subject was encouraged to perform voluntary pedaling with visual instructions (See Figure 3.5(a)). The experiment consisted of two sessions, implemented in three steps.

- The subject rests their foot on the minibike pedals and fixes their attention on a black screen for 5 s without engaging in any mental activity.

- A green cross is displayed on the screen, after which the subject pedals the minibike for 5 s.
- The subject rests for 5 to 7 s, and the cycle is repeated 30 times.

3.2.3.2. Passive pedaling and MI

This protocol was intended to acquire EEG and kinematic information during the execution of passive pedaling, combined with MI tasks. For this, the subject was instructed to perform MI tasks subsequent to passive pedaling at different velocities, considering that, according to the literature, this may increase the variation in cortical rhythms [20, 21, 13]. In this case, visual instructions were not implemented, and the MMEB executed three velocities (30, 45, and 60 rpm) randomly (See Figure 3.5(b)). The experiment consisted of two sessions, implemented in four steps.

- The subject rests their foot on the minibike pedals and fixes their attention on a black screen for a baseline of 60 s without engaging in any mental activity.
- The MMEB is activated in a time lapse between 7.5 and 10 s for passive assitance.
- The subject has to perform the pedaling MI for the same amount of time as before.
- A break of approximately 2 s without mental task is taken by the subject, which is indicated by a beep.

Each session of the above protocol consisted of 10 trials per speed (30 trials per session), for a total of 60 trials performing MI and passive pedaling.

3.2.3.3. MI with Visual-Neurofeedback

During the performance of this protocol the subject was always executing passive pedaling by the MMEB at a speed of 30 rpm, considering that the objective of this protocol is focused on neuromodulation. For visual neurofeedback, a percentage box was implemented on the screen where 100% means that the subject is modulating correctly during MI tasks, while 0% means that the subject is not modulating or performing MI. When modulation is detected for values above 40%, the box is green, whereas for a lower value the box is red (See Figure 3.5(c)).The protocol is divided into three parts.

- The subject puts their foot on the MMEB pedals while is performing passive pedaling but withouth executing mental tasks (baseline) for 150 s. During this time, visual stimulus are randomized.
- The subject is encouraged to perform MI tasks during passive pedaling. Here, the ERD percentage is calculated and displayed on the screen with the aim of motivating

the individual to neuromodulate for 150 s. Meanwhile, the ERD percentage computed with the actual values of power by using a time window of 1 s (overlapping 50%) computed with Equation 2-1 is presented in the screen.

- The subject proceeds to perform pedaling MI for 5 minutes continous, using visual neurofeedback-based BCI, which is going to be presented later.

(a)

(b)

(c)

Figure 3-5: Different protocols performed during this research based on (a) active pedaling; (b) passive pedaling combined with MI; (c) BCI based on MI and visual neurofeedback.

3.2.4 Participants

A sufficient number of subjects was determined based on a statistical power analysis realized in G*power software [112]. An analysis was performed to verify the appropriate number of subjects for model generalization based on the results reported in the literature. For

this purpose, a G*power $d = 2.13$, a value of $\alpha = 0.05$, and a power of 0.90 were used, as recommended in previous studies focused on BCI systems [84]. The minimum number of subjects calculated by the G* Power software for the Wilcoxon signed-rank test was seven; however, in this study, a deviation of 20% was considered as the final sample size.
Eight healthy subjects (five men and three women, aged 22 – 32 years) with no history of neurophysiological disorders participated in the study by validating the first two protocols. In contrast, real-time validation of the proposed visual-neurofeedback-based BCI was performed in a case study involving a 35-year-old male subject with no reported neurological diseases. The participants voluntarily signed an informed consent form following the guidelines of the Declaration of Helsinki, and the experimental protocol was approved by the Ethics Committee of the Federal University of Espirito Santo (UFES), Brazil, under the number CAAE:39410614.6.0000.5060. All subjects were instructed on the experimental design and correct execution of the experiment.

3.3 Motor tasks classification

3.3.1 Classification of AM

Considering some strategies published in the literature for motor task classification, simple strategies of low computational cost were initially used to classify AM tasks during pedaling tasks executed by the subjects, as shown in Figure 3.5(a). Two strategies were implemented, as described below.

3.3.1.1 Using ELM and PSD:

After preprocessing techniques performed based on CAR filter and a butterworth filter of order 4 between frequencies from 3 to 30 Hz, PSD values were used together with the ELM in 4 frequency bands (**FB1**:3-7 Hz, **FB2:** 7-13 Hz, **FB3:** 7-30 Hz, and **FB4:** 3-30 Hz) to classify pedaling vs. rest execution tasks. Notably, the literature does not report this combination for the classification of target movements. In addition, PSD has worked with adequate ACC with other approaches, as well as ELM [31, 113, 114, 96, 97].
The methodology for classifying the PSD feature extraction (see Algorithm 1) and classifying them using ELM (see Section 2) is summarized in Figure **3-6**. Then, to find the most suitable configuration of the ELM, the hidden layer was adjusted and validated for 13 values: 10, 20, 30, 40, 50, 60, 70, 80, 90, 100, 200, 500, and 1000, using information from FB1. To generalize ELM, a k-fold cross-validation methodology was performed, where the total feature dataset was separated into two parts (training and validation) with a random number of k times. The process was then repeated for a value of $k = 5$, and the validation metrics were computed and averaged. This process was performed for the features extracted from each frequency configuration (FB1, FB2, FB3, and FB4).

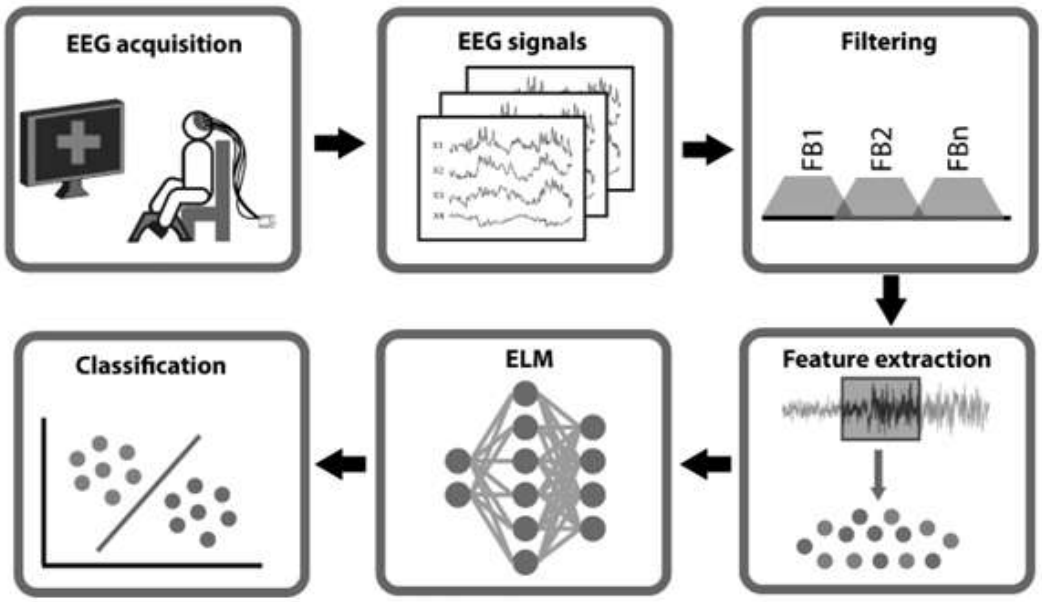

Figure 3-6: Block diagram of the methodology for the identification of pedaling tasks using PSD and ELM.

3.3.1.2. Using CSP-based methods and LDA:

Another strategy widely explored in the literature for classification of limb tasks movements corresponds to those based on CSP, such as FBCSP or FBCSSP [32, 87]. However, these methodologies have not yet been fully explored for pedaling [21]. Thus, these methods were used to classify pedaling vs. rest, and to find a suitable frequency band along with a suitable time window.

To address this methodology, a pre-processing was performed with a frequency band between 8 and 30 Hz, and then different filter banks and time windows were evaluated. Considering that the protocol contains 5 s for each task, the size of the windows was selected according to Figure **3-7**, and the frequency bands were selected according to table **3-1**.

Table 3-1: Configuration of Filter Bank for FBCSP and FBCSSP methods.

Filter Bank Configurations	Bandpass filter 1 (Hz)	Bandpass filter 2 (Hz)	Bandpass filter 3 (Hz)	Bandpass filter 4 (Hz)
FB1	8-13	13-30	-	-
FB2	8-19	19-30	-	-
FB3	8-16	14-22	20-28	-
FB4	8-15	15-22	22-29	-
FB5	8-15	13-20	18-25	23-30
FB6	8-13	13-18	18-23	23-28

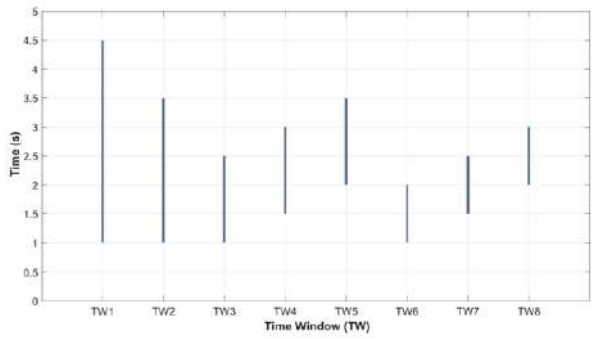

Figure 3-7: Configuration of time-windows used for feature extraction in CSP-based methods. Time 0 represents the trigger time (onset of the AM task).

For this research, the number of patterns was established and analyzed for the values 1, 2, 3, and 4, which allows for obtaining 2, 4, 6, and 8 CSP, respectively. Once the filters are obtained and implemented, the logarithm of variance (*logvar*) was extracted considering the different Time Window (TW) and FB. Then, LDA classifier was implemented to discriminate the pedaling tasks vs. rest, where the input came from the obtained features from algorithm 2. The k-fold cross trial-validation was used to validate the method according to the performance metrics with a $k = 5$, considering of 70% of the trials for training and 30% for the testing. Subsequently, considering previous studies and the CSP, FBCSP and FBCSSP were implemented under the same methodology. These methodologies are summarized in Figure **3-8**.

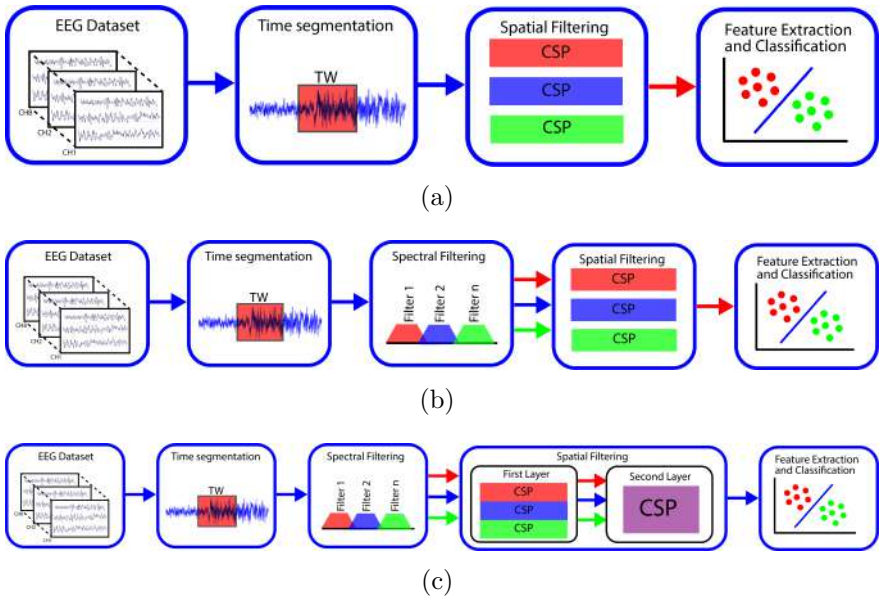

Figure 3-8: Spatial filtering and feature extraction for classification of pedaling tasks by using (a) CSP; (b) FBCSP; (c) FBCSSP.

To evaluate the performance of the above classification methods, metrics based on the confusion matrices obtained were used, especially using ACC.

3.3.2 Classification of MI

For the classification of MI after passive pedaling, strategies previously reported in the literature were considered [13, 21]. For this, information obtained from covariance matrices and calculations using Riemannian geometry were used as features.
Here the objective was to classify the MI with respect to the baseline, however, it is necessary to highlight that the protocol 3.5(b) presents a novelty with respect to the experimental designs reported in the literature [21, 13]. This novelty consists of the implementation of different time lapses and different passive assistance speeds, whereby the subject had to perform the MI task based on a previous stimulation with any of the three available velocities performed by the MMEB: 30 rpm, 45 rpm, and 60 rpm. Here the hypothesis was to analyze whether it is possible to discriminate these tasks using Riemannian geometry, as seen in multiclass classification studies.
Initially a filtering process was carried out, considering previous experiences with MI tasks [21, 32], where signals were segmented considering the triggers of the protocol and filtered in a range from 8 to 30 Hz using a 4 order Butterworth filter. Initially, the MI vs. baseline tasks were classified without considering the velocities to validate the performance of Algorithm 3. Subsequently, the one vs one strategy with LDA reported for multiclass classification was used, where different reference matrices were computed to classify the MI tasks for each speed. Additionally, the k-fold cross validation strategy with $k = 5$ was used to find the Riemann matrix that allowed the best discrimination for each class, using the ACC as a reference. In addition. considering that this is a multiclass problem, also in this case it is important to calculate the Area Under Curve (AUC) of ROC curve as metric, since this metric allows evaluating how well a class was discriminated with respect to the others [54]. A summary of this methodology is presented in Figure **3-9**.

3.3.3 Pedaling tasks decoding

In recent years, kinematic decoding through EEG signals has been of interest because this type of strategy generates continuous outputs that can be used as controllers of rehabilitation devices in a more robust way compared to discrete outputs by classifiers [37, 38].
However, these strategies for reconstruction of pedaling tasks have been little explored in the literature. For this reason, part of this research was to establish strategies to decode kinematic information of the lower limbs through EEG signals. To obtain the kinematic information, videos of the sagittal plane together with the position of the reflective markers were used (see Figure 3.4(a)), using the freely available software Deeplabcut [107].
The points were obtained according the reflective markers located in the hip, knee, and

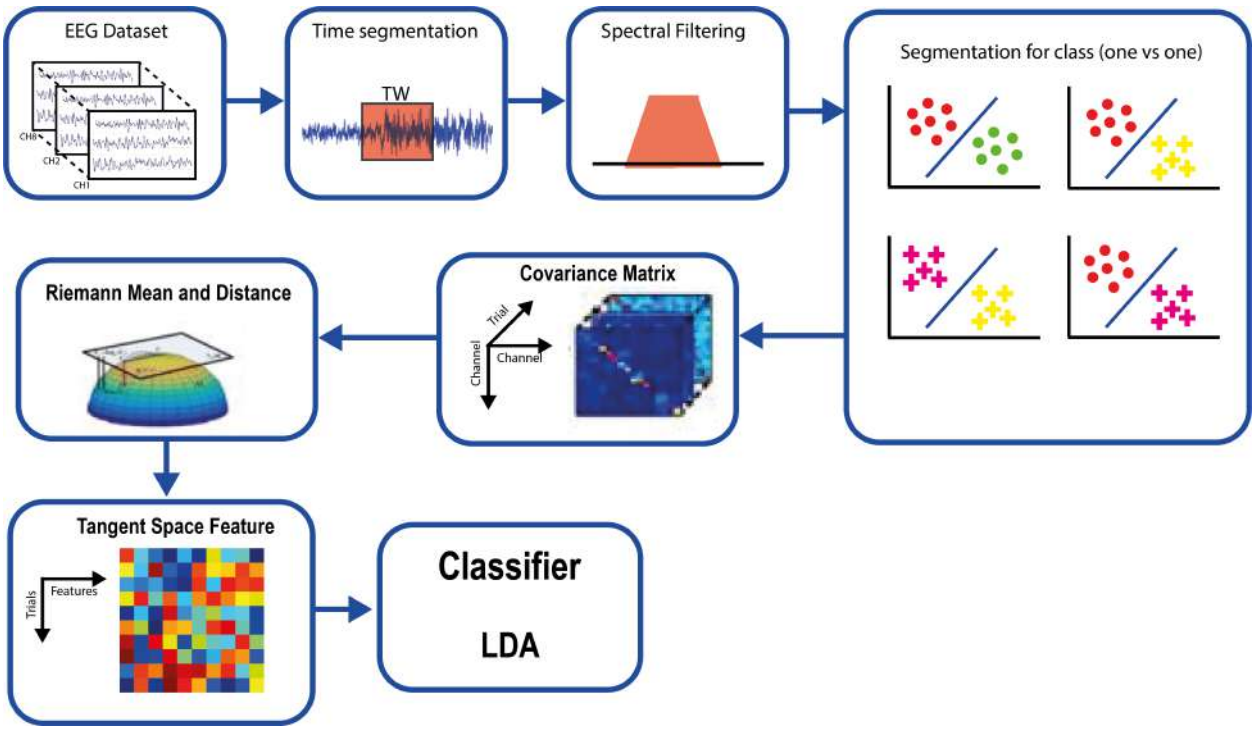

Figure 3-9: Feature extraction based on Riemannian geometry and classification with LDA for a multiclass approach.

ankle, considering that these are the joints involved in the pedaling tasks [111] (see Figure **3-10**).

Subsequently, Deeplabcut generates the kinematic signals, which were filtered with a Butterworth type low-pass filter to eliminate interference produced by occlusion. Two methods were used for the decoding of kinematics during pedaling tasks which are based on the Unscented Kalman Filter and Deep learning (CNN and LSTM).

3.3.3.1. Unscented Kalman Filter for velocities reconstruction:

To decode the pedaling tasks, EEG signals were filtered using a Butterworth filter in the frequency band of 0.1 to 4 Hz (δ band) [18, 38]. A CAR filter was used to reject the common noise involved in all EEG channels. In this case, four channels of EEG were used: C_Z, C_3, C_4, and P_Z, considering that literature reports Cz corresponds to more discrimant channel for decoding lower members [18, 13, 115].

In this case, EEG data was used to decode the kinematic behavior of the ankle joint, which is the most variable joint involved in pedaling tasks, and the knee angle, which is the most important joint involved in lower-limb movements [38]. Specifically, the velocities in the x and y axis were decoded for the ankle joint, according 2D registration, and the knee angular velocity was formed between the ankle, knee, and hip joints. To estimate the performance of the actual and decoded kinematic data, Equation 3-3 computed the knee angular velocity.

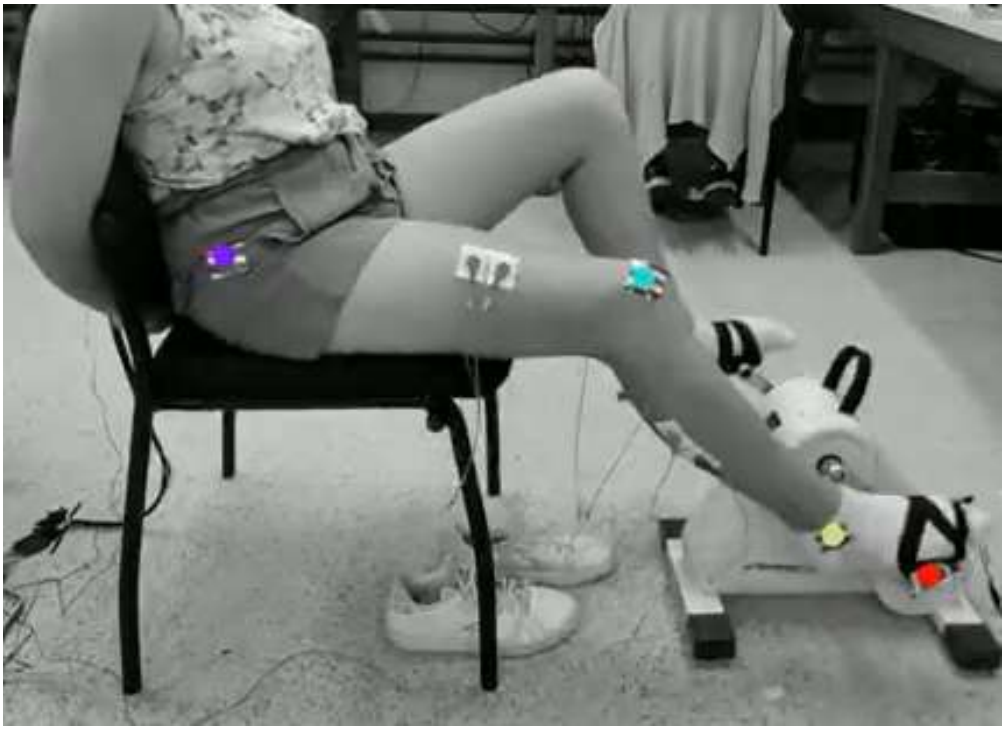

Figure 3-10: Reference points generated by Deeplabcut considering the three main joints: hip, knee, and ankle.

$$\dot{\theta} = \frac{\mathrm{d}}{\mathrm{d}x}\left[cos^{-1}\left(\frac{\bar{a}\cdot\bar{b}}{|\bar{a}|\cdot|\bar{b}|}\right)\right], \tag{3-1}$$

where a corresponds to the vector formed between the hip and knee, b corresponds to the vector formed between the knee and ankle, and $\dot{\theta}$ corresponds to the knee angle velocity. The first derivative was applied to Equation 3-3 to compute the angular velocity. In addition, the envelope of each kinematic signal was calculated using the spline interpolation method over the local maxima in a specific number of samples (50 in this case) to compare the real and estimated data [110]. Finally, considering that it is necessary for the kinematic and EEG signals to have the same sampling frequency, they were resampled and subsampled at 100 Hz [38].

The UKF is an improved version of the Kalman Filter due to its robustness in nonlinear applications. This method generates sigma points that are separated by the covariance of the estimated current state, which allows for better performance considering noise that affects the system. The UKF uses an Unscented Transform (UT) to incorporate nonlinearity into the model, which is important considering the nonlinear relationship between neural signals and limb motion [91, 18, 38].

In this study, the UKF was used as a decoder for the reconstruction of three kinematic

signals. For this, the nonlinear system consists of a motion model named state model, and a neural model (observation model). More information about these models is available in [56, 91]. In this case, the variables to estimate correspond as follow:

$$x_t = [\dot{\theta}_{knee}, \dot{x}_{ankle}, \dot{y}_{ankle}]^T, \tag{3-2}$$

where $\dot{x}_{ankle}$ denotes the velocity in x-axis of the ankle joint, $\dot{y}_{ankle}$ corresponds to the velocity in y-axis of the ankle joint, and $\dot{\theta}_{knee}$ denotes the knee angle velocity.

Considering the matrices that allow relating the neural behavior with respect to the kinematics, it is possible to obtain a vector of predictions for Equation 3-2. The methodology consisted of evaluating different time windows to predict the kinematic variable (lags), as shown in Figure **3-11**. In this case, information from TWs of 10, 20, 50, and 100 ms were used, which correspond to lag values of 1, 2, 5 and 10, respectively. Here, the PCC is computed to evaluate the performance of the implemented method to estimate the kinematics [110].

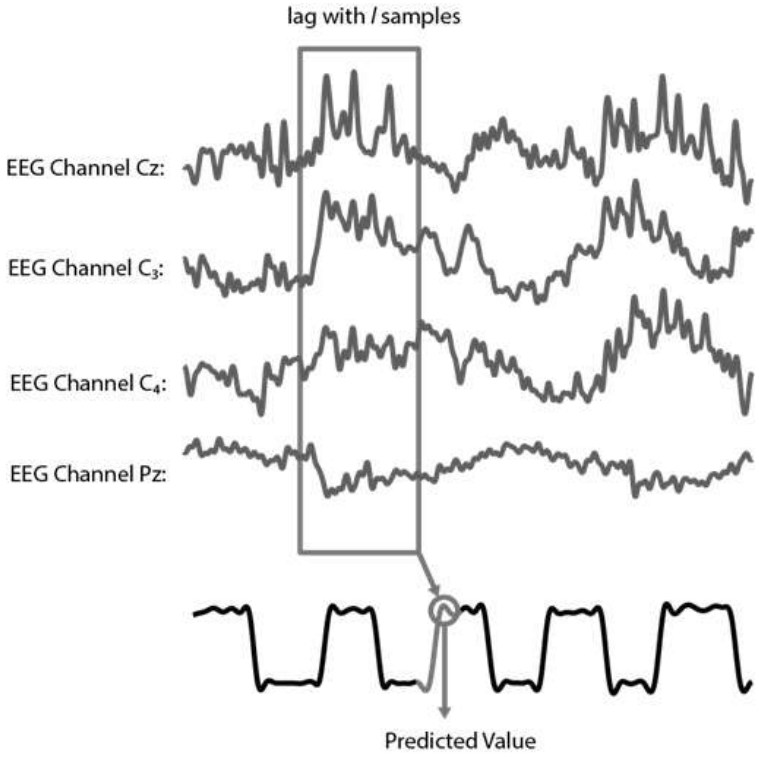

Figure 3-11: Decoding schematic for tap size = l. When running multiple experiments, the tap sizes ranged from 1, 2, 5, 10, which correspond to 10, 20, 50, 100 ms, respectively.

3.3.3.2. Deep learning for trajectory estimation:

Unlike the previous method, where it was possible to estimate the kinematic velocities present in the pedaling movement, in this case the trajectories were estimated [83]. For this, the information of the x and y axis of the ankle was used, together with the joint angle, obtained from the Equation 3-3.

$$\theta = cos^{-1}\left(\frac{\bar{a}\cdot\bar{b}}{|\bar{a}|\cdot|\bar{b}|}\right), \tag{3-3}$$

where a corresponds to the vector formed between the hip and knee, b corresponds to the vector formed between knee and ankle, and θ corresponds to the knee joint amplitude. Finally, this kinematic information is normalized by using max-min normalization technique, considering previous results [83]. After, the signals were segmented in TWs similar to estimate the kinematic parameter, such as the procedure shown in Figure **3-11**. After, the CNN and the LSTM were used in regression mode to estimate the angle.

- The CNN structure used in this study is shown in Fig. 3.12(a), which consists of different convolution and pooling layers. This architecture is based on related works of DL in decodification with EEG [83, 116, 117]. Furthermore, the size of the intermediate layers as well as the chosen hyperparameters were applied considering literature studies [83]. All the intermediate layers use ReLU as an activation function, as using this activation function the gradient has a constant value. In addition, different TWs were evaluated, where the lags had numbers equal to 50, 100, 150, 200, 250, and 300 ms. The input layer was based on features which correspond to the AM potentials in the delta band. The output layers were the estimated knee angle and ankle position, which were configured as a regression problem [117].

- LSTM was used considering the configuration shown in Fig. 3.12(b). The architecture used along with the established hyperparameters were chosen considering the reports of Nakagome *et al.* and Jain *et al.* [38, 83]. ReLu was used as the activation function for the hidden layers. The process was similar to the CNN methodology, where the features correspond to the AM potentials in the delta band for each lag (50, 100, 150, 200, 250, and 300 ms), and the output layers are the estimated kinematic parameters that were configured as a regression problem [117].

Training and Testing

After pre-processing and segmentation by time windows for EEG and kinematic samples, the data from the two sessions for each test subject were concatenated. Subsequently, the data

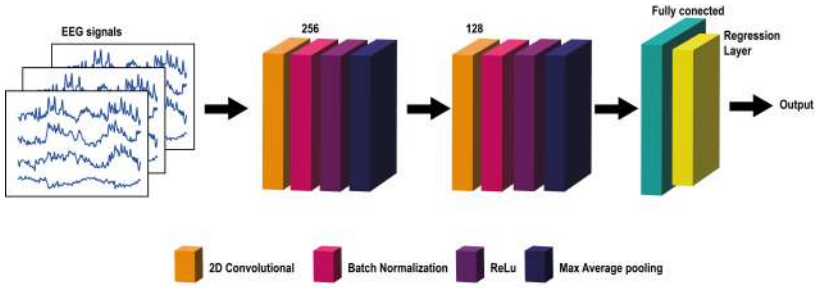

(a)

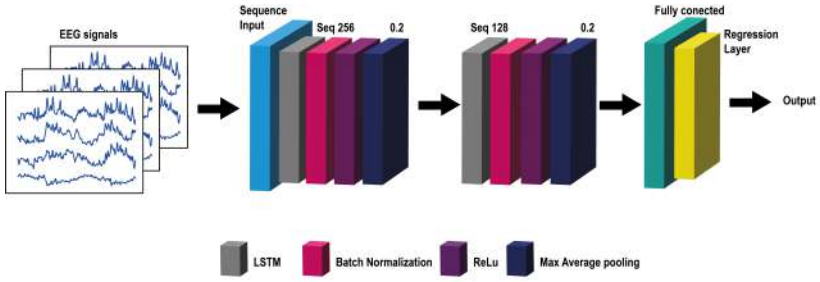

(b)

Figure 3-12: Proposed ANN-based structures for pedaling task identification. Above each block the configuration value set for each layer and the method is presented. Seq corresponds to sequence.

were randomized using the 70-15-15 strategy [110, 83], where 70% of the trials were used to train the ANNs, 15% were used to validate and generalize the algorithms, and finally 15% of the data were used to evaluate the efficiency of the network. The latter are presented in the results section. In total, 42 trials were used for training, 9 were used for validation and 9 for evaluation.

3.4 Visual Neurofeedback-based BCI

Finally, a real-time BCI system is proposed for the evaluation of a visual neurofeeback. For this, the Baseline and MI information shown in the protocol 3.5(c) are used to train the classification model. To address this, the features of the Riemannian geometry presented in the algorithm 3 were used.

Furthermore, the approach computes Euclidean distances of feature vectors extracted in a multi-channel EEG scenario with respect to cluster centers to help individuals regulate their cortical rhythms associated with MI. As explained below, two clusters are defined in this approach, one composed of baseline, and other composed of MI. This strategy was based on previous studies presented by [118]. Let be a feature vector $F = \{f_1, \cdots, f_i \cdots, f_K\}$

considering that i equals the epochs, and the features obtained by the Reimanian geometry for the class when MI is running. Subsequently, the visual neurofeedback percentage is calculated based on the Euclidean distance, considering a marker that allows weighting the features. According the above:

$$d_i = \sqrt{(f_i - u)(f_i - u)^T}, \tag{3-4}$$

$$u = \sum_i w_i \times f_i, \tag{3-5}$$

where

$$w_i = B_i \times \left[\sum_{l=1}^{N} B_l\right]^{-1} \tag{3-6}$$

where B_i is the biomarker considering electrodes $E = \{e_1, \cdots, e_L\}$, f_i is a feature recognized as MI task, d_i is the Euclidean distance of f_i with respect to the mean vector of its corresponding set, and N is the total number of feature vectors in the subset. For this case, the relative power in the band mu and beta is used as biomarker. In Equation 3-7, the biomarker increases for MI. In this study, the electrodes closer to C_z play an important role during lower MI activity. For this reason, CP_1, CP_2, and C_Z, were used to calculate the biomarker by:

$$B_i = \left(\left(\frac{\mu_{MI} + \beta_{MI}}{P_{MI}}\right) - \left(\frac{\mu_b + \beta_b}{P_b}\right)\right)_i = \sum_{e=1}^{L}\left(\left(\frac{\mu_{MI_e} + \beta_{MI_e}}{P_{MI_e}}\right) - \left(\frac{\mu_{b_e} + \beta_{b_e}}{P_{b_e}}\right)\right), \tag{3-7}$$

where e represents each specific EEG location, L is the number of total specific electrodes that f_i is computed, μ is the power in mu band, β is the power in beta band, P is the total power, b corresponds to baseline, MI corresponds to the MI. Subsequently, an interpolation-based strategy was used to establish the Eucladian distances and convert them into a percentage. The lower the Eucladian distance to the MI clusters, the higher the percentage rate, with a maximum value of 100% and a minimum value of 40%. This is presented to the individual as visual neurofeedback in green color. On the other hand, when the subject does not perform MI, a value of 0% is presented in red. A summary of the proposed BCI can be seen in Figure **3-13**. It should be noted that for the calibration phase the data from the baseline and MI phase with neurofeedback calculated by the protocol depicted in Figure 3.5(c) are used.

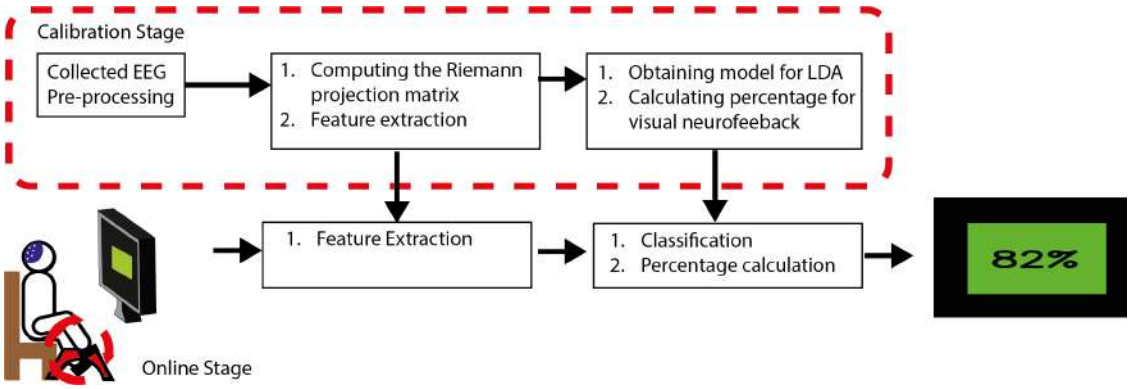

Figure 3-13: Block diagram of the proposed BCI.

4 Results and Discussion

4.1 Data Analysis

First, before performing the classification tasks, it is possible to make a Time-Frequency (TF) representation of the cortical rhythms during the pedaling tasks [108]. For this, the Morlet wavelet transform was used on the Cz channel between the 8 to 30 Hz frequency bands, after a CAR filter. Additionally, Equation 2-1 was used to calculate the ERD percentage in each case. Figure **4-1** shows the ERD for the active pedaling tasks per subject, whereas Figures **4-2** and **4-3** show the ERD for the MI tasks after performing passive pedaling for each of the 3 MMEB speeds.

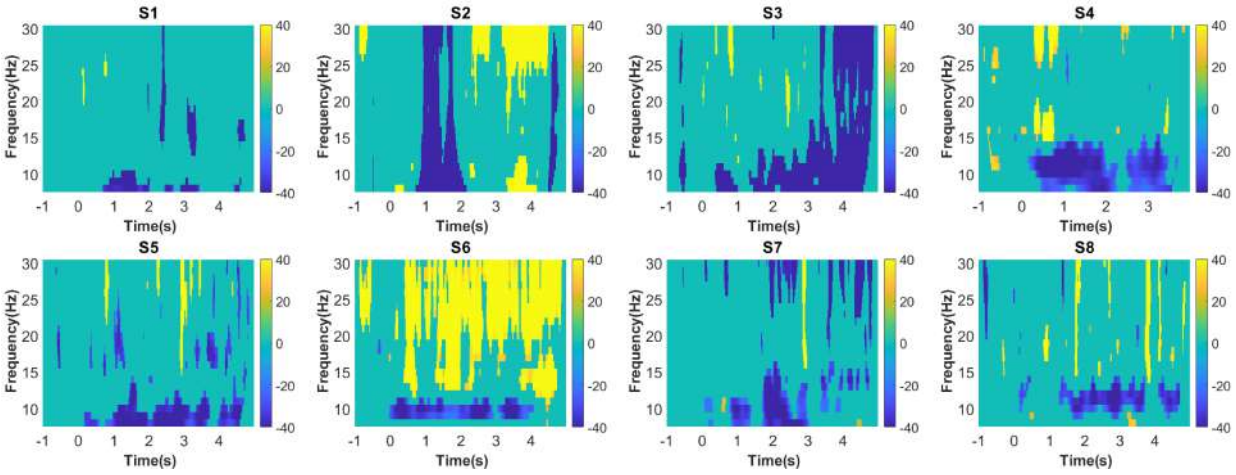

Figure 4-1: Quantification of ERD cortical changes for all subject while performing active pedaling tasks, where the x-axis corresponds to time, the y-axis is the frequency domain, and the z-axis corresponds to the ERD in channel C_Z.

From Figure **4-1** it can be argued that there is an evident behavior of power decrease in the Mu band, for all subjects, which is in accordance with the literature in previously presented studies [20, 108]. For instance, these findings were similar to the results of Pfurtscheller *et al.*[119], who determined that the ERD behavior of lower limb movements are similar between frequency bands between 8 and 30 Hz and time segments after the trigger for approximately 1 s. On the other hand, this phenomenon also arises when the subject performs MI, as presented in Figures **4-2** and **4-3**, considering that these last two figures also indicate a power increase (synchronization) in the beta band at the beginning and end of the MI cycle,

which are similar to the results reported by Storzer *et al.* between the frequency ranges of 28 to 35 Hz [108].

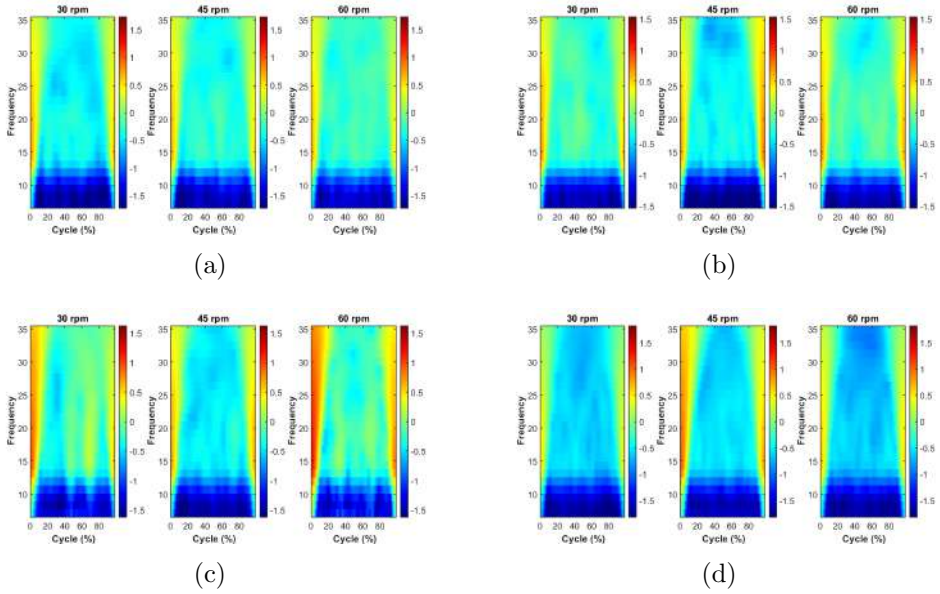

Figure 4-2: Quantification of ERD cortical changes for all subject while performing MI pedaling tasks after passive pedaling for the three velocities, where the x-axis corresponds to time, the y-axis is the frequency domain, and the z-axis corresponds to the ERD in the channel C_Z for the subjects S1-S4 ((a)-(d)).

4.2 Classification

4.2.1 PSD-ELM

The results of the ELM evaluated for different number of hidden neurons is shown in Figure **4-4**, which shows the variation of ACC and FPR parameters by changing the number of hidden neurons in the network structure. From the figure, it can be noted that a higher number of neurons in the hidden layer does not mean a better performance. Thus, a configuration with 20 neurons in the hidden layer was selected for additional post-processing. This configuration initially achieved an ACC of 0.706±0.12, and a FPR of 0.29±0.11.

Four frequency bands were evaluated, and the results are shown in Fig **4-5**. Figure 4.5(a) represents the ACC results for each frequency band, where the best performance was achieved with the FB2 with an ACC of 0.73±0.12, and the lowest behavior was obtained with the FB3 with an ACC of 0.67±0.15. It is worth nothing that for this case, Subject 5 obtained the highest performance with an ACC of 0.89 using the FB2.

On the other hand, Figure 4.5(b) represents the average FPR results for all subjects, where the lowest FPR value was achieved for Subject 5 with the FB1 of approximately 0.07. In

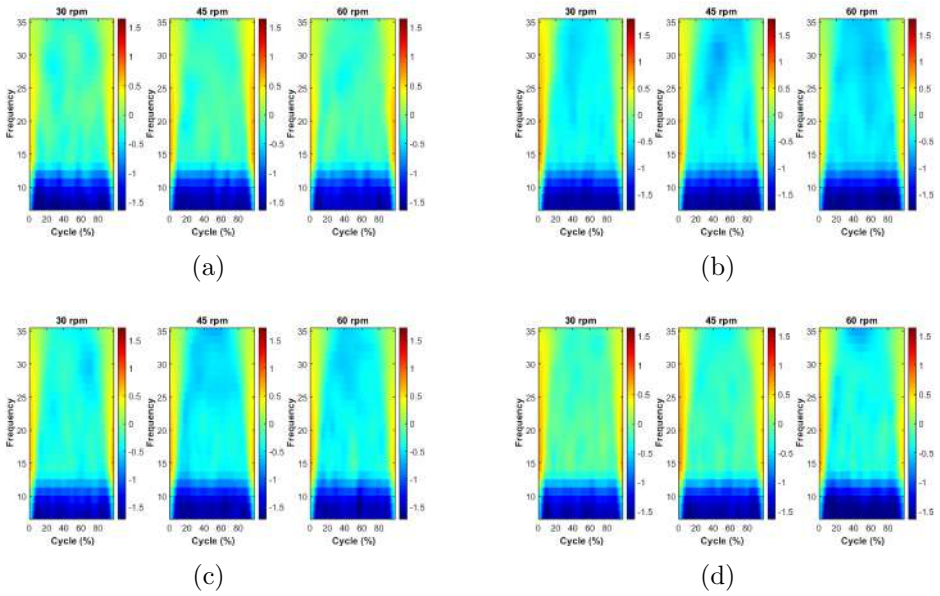

Figure 4-3: Quantification of ERD cortical changes for all subject while performing MI pedaling tasks after passive pedaling for the three velocities, where the x-axis corresponds to time, the y-axis is the frequency domain, and the z-axis corresponds to the ERD in the channel C_Z for the subjects S5-S8 ((a)-(d)).

addition, The lowest average FPR value obtained was with the FB1 of 0.26±0.13, while the worst performance was obtained with 0.33±0.17 by implementing FB4. The FB2 configuration achieved an FPR of 0.28±0.14. It is worth mentioning that the best results mean an ACC close to 1 and an FPR close to 0.

The results indicated that the highest ACC was obtained with the FB2 configuration to indentify pedaling tasks through EEG signals, whereas the best FPR performance was obtained with FB1. These two frequency bands are according to the literature, where suggestions are that the most discriminating information for movement execution with the lower limbs should be obtained in the frequency ranges of 3-7 Hz (delta band) and 7-13 Hz (mu band) [115, 18, 110]. This study provides an extension in the literature, where frequency analysis across filter banks has not been fully explored, and the most reported studies for pedaling tasks were acquired between 7-30 Hz or 3-30 Hz (FB3 and FB4, respectively) [115, 13]. This suggests that selective filtering in frequency bands may improve the performance of BCIs for movement detection with EEG, as reported for upper limb motor tasks [32], but not necessarily for lower limb pedaling tasks.

Compared to the previous literature, this study obtained a mean ACC of 0.73 and a maximum of 0.89 using ELM as a classifier, and PSD as feature, which surpasses techniques for lower limb recognition, such as that of Ugarte *et al.*, where an ACC of 0.61 was obtained [120]. In addition, Liu *et al.* proposed a study for the identification of ankle movements, obtaining an ACC higher than 0.81 [121]. However, the latter is not fully comparable be-

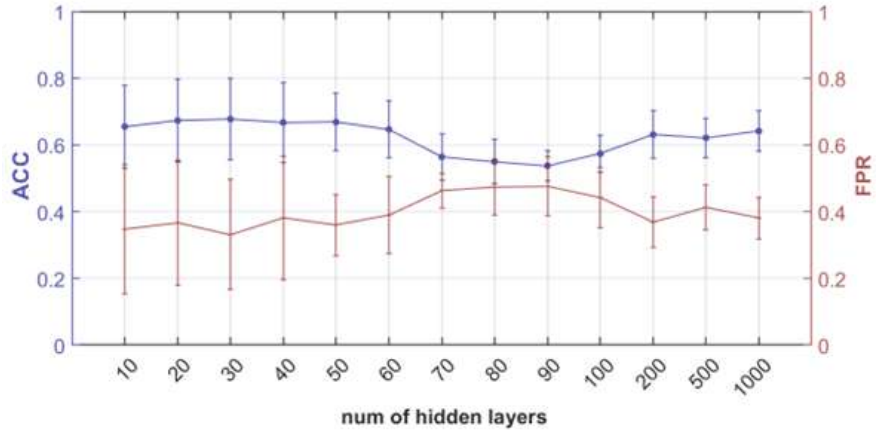

Figure 4-4: ACC and FPR for the different configurations of number of hidden neurons.

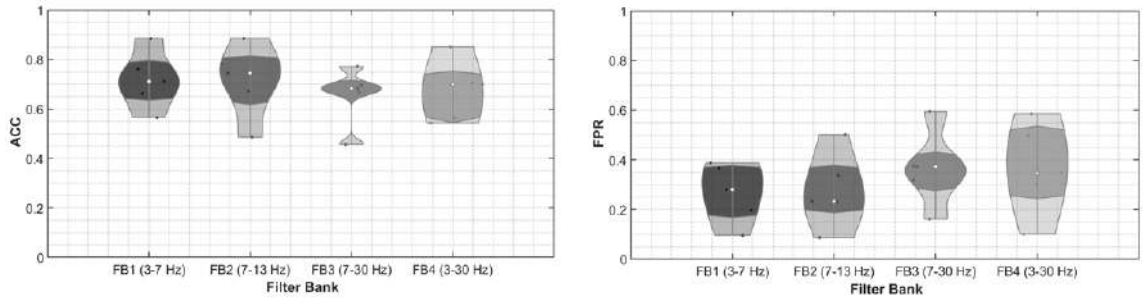

(a) (b)

Figure 4-5: Average classification metrics for ELM for the different frequency band configurations for all subjects. Considering (A) ACC; (B) FPR.

cause the movements are different. Studies related to pedaling MI tasks have reported ACC of approximately 0.85 or FPR of approximately 0.18 by using Riemannian computational strategies [13]. However, this technique has not been explored to active movement. It is worth commenting that these strategies based on MI may be not useful in some cases whether the idea is implement more personalized systems, considering that their functioning is based on on/off methodology. Furthermore, movements related to pedaling have not been explored extensively using different spectral analyses [115, 13], whereas the use of ELM and PSD for the classification of lower limb tasks is not well documented in the literature.

4.2.2 CSP-based Methods and LDA

Fig **4-6** represents the results for ACC and FPR according to the different TWs and the number of patterns for CSP. It is possible to see that the best performance is achieved with 4 patterns. On the contrary, for the TW normally used in the literature in motor tasks (TW1) it is possible to observe an ACC of 0.73±0.17 and FPR of 0.26±0.17. Meanwhile,

the best result was obtained with TW7 and 4 patterns, representing an average accuracy of 0.79±0.13 and FPR of 0.20±0.14.

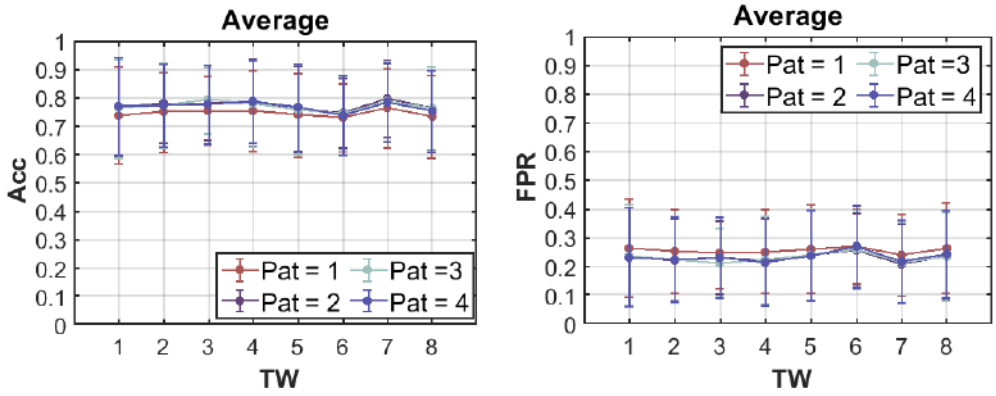

(a) ACC (b) FPR

Figure 4-6: Average classification (a)ACC; (b) FPR for CSP for the different TWs and number of patterns for all subjects.

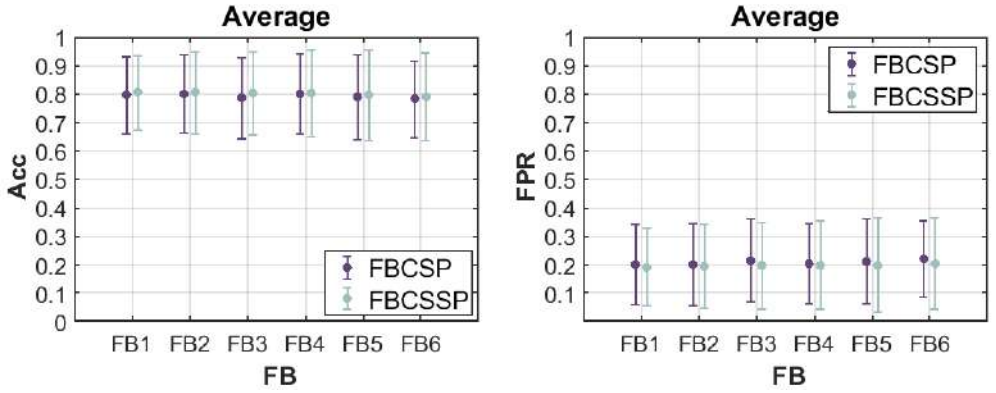

(a) ACC (b) FPR

Figure 4-7: Average performance metrics for FBCSP and FBCSSP for the different Filter Bank cosidering all subjects by using as metrics: (a) ACC; (b) FPR.

Figure **4-7** shows a better performance with the FBCSSP concerning the FBCSP method, where the FB2 was the best with an ACC of approximately 0.80±0.12 and 0.80±0.14 for the FBCSP and FBCSSP, respectively. On the other hand, the minimum FPR was 0.19±0.14 and 0.19±0.14, for the FBCSP and FBCSSP, respectively.

In order to distinguish between active pedaling tasks and resting tasks by using EEG, this section presents a comparative study of various combinations of configurations for CSP, FBCSP, and FBCSSP methods based on the variation of number of patterns in spatial filtering, TW in temporal segmentation, and filter banks during frequency filtering. The

best results are obtained with a number of 4 patterns, a non-overlapping 2 filter bank (FB2), and a TW between 1.5 and 2.5 s (TW7), according to the evaluation metrics.
Furthermore, the lower performance was obtained with the CSP method using the TW6 (between 1 and 2 s) and 2 patterns. On the other hand, for the frequency filtering, the lower performance was obtained using a bank of 4 filters without overlap. These results provide a contribution to the challenge of scientific community for the recognition of lower limb motor tasks, considering the fact that the variations of spatial and frequency filtering together with TW segmentation for pedaling execution detection has not been deepened in the literature, making it difficult to compare among decoding techniques. Related studies have proposed this type of analysis, where Blanco *et al.*[32] reported the use of CSP, FBCSP and FBCSSP for the discrimination of upper-limb tasks, in which an approximate average ACC of 74% was obtained, using 3 filter banks with no overlap and a window between the segment of 1.5 and 3 s.
Liu *et al.*[121] proposed a study for the identification of ankle planter flexion MI using 1.5 s time windows, a filter between 4-48 Hz, and 32 EEG channels, obtaining ACC about 81%. Additionally, similar studies have been proposed for the decoding of pedaling MI, where Ugarte *et al.*[120] reported an ACC of 61% using a frequency range between 6-30 Hz and 30 EEG channels; Romero *et al.*[13] reported FPR of 0.18 using 8 EEG channels and a filter between 0.1-30 Hz; Rodriguez-Ugarte *et al.*[122] reported ACC of 0.85 using a 4 s time window; and Gurve *et al.*[123] reported ACC of 0.96 using a filter between 0.1-30 and 19 EEG channels. Nevertheless, these studies do not propose to delve into the different variations of temporal segmentation, spectral and spatial filtering, can increase the performance of standard methods, as evidenced in this study.

4.3 Classification of MI

For MI classification using Riemannian geometry, was initially validated to identify baseline vs. MI for all subjects, which has reported ACC near 98% in previous studies [21]. To perform this procedure, the data were segmented using k-fold cross validation, where 70% of the dataset was used for training, 15% for validation and 15% for evaluation. Here, the projection matrix that generated the highest ACC was used on the evaluation data for model generalization. The confusion matrices using this methodology for each test subject on the evaluation data for all subjects are presented in Figure **4-8**.
Considering the confusion matrices, ACC is computed for each subject, which are presented in Table **4-1**. These results are in line with expectations, considering that previous studies have reported MI combined with passive pedaling, obtaining ACC around 0.98 [21].
Subsequently, the methodology of Figure **3-9** is used to decode the MI task after passive pedaling at the three different speeds. As before, the dataset was validated using k-fold cross validation with $k = 5$ to obtain the best Riemannian distance projection matrices in addition to the LDA classifier. Considering that it is a multi-class task, the one .vs one

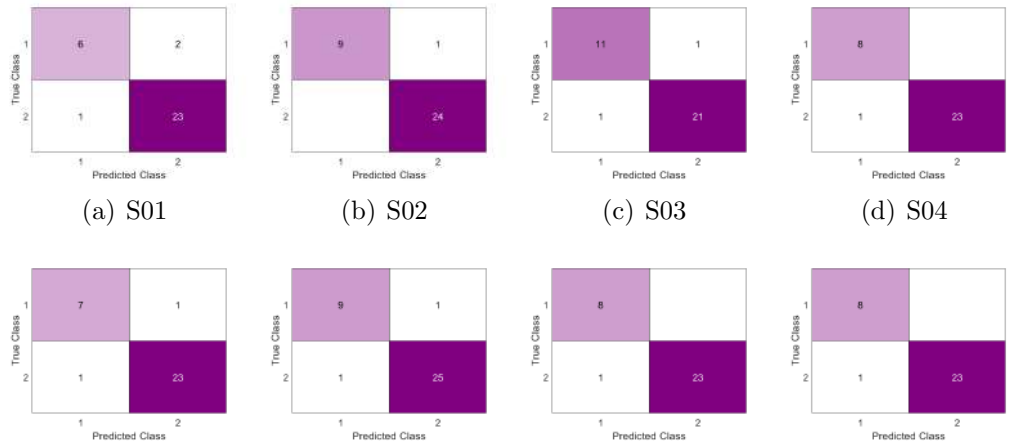

(a) S01 (b) S02 (c) S03 (d) S04

(e) S05 (f) S06 (g) S07 (h) S08

Figure 4-8: Confusion matrices for the 8 Subjects using Riemannian geometry-based Feature Extraction, and LDA to classify Baseline (Class 1) and MI(Class 2).

Table 4-1: ACC for classification of MI tasks by using Riemannian geometry and LDA

Subject	**S01**	**S02**	**S03**	**S04**	**S05**	**S06**	**S07**	**S08**	**Average**
ACC	0.9062	0.9706	0.9412	0.9687	0.9375	0.9444	0.9687	0.9687	0.9507

strategy was used so that different ACCs were obtained in the identification of binary tasks. The ACC results are shown in Figure **4-9** for each test subject.

The results in Figure 4.9(i) allow verifying that the methodology to identify pedaling MI tasks at different speeds were the most discriminant class correspondent to the Baseline, which is in accordance with the results presented in Table **4-1**. It was also possible to determine that the most discriminant class of the 3 MIs corresponds to the 60 rpm, with respect to the 30 rpm, with an ACC of 0.78, whereas the other two speeds obtained average performance close to 0.68.

Some related studies have been focused on evaluating EEG at different walking speeds, either using exoskeletons or treadmills. For the case of exoskeletons, Quiles *et al.* have conducted a methodology related to intentionality to change the velocities of an exoskeleton in a pseudo-online phase [124]. In this study, non-linear extraction techniques were used where was possible to obtain an ACC close to 0.68. On the other hand, Wu *et al.* used strategies to classify SSVEP at different speeds of a treadmill, and evaluate through an ANN whether it was possible to classify the speeds [125]. Through the aforementioned methodology, they got an ACC of 0.77 to discriminate higher speeds from lower speeds.

In this study, a strategy for classifying pedaling MI tasks at different speeds was presented for the first time. To address this, passive pedaling at different speeds was performed by a passive-assistive MMEB. The results allowed determining that the most discriminative task corresponds to differentiating the highest available speed (60 rpm) with respect to the lowest

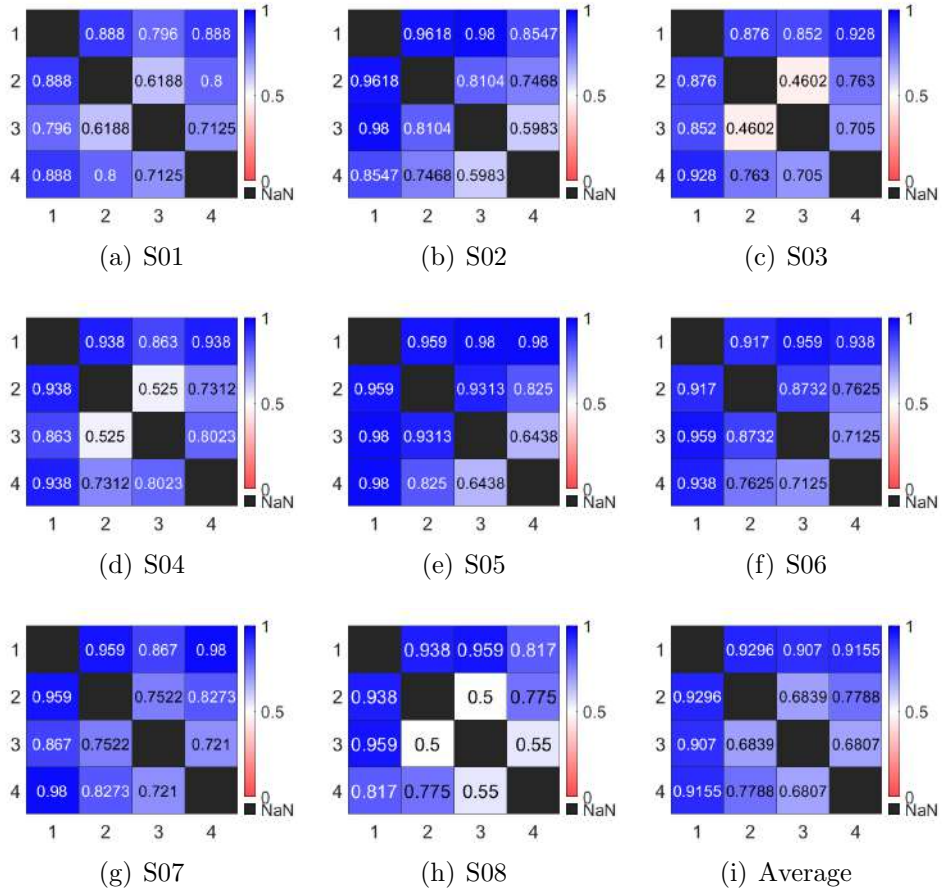

(a) S01 (b) S02 (c) S03

(d) S04 (e) S05 (f) S06

(g) S07 (h) S08 (i) Average

Figure 4-9: Confusion matrices for the 8 Subjects using Riemannian geometry-based Feature Extraction, and LDA to classify the MI after passive pedaling with three different velocities (Class 1 = Baseline; Class 2= MI after 30 rpm; Class 3= MI after 45 rpm; Class 4= MI after 60 rpm).

speed (30 rpm). This is somewhat related to the results of Wu *et al.* where for the case of walking it was possible to identify SSVEP responses during walking at high speeds compared to low speeds in a more feasible way using ANN [125]. On the other hand, discrimination between the other speeds (30-45rpm and 45-60 rpm) generated adequate ACCs considering the binary classification problem and the randomized probability (50%).

4.4 Kinematics reconstruction of continuous active pedaling tasks with UKF

An hiperparameter to be considerend when UKF is used corresponds to the system order [91]. For this reason, Figure **4-11** presents the results of the variation by using the PCC as metric. It is possible to highlight that for the angular velocity variable of the knee, the most adequate order of the system corresponds to order 9 with a $PCC = 0.20 \pm 0.04$; whereas, for the values of the ankle velocities, the best PCC is obtained with order 3 for an average value of 0.212 ± 0.04 in x-axis and 0.22 ± 0.05 for y-axis with order 9. Therefore, all UKFs were set in the order of 9.

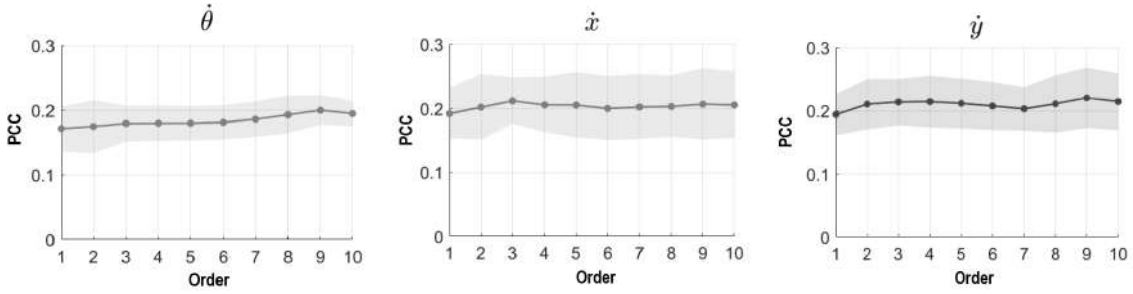

(a) (b) (c)

Figure 4-10: PCC values obtained by varying the UKF order for the kinematic variables: (a) knee angular velocity (θ), (b) ankle velocity in x-axis ($\dot{x}$), and y-axis ($\dot{y}$).

Figure 4.11(a) represents the obtained PCC values for angular velocity ($\dot{\theta}$) prediction, where it is possible to observe a maximum PCC of approximately 0.24 with five lags and a mean of 0.21±0.02. Figure 4.11(b) represents the obtained PCC values for linear velocity in the x-axis ($\dot{x}$) prediction, with a maximum value of 0.30 with two lags, and an average of 0.20±0.04. Figure 4.11(c) presents the obtained PCC values for linear velocity in the y-axis ($\dot{y}$), where a maximum value of 0.33 was obtained by using two lags, and an average of 0.21±0.03.

Finally, considering the most appropriate order of the system, the reconstructed kinematic information for the best subject (S06) is presented in Figure **4-12**.

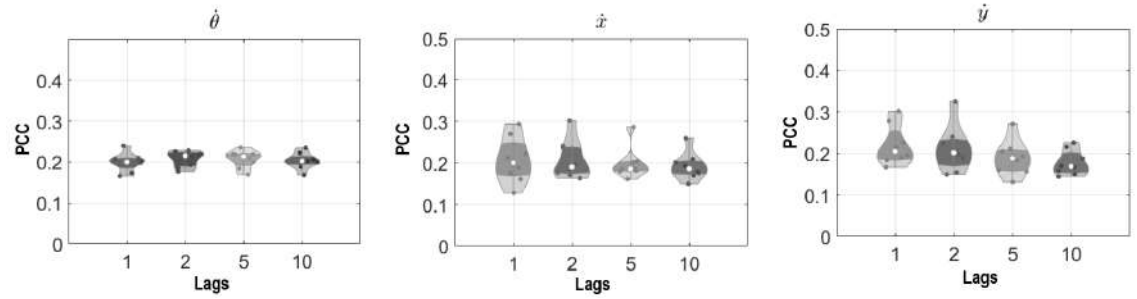

(a) (b) (c)

Figure 4-11: Average PCC for the prediction of lower limb joint from EEG signals for all subjects for each evaluated lag.

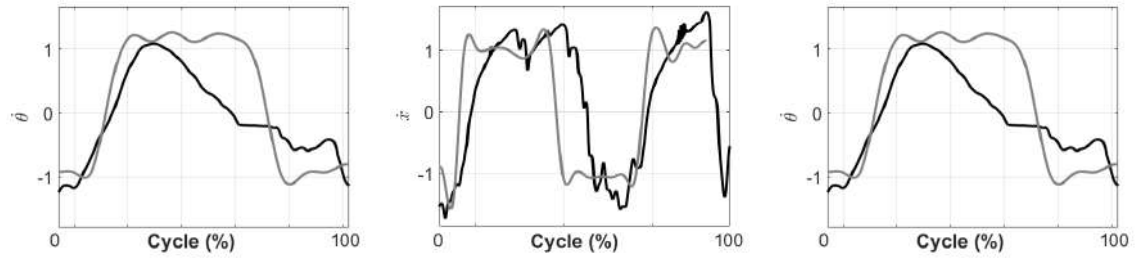

(a) (b) (c)

Figure 4-12: Measured and reconstructed lower limb joint parameters during a cycle of pedaling task from EEG signals for the Subject S06. Light gray represents the true measurement, and black the estimated parameter.

4.5 Decoding trajectories of continuous active pedaling tasks with DL approaches

The analyses of this study were performed for each of the subjects considering the inter-subject variability, the lags of interest, and the decoders presented for each of the three kinematic parameters (θ, x, and y). The reconstructionof of PCC during the pedaling tasks is given in Table **4-2** for each EEG TW, each ANN, for each subject.

In this table it is possible to see that the decoders improve as the TW is increased, which is the expected result. This average behavior can be seen more clearly in Figure **4-13**. On the one hand, it can be observed that the variable that obtained the best decoding corresponded to the knee joint angle, which is in agreement with the previous results. On the other hand, the LSTM-based decoder obtained higher average PCC values compared to the CNN for the decoding of the θ angle, however, on average for the position of the ankle in the x and y axes, the highest PCC values were obtained with the CNN. The best PCC values obtained

Table 4-2: Analysis per subject of neural decoders (CNN and LSTM) with TW of 50, 100, 150, 200, 250m and 350 ms.

Lag	ANN	Variable	Subject								
			S01	**S02**	**S03**	**S04**	**S05**	**S06**	**S07**	**S08**	**Average**
50 ms	**CNN**	**Theta**	**0.3713**	0.3894	**0.3643**	0.4054	0.5255	0.4280	0.4566	0.4282	**0.4211**
		X	0.3442	0.4032	0.3578	**0.4150**	0.5222	0.4341	0.4456	0.4063	0.4160
		Y	0.3624	**0.4295**	0.3553	0.4018	0.4804	0.3986	0.4343	0.3942	0.4071
	LSTM	**Theta**	0.2577	0.3600	0.3331	0.3827	**0.6032**	**0.4586**	**0.4621**	**0.4553**	0.4141
		X	0.2391	0.3600	0.3207	0.3751	0.5942	0.4330	0.4436	0.4199	0.3982
		Y	0.2832	0.3828	0.2480	0.3378	0.4386	0.3634	0.3928	0.3402	0.3484
100 ms	**CNN**	**Theta**	0.3462	0.3691	0.3877	0.4088	0.5536	0.4606	0.4626	0.4386	0.4284
		X	0.3494	0.3938	0.3799	0.4357	0.5518	0.4534	0.4589	0.4251	0.4310
		Y	0.3686	0.4157	**0.4023**	0.3816	0.4883	0.4720	0.4686	0.4086	0.4257
	LSTM	**Theta**	**0.4111**	0.3932	0.3890	**0.4799**	**0.6406**	**0.5149**	**0.5127**	**0.5430**	**0.4855**
		X	0.3666	0.3707	0.3687	0.4700	0.6219	0.4686	0.4786	0.5219	0.4584
		Y	0.3443	**0.4225**	0.3466	0.3589	0.5105	0.4529	0.4524	0.4262	0.4143
150 ms	**CNN**	**Theta**	0.3646	0.4130	0.4185	0.4473	0.5705	0.5224	0.4723	0.5119	0.4651
		X	0.3723	0.3798	0.4314	0.4363	0.5767	0.5104	0.4543	0.4997	0.4576
		Y	**0.4113**	0.4184	0.4141	0.4362	0.5365	0.5023	0.4519	0.4734	0.4555
	LSTM	**Theta**	0.3987	0.4184	**0.4546**	**0.4670**	**0.6958**	**0.5482**	**0.5475**	**0.5633**	**0.5117**
		X	0.3541	**0.4211**	0.4498	0.4623	0.6885	0.5113	0.5197	0.5300	0.4921
		Y	0.4090	0.3900	0.3861	0.3816	0.5189	0.4798	0.4844	0.4915	0.4427
200 ms	**CNN**	**Theta**	0.4518	0.4534	0.4835	0.5043	0.6883	0.5210	0.5798	0.6133	0.5369
		X	0.4487	**0.4657**	0.4750	0.5046	0.6710	0.5187	0.5815	0.6006	0.5332
		Y	**0.4612**	0.4392	0.4820	0.4973	0.6152	0.5054	0.5497	0.6006	0.5188
	LSTM	**Theta**	0.4039	0.4314	**0.5691**	**0.5197**	**0.7364**	**0.6240**	**0.5823**	**0.6422**	**0.5636**
		X	0.3886	0.4514	0.5430	0.4918	0.7131	0.5869	0.5697	0.6106	0.5444
		Y	0.3824	0.4211	0.4620	0.4024	0.5526	0.5202	0.4903	0.4970	0.4660
250 ms	**CNN**	**Theta**	0.5059	0.4784	0.5252	0.5895	0.6856	0.5854	0.6239	0.6630	0.5821
		X	0.5115	0.5057	0.5374	**0.6158**	0.6727	0.5836	**0.6355**	0.6359	0.5873
		Y	**0.5261**	0.4927	0.4911	0.5408	0.6206	0.5524	0.6004	0.6158	0.5550
	LSTM	**Theta**	0.4596	0.4852	**0.5455**	0.5827	**0.8273**	**0.6360**	0.6057	**0.6974**	**0.6049**
		X	0.4389	**0.5103**	0.5154	0.5608	0.7888	0.5792	0.5791	0.6640	0.5796
		Y	0.4043	0.3903	0.4513	0.4789	0.6374	0.5653	0.5129	0.5233	0.4955
300 ms	**CNN**	**Theta**	**0.5208**	0.4612	0.5635	**0.6114**	0.7224	0.6506	**0.6605**	0.6749	0.6082
		X	0.5139	0.4627	0.5589	0.6071	0.7032	0.6570	0.6560	0.6656	0.6031
		Y	0.5382	**0.5317**	0.5694	0.5965	0.6443	0.6345	0.6439	0.6431	0.6002
	LSTM	**Theta**	0.4638	0.4524	**0.5817**	0.5775	**0.8024**	**0.6693**	0.6601	**0.7133**	**0.6150**
		X	0.4065	0.4709	0.5607	0.5298	0.7657	0.6088	0.6146	0.6578	0.5769
		Y	0.4406	0.4209	0.4470	0.5079	0.6524	0.6005	0.5861	0.5921	0.5309

were 0.6150 for θ with LSTM, and 0.6031 and 0.6002 for the x and y direction of the ankle, respectively, using a TW of 300 ms.

On average, the decodings using a lag of 300 ms obtained average PCCs of 0.6150, 0.5769, and 0.5309 for θ, x, and y, respectively with LSTM; whereas using CNN obtained PCCs of 0.6082, 0.6031, and 0.6002 for θ, x, and y, respectively. Additionally, in Table **4-2** it can be observed that the variable θ obtained best PCCs using LSTM in comparison to the CNN. For instance, it can be observed for subjects S03-S08 using TWs of 100 and 150 ms. The highest performance was achieved by subject S05 for a 250 ms window, with a PCC of 0.8273, using the LSTM to decode the θ parameter. On the other hand, the lowest performance was obtained using the shortest time window by subjects S01 and S03 and the LSTM decoder, with PCC values near 0.30.

It is worth noting that this is the first time that a continuous decoding approach is made

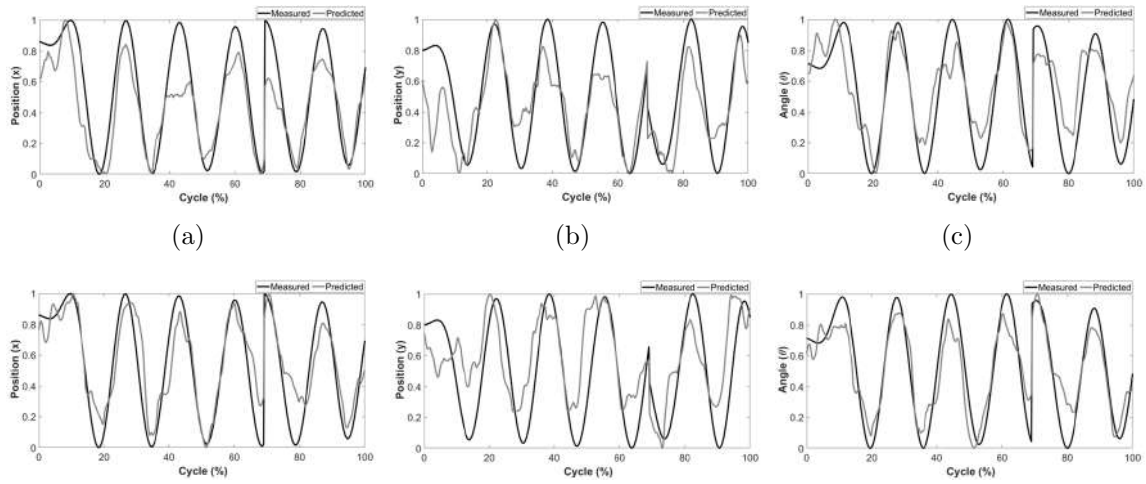

Figure 4-13: Kinematic trajectory decoding for θ, x and y-directions for subject S05 using CNN decoder in (a)–(c), and LSTM decoder in (d)–(f). A 300 ms lag window was taken. Light gray represents the true measurement, and black the estimated parameter.

in pedaling tasks, therefore, there is no literature reported towards these approaches [110]. Nevertheless, it is necessary to compare the results obtained in this study with those in the literature. Hosseini *et al.* implemented a regressor based on Gaussian processing to decode random hand trajectory tasks, where they obtained PCC close to 0.37 [84]. Under similar motions, Jain *et al.* obtained PCC about 0.63 for upper limb movement prediction by using ANN [83]. Additionally, for lower limb tasks the focus has been put on tasks such as walking, where Pressaco *et al.* were the pioneers to report a Wiener Filter based decoder to decode lower limb parameters during walking, obtaining PCC of about 0.68 [126]. Years later, Luu *et al.* started using nonlinear classifiers for estimating kinematics during gait, obtaining PCCs close to 0.75 with Kalman filters (KF) [127]. Subsequently, ANN for decoding was used to decode movements of gait joints, such as hip, knee and ankle, obtaining PCC values between 0.55 and 0.65 [38, 37, 128]. Some of this works are presented and compared in Table **4-3**.

4.6 Visual neurofeedback-based BCI

To evaluate the use of BCI in real time, it was first necessary to perform training with the data from the first two phases of the protocol 3.5(c). Subsequently, 1 s windows with 0.5 overlapping were calculated for both baseline and MI. A strategy based on k-fold cross-validation was performed, where 150 s were divided into 120 s to train the models and 30 s to evaluate them. The first 120 s were divided into 12 segments of 10 s, where the data were

Table 4-3: Summary of the proposed method and others reported for lower limb movement prediction.

Ref	Task	Method	PCC
[128]	Gait	CLDA	0.53
[38]	Gait	LSTM	0.32
[18]	Gait	UKF	0.47
[126]	Gait	LWF	0.56
[127]	Gait	UKF	0.40
Proposed	**pedaling**	**UKF**	**0.33**
Proposed	**pedaling**	**CNN/LSTM**	**0.60**

Note: CLDA: Close-Loop Decoder Adaptation Algorithm
LWF: Linear Wiener Filter

randomized and validated using the extraction techniques based on Riemannian geometry. The process was repeated for a value of $k = 10$, where at the end the Riemannian matrix that provided the maximum ACC in validation set was chosen to project into Tangent space. Subsequently, all data were used to re-train the LDA model in the real-time implementation. The ACC confusion matrices for the cross-validation and generalized model are shown in Figure 4.15(a) and 4.15(b), respectively. From these confusion matrices, the ACC values are 0.6957 and 0.7978 for the ACC test and for the ACC of the re-trained model, respectively.
Subsequently, the system was evaluated in real time as shown in Figure **4-14**. Here the subject is instructed to perform MI which is quantified to a percentage through the Euclidean distance calculated in section 3.2.3. The phenomenon is that when the neuromodulation is higher (the Euclidean distance is closer to the MI cluster) the green box has a score closer to 100. On the contrary, if the MI task is not performed correctly, the system indicates a 0% (red color). The ACC in real time was of approximately 0.80 as is presented in the Figure 4.15(c).
The average percentages of neuromodulation for each minute of the evaluation phase is presented in Figure **4-16**. Additionally, the brain behavior of the biomarker calculated in section 3.2.3 for each minute is shown in Figure **4-17**.
It is possible to observe the variation of percentages in Figure **4-16**, where it is interesting to analyze that during the first minute the subject had a low percentage of neuromodulation, which subsequently rose and was attempted to be maintained until the end. This allows determining the learning that the person had during the performance of the task. On the other hand, the biomarker showed a similar behavior during each minute for the Cz channel, which is important to highlight, considering that this is the most influential eletrode during lower limb MI tasks [119].

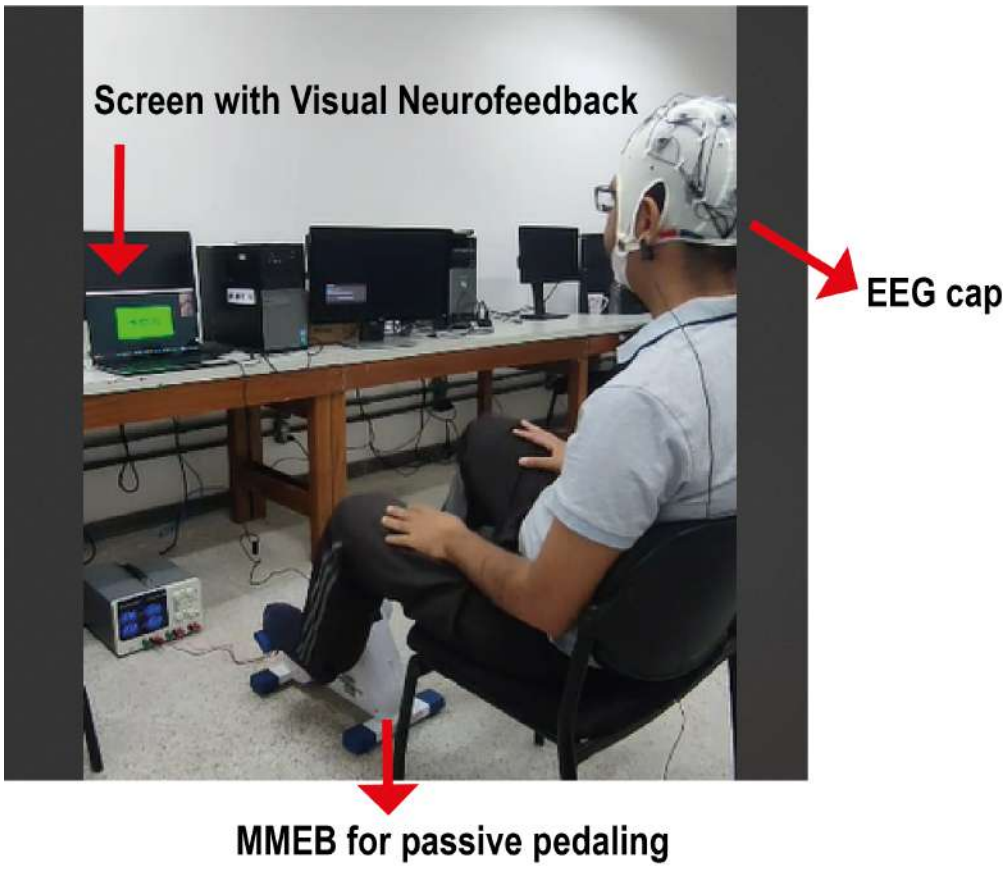

Figure 4-14: MMEB-based BCI with MI and visual neurofeedback in real-time.

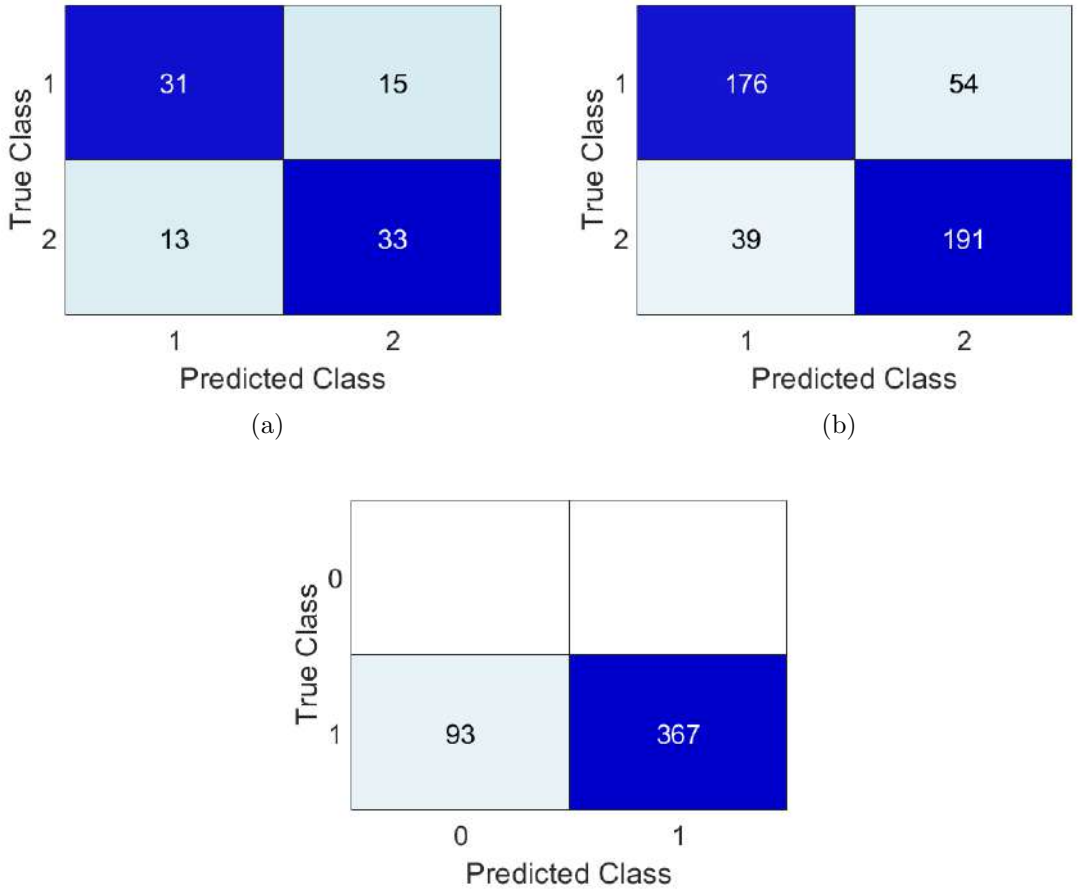

Figure 4-15: Confusion matrices obtained in the calibration phase for the visual neurofeedback-based BCI, where (a) confusion matrix for test set; (b) confusion matrix obtained from the general model; (c) confusion matrix from online phase.

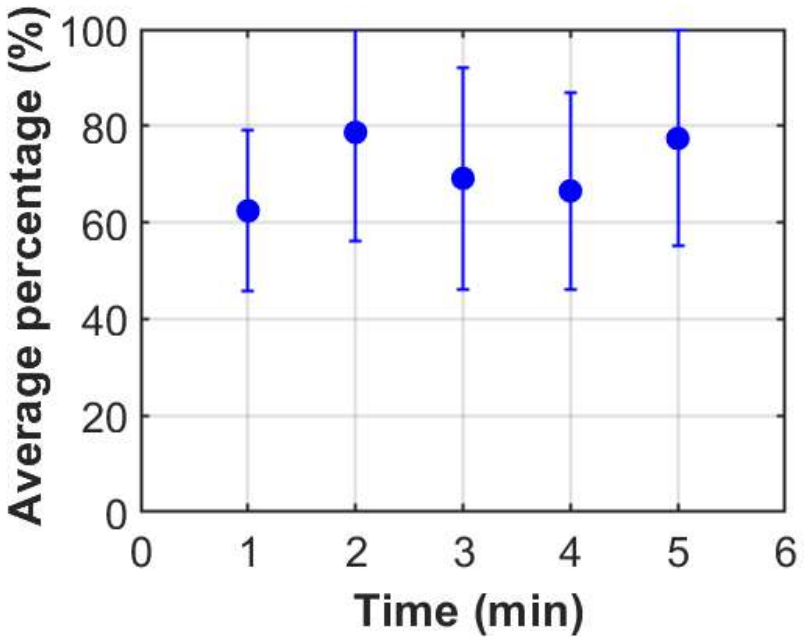

Figure 4-16: Performance of the participant using the BCI to control the percentage presented in the screen by using MI.

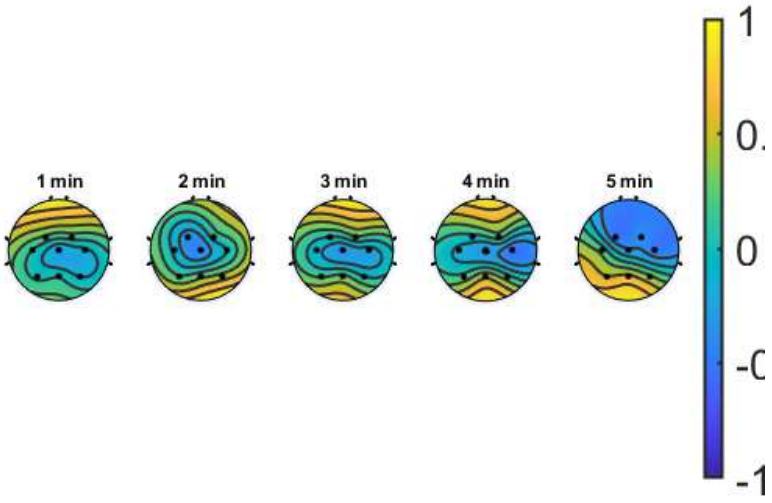

Figure 4-17: Representation of the ratio (mu+beta)/total, of the test subject using the visual neurofeeback-based BCI calculated after each minute of the online phase.

5 Discussion

5.1 General Discussion

In this study it was possible to determine that there is a lack of literature regarding the implementation of BCIs based on pedaling tasks, considering that some studies have reported the use of brain signals for the on/off control of MMEB at constant speeds [21, 13, 20]. This has been of significant progress, however, this may limit rehabilitation and HMI. In view of this, this dissertation aimed to extend the knowledge acquired for the analysis of pedaling tasks through signal processing in different approaches towards the design and practical application of real-time BCI systems for rehabilitation.

To address this, three protocols based on pedaling tasks and the use of an MMEB were proposed: one based on active pedaling, one based on passive pedaling and MI, and one based on visual neurofeedback during passive pedaling and MI. Initially, some guiding methodologies from the literature were performed to analyze the acquired data, where it was possible to demonstrate the ERD that is highly reported in the literature on the Cz electrode for the performance of lower limb tasks [119, 108].

Subsequently, different classification algorithms were performed. First, PSD features were used together with ELM to classify active pedaling, where it was possible to obtain ACC values close to 0.73 with a maximum of 0.89, which exceeds some results reported in the literature [120, 122] and shows viability in the classification. However, it is necessary to deepen the optimization of the ANN hyperparameters. In contrast, a study that imparted CSP-based methods was applied. This study showed that spatial, spectral and temporal configurations have a significant effect on the performance of a BCI based on the CSP, FBCSP, and FBCSSP methods for decoding pedal motor execution tasks, considering ACC and FPR. The best results were obtained with four patterns for the CSP, a 2-filter bank without overlap (8-19 Hz, 19-30 Hz), and a TW between 1.5 and 2.5 s after indication. A maximum ACC of 0.80 and minimum FPR of 0.19 were obtained, for all subjects, which indicates that the CSP-based algorithms are adequate for the discrimination of pedaling tasks. Furthermore, the worst configuration obtained was a bank with four filters without overlap, a TW between 1 and 2 s, and two CSP patterns. Interestingly, in the literature, this joint temporal, spectral, and spatial domain feasibility analysis has not been fully explored with lower limbs during active pedaling tasks, but only for upper limb tasks.

Another variation used in this dissertation corresponded to the use of Riemannian geometry to decode pedaling MI tasks after passive pedaling. This has been addressed previously,

where ACCs of approximately 0.97 have been reported [115, 123, 13]. However, in our study an ACC of 0.95 was obtained, which is not a significant difference. Nevertheless, for the first time, this algorithm was used in a multiclass variation to discriminate MI tasks at different speeds, obtaining ACCs close to 0.78 and 0.69. The results indicate that the most discriminating speed corresponds to the maximum speed (60 rpm), which is consistent with the study performed in [125]. In a previous study, the authors concluded that higher walking speeds are easier to discriminate using EEG than lower speeds. Likewise, the implemented methodology of feature extraction using Riemannian geometry proved to be feasible for identifying MI under different conditions, which is an advance and can be applied to control MMEBs at different speeds, allowing for a more personalized rehabilitation therapy.

In recent years, some authors have expressed in the literature to leave aside the discrete decoding of mental tasks for the design of BCIs and opt for the use of continuous decoding. Among these, Presaco *et al.*, Luu *et al.*, Nakagome *et al.*, and others have focused on decoding gait using brain signals in the delta band [126, 18, 37, 38]. Thus, the continuous decoding of pedaling tasks is not known in the literature. For this reason, this dissertation includes two new strategies that allow decoding knee and ankle kinematics using two different approaches. To reconstruct the velocities, the UKF was used with delta band information to obtain PCCs close to 0.33, whereas for trajectory decoding, ANN with CNN and LSTM structures were used to obtain PCCs close to 0.70. It was possible to identify reasonable metrics with TWs of 200 ms and 300 ms, which are acceptable in the implementation of BCIs. These results demonstrate the proposed methods show feasibility of decoding the kinematic parameters of the lower limb during pedaling, where the above findings leave the door open to implementation in the development of new BCIs based on continuous decoding for better accuracy in intentionality detection and control strategies, as done by Luu *et al.* in the interactive implementation of games based on EEG-controlled avatars [127].

Last but not least, the visual neurofeedback has been explored in recent years because it promotes brain regulation and thus reorganizes synaptic configurations [24]. Therefore, in this dissertation, a BCI proposal is proposed based on passive pedaling through MMEB and MI-controlled neurofeedback. The results showed that the algorithms based on Riemannian geometry allowed the classification of MI with an ACC of 0.80. This metric is a little low compared to the literature, however, in this study, a protocol was presented where the baseline was driven by passive pedaling tasks, while studies reported a static baseline [13, 123]. In addition, it was possible to quantify the percentage of task completion, where percentage stabilization was obtained after the first minute of the session. This allows determining the learning that the subject had during the passage of the session, which is an important factor in neuromodulation. It is worth commenting that this strategy can be used in the neurorehabilitation of people with disabilities because it promotes the use of passive pedaling driven by an MMEB while performing MI tasks, which motivates the performance of simultaneous mental tasks. Based on the literature, this may lead to the restoration of neural activity lost during the development of a neurological disease [25, 26].

5.2 Limitations

Some of the limitations during the execution of this dissertation correspond to the fact that the protocols were executed in healthy people, which limits the final objective as a rehabilitation device. Nevertheless, different strategies were addressed in the exploration of EEG signals and applications of BCI systems based on pedaling tasks, which can be oriented in future studies to post-stroke or SCI populations.

5.3 Clinical and potential applications

Passive assistance has been of importance in post-stroke rehabilitation therapies. Additionally, the use of MMEBs brings with it many advantages because it is a lower limb assistance and rehabilitation device that is portable, does not require a complex structure, relatively very low cost compared to exoskeletons, among others. Therefore, the techniques used here may be of interest to the neuroscientific community because it broadens the understanding of EEG signals during pedaling tasks, while different algorithms have potential use in more personalized neurorehabilitation therapies, such as the strategy for MI detection at different speeds or continuous decoding of movement.
Additionally, a BCI proposal based on MMEB for passive assistance and MI was presented, where the objective was to encourage the subject to neuromodulate brain signals, which may increase neuroplasticity in a person with neurological impairment. However, it should be noted that this type of approach is being simultaneously implemented in lower limb assistive devices, such as the Lokomat exoskeleton, for intervention towards the neurorehabilitation of people with SCI in the Edmond and Lily Safra International Institute of Neurosciences (see figure **5-1**), which demonstrates the importance of this study.

Figure 5-1: Proposal based on passive lower limb movement during the use of a BCI based on visual neurofeeback and MI and Lokomat by a person with SCI.

6 Conclusions and Future works

During the last years the development of BCIs using EEG has been of interest for the Engineering community, because it has allowed the implementation of robotic systems in therapeutic interventions, giving progressive results in the increase of plasticity and restoration of mobility of post-stroke and SCI population. Additionally, the use of MMEB has expanded the usability of BCIs, since it has allowed controlling the device with MI tasks, which encourages the patient during their passive pedaling sessions. However, this has brought challenges related to long calibration phases, intersubject variability, and the lack of customization of these devices for each patient.

Thus, according to the objectives initially stated in this dissertation, it was possible to expand the knowledge regarding pedaling tasks and their relationship with EEG signals. Different protocols were executed with different approaches, which were processed using different resources, classification and/or regression algorithms, which generated alternatives for the practical implementation of real-time BCIs. These algorithms were feasible for the detection of movement intentionality of the subjects with respect to MI tasks or actual executed pedaling movement, showing ACC close to 0.95 and 0.80, respectively.

Other approaches were carried out, aiming at the development of personalized rehabilitation systems with MMEBs, where the implemented methodologies were adequate for the detection of MI in different velocity conditions or the exploration of continuous kinematics with information of low brain frequencies, highlighting ACC close to 0.78 for velocity identification or PCCs close to 0.70 for continuous decoding. This has been little known in the literature.

Finally, some methodologies were involved for the design of a BCI based on visual neurofeedback and MI, where an ACC, in online phase, of approximately 0.80 was reported, and it was possible to analyze the cortical response of the subject during the development of the experimental methodology, observing a better neuromodulation after the first minute of the session. Therefore, it is possible to conclude that the results of this dissertation can be used for the design of more personalized lower limb neurorehabilitation systems that allow a better usability for the subject and a better HMI.

As future work, it is recommended to deepen in the processing of brain signals during execution of pedaling tasks (either active, passive or imagined), which will allow developing different approaches that can be used as control signals for robotic rehabilitation devices, such as MMEB. Additionally, future research will be focused on the implementation of the generated BCI, which is based on passive motion and neurofeedback for the therapeutic

intervention of people with SCI with other approaches, such as walking.

Bibliography

[1] World Health Organization, *World Report on Disability*. WHO, Geneve, 2011. ISBN 9789241564182.

[2] C. Marquez-Chin and M. R. Popovic, "Functional electrical stimulation therapy for restoration of motor function after spinal cord injury and stroke: a review," *Biomedical engineering online*, vol. 19, no. 1, pp. 1–25, 2020.

[3] P. A. Lim and A. M. Tow, "Recovery and regeneration after spinal cord injury: a review and summary of recent literature," *Annals-Academy of Medicine Singapore*, vol. 36, no. 1, p. 49, 2007.

[4] J. El-Sayes, D. Harasym, C. V. Turco, M. B. Locke, and A. J. Nelson, "Exercise-induced neuroplasticity: a mechanistic model and prospects for promoting plasticity," *The Neuroscientist*, vol. 25, no. 1, pp. 65–85, 2019.

[5] A. Vourvopoulos, C. Jorge, R. Abreu, P. Figueiredo, J.-C. Fernandes, and S. Bermudez i Badia, "Efficacy and brain imaging correlates of an immersive motor imagery bci-driven vr system for upper limb motor rehabilitation: A clinical case report," *Frontiers in human neuroscience*, vol. 13, p. 244, 2019.

[6] K. He, L. Wu, F. Ni, X. Li, K. Liang, and R. Ma, "Efficacy and safety of mirror therapy for post-stroke dysphagia: A systematic review and meta-analysis," *Frontiers in Neurology*, vol. 13, p. 874994, 2022.

[7] H.-Y. Hsu, L.-C. Kuo, Y.-C. Lin, F.-C. Su, T.-H. Yang, and C.-W. Lin, "Effects of a virtual reality–based mirror therapy program on improving sensorimotor function of hands in chronic stroke patients: a randomized controlled trial," *Neurorehabilitation and Neural Repair*, vol. 36, no. 6, pp. 335–345, 2022.

[8] M. S. Al-Quraishi, I. Elamvazuthi, S. A. Daud, S. Parasuraman, and A. Borboni, "Eeg-based control for upper and lower limb exoskeletons and prostheses: A systematic review," *Sensors*, vol. 18, no. 10, p. 3342, 2018.

[9] M. Ortiz, E. Iáñez, J. L. Contreras-Vidal, and J. M. Azorín, "Analysis of the eeg rhythms based on the empirical mode decomposition during motor imagery when using a lower-limb exoskeleton. a case study," *Frontiers in Neurorobotics*, vol. 14, p. 48, 2020.

[10] J. Hidler, D. Brennan, D. Nichols, K. Brady, T. Nef, *et al.*, "Zerog: overground gait and balance training system.," *Journal of Rehabilitation Research & Development*, vol. 48, no. 4, 2011.

[11] O. Lennon, M. Tonellato, A. Del Felice, R. Di Marco, C. Fingleton, A. Korik, E. Guanziroli, F. Molteni, C. Guger, R. Otner, *et al.*, "A systematic review establishing the current state-of-the-art, the limitations, and the desired checklist in studies of direct neural interfacing with robotic gait devices in stroke rehabilitation," *Frontiers in Neuroscience*, vol. 14, p. 578, 2020.

[12] A. R. Dawson-Elli and P. G. Adamczyk, "Design and validation of a lower-limb haptic rehabilitation robot," *IEEE Transactions on Neural Systems and Rehabilitation Engineering*, vol. 28, no. 7, pp. 1584–1594, 2020.

[13] M. A. Romero-Laiseca, D. Delisle-Rodriguez, V. Cardoso, D. Gurve, F. Loterio, J. H. P. Nascimento, S. Krishnan, A. Frizera-Neto, and T. Bastos-Filho, "A low-cost lower-limb brain-machine interface triggered by pedaling motor imagery for post-stroke patients rehabilitation," *IEEE Transactions on Neural Systems and Rehabilitation Engineering*, vol. 28, no. 4, pp. 988–996, 2020.

[14] C.-Y. Au, P. Mehra, K. W. Leung, and R. K. Tong, "Effects of electromyographically-driven neuromuscular stimulatio cycling system on the lower-limb of stroke survivors," in *2019 IEEE 16th International Conference on Rehabilitation Robotics (ICORR)*, pp. 300–304, IEEE, 2019.

[15] M. E. Dohring and J. J. Daly, "Automatic synchronization of functional electrical stimulation and robotic assisted treadmill training," *IEEE Transactions on Neural Systems and Rehabilitation Engineering*, vol. 16, no. 3, pp. 310–313, 2008.

[16] D. Esposito, J. Centracchio, E. Andreozzi, G. D. Gargiulo, G. R. Naik, and P. Bifulco, "Biosignal-based human–machine interfaces for assistance and rehabilitation: A survey," *Sensors*, vol. 21, no. 20, p. 6863, 2021.

[17] C. F. Blanco-Díaz, C. D. Guerrero-Méndez, T. Bastos-Filho, S. Jaramillo-Isaza, and A. F. Ruiz-Olaya, "Effects of the concentration level, eye fatigue and coffee consumption on the performance of a bci system based on visual erp-p300," *Journal of Neuroscience Methods*, vol. 382, p. 109722, 2022.

[18] T. P. Luu, Y. He, S. Nakagame, J. Gorges, K. Nathan, and J. L. Contreras-Vidal, "Unscented kalman filter for neural decoding of human treadmill walking from non-invasive electroencephalography," in *2016 38th Annual International Conference of the IEEE Engineering in Medicine and Biology Society (EMBC)*, pp. 1548–1551, 2016.

[19] L.-W. Ko, C. Stevenson, W.-C. Chang, K.-H. Yu, K.-C. Chi, Y.-J. Chen, and C.-H. Chen, "Integrated gait triggered mixed reality and neurophysiological monitoring as a framework for next-generation ambulatory stroke rehabilitation," *IEEE Transactions on Neural Systems and Rehabilitation Engineering*, vol. 29, pp. 2435–2444, 2021.

[20] V. F. Cardoso, D. Delisle-Rodriguez, M. A. Romero-Laiseca, F. A. Loterio, D. Gurve, A. Floriano, C. Valadão, L. Silva, S. Krishnan, A. Frizera-Neto, *et al.*, "Effect of a brain–computer interface based on pedaling motor imagery on cortical excitability and connectivity," *Sensors*, vol. 21, no. 6, p. 2020, 2021.

[21] D. Delisle-Rodriguez, L. Silva, and T. Bastos-Filho, "Eeg changes during passive movements improve the motor imagery feature extraction in bcis-based sensory feedback calibration," *Journal of Neural Engineering*, vol. 20, no. 1, p. 016047, 2023.

[22] I. Cajigas and A. Vedantam, "Brain-computer interface, neuromodulation, and neurorehabilitation strategies for spinal cord injury," *Neurosurgery Clinics*, vol. 32, no. 3, pp. 407–417, 2021.

[23] K. Patel, H. Sutherland, J. Henshaw, J. R. Taylor, C. A. Brown, A. J. Casson, N. J. Trujillo-Barreton, A. K. Jones, and M. Sivan, "Effects of neurofeedback in the management of chronic pain: A systematic review and meta-analysis of clinical trials," *European Journal of Pain*, vol. 24, no. 8, pp. 1440–1457, 2020.

[24] R. Carvalho, N. Dias, and J. J. Cerqueira, "Brain-machine interface of upper limb recovery in stroke patients rehabilitation: a systematic review," *Physiotherapy Research International*, vol. 24, no. 2, p. e1764, 2019.

[25] A. Zulauf-Czaja, B. Osuagwu, and A. Vuckovic, "Source-based eeg neurofeedback for sustained motor imagery of a single leg," *Sensors*, vol. 23, no. 12, p. 5601, 2023.

[26] A. Behboodi, W. A. Lee, V. S. Hinchberger, and D. L. Damiano, "Determining optimal mobile neurofeedback methods for motor neurorehabilitation in children and adults with non-progressive neurological disorders: a scoping review," *Journal of NeuroEngineering and Rehabilitation*, vol. 19, no. 1, pp. 1–23, 2022.

[27] J. Mackay and G. A. Mensah, *The atlas of heart disease and stroke*. World Health Organization, 2004.

[28] C. W. Tsao, A. W. Aday, Z. I. Almarzooq, A. Alonso, A. Z. Beaton, M. S. Bittencourt, A. K. Boehme, A. E. Buxton, A. P. Carson, Y. Commodore-Mensah, *et al.*, "Heart disease and stroke statistics—2022 update: a report from the american heart association," *Circulation*, vol. 145, no. 8, pp. e153–e639, 2022.

[29] World Health Organization, *Spinal cord injury*. WHO, Geneve, 2013.

[30] P. Vinoj, S. Jacob, V. G. Menon, S. Rajesh, and M. R. Khosravi, "Brain-controlled adaptive lower limb exoskeleton for rehabilitation of post-stroke paralyzed," *IEEE Access*, vol. 7, pp. 132628–132648, 2019.

[31] N. Padfield, J. Zabalza, H. Zhao, V. Masero, and J. Ren, "Eeg-based brain-computer interfaces using motor-imagery: Techniques and challenges," *Sensors*, vol. 19, no. 6, p. 1423, 2019.

[32] C. F. Blanco-Diaz, J. M. Antelis, and A. F. Ruiz-Olaya, "Comparative analysis of spectral and temporal combinations in csp-based methods for decoding hand motor imagery tasks," *Journal of Neuroscience Methods*, vol. 371, p. 109495, 2022.

[33] N. Robinson, R. Mane, T. Chouhan, and C. Guan, "Emerging trends in bci-robotics for motor control and rehabilitation," *Current Opinion in Biomedical Engineering*, vol. 20, p. 100354, 2021.

[34] T. C. Bulea, S. Prasad, A. Kilicarslan, and J. L. Contreras-Vidal, "Sitting and standing intention can be decoded from scalp eeg recorded prior to movement execution," *Frontiers in neuroscience*, vol. 8, p. 376, 2014.

[35] C. M. McCrimmon, C. E. King, P. T. Wang, S. C. Cramer, Z. Nenadic, and A. H. Do, "Brain-controlled functional electrical stimulation therapy for gait rehabilitation after stroke: a safety study," *Journal of neuroengineering and rehabilitation*, vol. 12, no. 1, pp. 1–12, 2015.

[36] Y. He, K. Nathan, A. Venkatakrishnan, R. Rovekamp, C. Beck, R. Ozdemir, G. E. Francisco, and J. L. Contreras-Vidal, "An integrated neuro-robotic interface for stroke rehabilitation using the nasa x1 powered lower limb exoskeleton," in *2014 36th annual international conference of the IEEE engineering in medicine and biology society*, pp. 3985–3988, IEEE, 2014.

[37] T. P. Luu, S. Nakagome, Y. He, and J. L. Contreras-Vidal, "Real-time eeg-based brain-computer interface to a virtual avatar enhances cortical involvement in human treadmill walking," *Scientific reports*, vol. 7, no. 1, pp. 1–12, 2017.

[38] S. Nakagome, T. P. Luu, Y. He, A. S. Ravindran, and J. L. Contreras-Vidal, "An empirical comparison of neural networks and machine learning algorithms for eeg gait decoding," *Scientific reports*, vol. 10, no. 1, pp. 1–17, 2020.

[39] S. Tortora, S. Ghidoni, C. Chisari, S. Micera, and F. Artoni, "Deep learning-based bci for gait decoding from eeg with lstm recurrent neural network," *Journal of neural engineering*, vol. 17, no. 4, p. 046011, 2020.

[40] M. Futrell and S. L. Rozzi, "Principles of rehabilitation," *Primary Care: Clinics in Office Practice*, vol. 47, no. 1, pp. 87–103, 2020.

[41] S. R. Belagaje, "Stroke rehabilitation," *CONTINUUM: Lifelong Learning in Neurology*, vol. 23, no. 1, pp. 238–253, 2017.

[42] S. M. Hatem, G. Saussez, M. Della Faille, V. Prist, X. Zhang, D. Dispa, and Y. Bleyenheuft, "Rehabilitation of motor function after stroke: a multiple systematic review focused on techniques to stimulate upper extremity recovery," *Frontiers in human neuroscience*, vol. 10, p. 442, 2016.

[43] D. G. Liebermann, A. S. Buchman, and I. M. Franks, "Enhancement of motor rehabilitation through the use of information technologies," *Clinical biomechanics*, vol. 21, no. 1, pp. 8–20, 2006.

[44] Q. Ai, Z. Liu, W. Meng, Q. Liu, and S. Q. Xie, "Machine learning in robot assisted upper limb rehabilitation: A focused review," *IEEE Transactions on Cognitive and Developmental Systems*, 2021.

[45] K. Nizamis, A. Athanasiou, S. Almpani, C. Dimitrousis, and A. Astaras, "Converging robotic technologies in targeted neural rehabilitation: a review of emerging solutions and challenges," *Sensors*, vol. 21, no. 6, p. 2084, 2021.

[46] J. S. Kumar and P. Bhuvaneswari, "Analysis of electroencephalography (eeg) signals and its categorization–a study," *Procedia engineering*, vol. 38, pp. 2525–2536, 2012.

[47] M. Teplan *et al.*, "Fundamentals of eeg measurement," *Measurement science review*, vol. 2, no. 2, pp. 1–11, 2002.

[48] G. Baura, *Medical device technologies:a system-based overview using engineering standars*. San Diego(CA): Oxford Academic Press, 2011.

[49] N. Nacional Center for Adaptative Neurotechnologies, "BCI2000." url https://www.bci2000.org/mediawiki/index.php/Main$_Page$, 2018.

[50] C. F. Blanco-Díaz, *Estudio comparativo de métodos para el reconocimiento de potenciales relacionados a eventos P300 para una interfaz cerebro-computador*. Undergraduate work, Universidad Antonio Nariño, May 2021.

[51] M. Orban, M. Elsamanty, K. Guo, S. Zhang, and H. Yang, "A review of brain activity and eeg-based brain–computer interfaces for rehabilitation application," *Bioengineering*, vol. 9, no. 12, p. 768, 2022.

[52] C. D. Guerrero-Mendez, C. F. Blanco-Diaz, and A. F. Ruiz-Olaya, "Identification of motor imagery tasks using power-based connectivity descriptors from eeg signals," in *2021 XXIII symposium on image, signal processing and artificial vision (STSIVA)*, pp. 1–6, IEEE, 2021.

[53] C. D. Guerrero-Mendez, C. F. Blanco-Diaz, A. F. Ruiz-Olaya, A. López-Delis, S. Jaramillo-Isaza, R. Milanezi Andrade, A. Ferreira De Souza, D. Delisle-Rodriguez, A. Frizera-Neto, and T. F. Bastos-Filho, "Eeg motor imagery classification using deep learning approaches in naïve bci users," *Biomedical physics amp; engineering express*, vol. 9, June 2023.

[54] C. F. Blanco-Díaz and A. F. Ruiz-Olaya, "A novel method based on regularized logistic regression and cca for p300 detection using a reduced number of eeg trials," *IEEE Latin America Transactions*, vol. 18, no. 12, pp. 2147–2154, 2020.

[55] C. D. Guerrero-Mendez, C. F. Blanco-Diaz, and A. F. Ruiz-Olaya, "How do factors of comfort, concentration, and eye fatigue affect the performance of a bci system based on ssvep?," in *2021 IEEE 2nd International Congress of Biomedical Engineering and Bioengineering (CI-IBBI)*, pp. 1–4, 2021.

[56] C. Blanco-Díaz, C. Guerrero-Méndez, and A. Ruiz-Olaya, "Enhancing p300 detection using a band-selective filter bank for a visual p300 speller," *IRBM*, vol. 44, no. 3, p. 100751, 2023.

[57] N. Nazmi, M. A. Abdul Rahman, S.-I. Yamamoto, S. A. Ahmad, H. Zamzuri, and S. A. Mazlan, "A review of classification techniques of emg signals during isotonic and isometric contractions," *Sensors*, vol. 16, no. 8, p. 1304, 2016.

[58] C. Fang, B. He, Y. Wang, J. Cao, and S. Gao, "Emg-centered multisensory based technologies for pattern recognition in rehabilitation: state of the art and challenges," *Biosensors*, vol. 10, no. 8, p. 85, 2020.

[59] M. Simao, N. Mendes, O. Gibaru, and P. Neto, "A review on electromyography decoding and pattern recognition for human-machine interaction," *Ieee Access*, vol. 7, pp. 39564–39582, 2019.

[60] W. Li, W. Lu, X. Sha, H. Xing, J. Lou, H. Sun, and Y. Zhao, "Wearable gait recognition systems based on mems pressure and inertial sensors: A review," *IEEE Sensors Journal*, vol. 22, no. 2, pp. 1092–1104, 2022.

[61] C. Gu, W. Lin, X. He, L. Zhang, and M. Zhang, "Imu-based mocap system for rehabilitation applications: A systematic review," *Biomimetic Intelligence and Robotics*, p. 100097, 2023.

[62] C. F. Blanco-Díaz, A. K. Q. González, S. J. Isaza, and A. D. Orjuela-Cañón, "A biomechanical analysis of free squat exercise employing self-organizing maps," in *2019 IEEE Colombian Conference on Applications in Computational Intelligence (ColCACI)*, pp. 1–5, IEEE, 2019.

[63] C. F. Blanco-Diaz, C. D. Guerrero-Mendez, M. E. Duarte-González, and S. Jaramillo-Isaza, "Estimation of limbs angles amplitudes during the use of the five minute shaper device using artificial neural networks," in *Applied Computer Sciences in Engineering: 8th Workshop on Engineering Applications, WEA 2021, Medellín, Colombia, October 6–8, 2021, Proceedings 8*, pp. 213–224, Springer, 2021.

[64] C. F. Blanco-Díaz, C. D. Guerrero-Méndez, M. E. Duarte-González, and S. Jaramillo-Isaza, "Implementation of computational methods to estimate lower limb angle amplitudes during squat," *TecnoLógicas*, vol. 25, no. 53, 2022.

[65] M. K. Sharma, V. S. Dhaka, T. Perumal, N. Dey, J. M. R. Tavares, *et al.*, *Innovations in Computational Intelligence and Computer Vision: Proceedings of ICICV 2020*. Springer, 2021.

[66] A. C. Plazas-Molano, M. E. Duarte-González, C. F. Blanco-Díaz, and S. Jaramillo-Isaza, "Exploring the facial and neurological activation due to predetermined visual stimulus using kinect and emotiv sensors," in *Applied Computer Sciences in Engineering: 7th Workshop on Engineering Applications, WEA 2020, Bogota, Colombia, October 7–9, 2020, Proceedings 7*, pp. 268–280, Springer, 2020.

[67] N. Peng, W. Meng, Q. Wei, Q. Ai, Q. Liu, and S. Xie, "Wearable optical fiber sensors for biomechanical measurement in medical rehabilitation: A review," *IEEE Sensors Journal*, 2023.

[68] A. X. GONZALEZ CELY, C. F. Blanco-Diaz, C. A. Rodriguez-Diaz, T. Bastos-Filho, and S. Krishnan, "Machine learning algorithm for wheelchair control through pof-based pressure sensors and neck movements," *Available at SSRN 4435617*.

[69] P. Zhang, "Chapter 13 - human–machine interfaces," in *Advanced Industrial Control Technology* (P. Zhang, ed.), pp. 527–555, Oxford: William Andrew Publishing, 2010.

[70] S. Y. Gordleeva, S. A. Lobov, N. A. Grigorev, A. O. Savosenkov, M. O. Shamshin, M. V. Lukoyanov, M. A. Khoruzhko, and V. B. Kazantsev, "Real-time eeg–emg human–machine interface-based control system for a lower-limb exoskeleton," *IEEE Access*, vol. 8, pp. 84070–84081, 2020.

[71] A. Palumbo, P. Vizza, B. Calabrese, and N. Ielpo, "Biopotential signal monitoring systems in rehabilitation: A review," *Sensors*, vol. 21, no. 21, p. 7172, 2021.

[72] B. Remeseiro and V. Bolon-Canedo, "A review of feature selection methods in medical applications," *Computers in biology and medicine*, vol. 112, p. 103375, 2019.

[73] K. L. Lew, K. S. Sim, S. C. Tan, and F. S. Abas, "Biofeedback upper limb assessment using electroencephalogram, electromyographic and electrocardiographic with machine learning in signal classification.," *Engineering Letters*, vol. 30, no. 3, 2022.

[74] I. Boukhennoufa, X. Zhai, V. Utti, J. Jackson, and K. D. McDonald-Maier, "Wearable sensors and machine learning in post-stroke rehabilitation assessment: A systematic review," *Biomedical Signal Processing and Control*, vol. 71, p. 103197, 2022.

[75] F. Aggogeri, T. Mikolajczyk, and J. O'Kane, "Robotics for rehabilitation of hand movement in stroke survivors," *Advances in Mechanical Engineering*, vol. 11, no. 4, p. 1687814019841921, 2019.

[76] F. Yuan, E. Klavon, Z. Liu, R. P. Lopez, and X. Zhao, "A systematic review of robotic rehabilitation for cognitive training," *Frontiers in Robotics and AI*, vol. 8, p. 605715, 2021.

[77] Z. Makhataeva and H. A. Varol, "Augmented reality for robotics: A review," *Robotics*, vol. 9, no. 2, p. 21, 2020.

[78] F. L. Da Silva, "Event-related eeg/meg synchronization and desynchronization: basic principles," *Clinical neurophysiology*, vol. 110, no. 11, pp. 1842–1857, 1999.

[79] Y. Xie and S. Oniga, "A review of processing methods and classification algorithm for eeg signal," *Carpathian Journal of Electronic and Computer Engineering*, vol. 13, no. 1, pp. 23–29, 2020.

[80] D. Delisle-Rodriguez, A. C. Villa-Parra, T. Bastos-Filho, A. López-Delis, A. Frizera-Neto, S. Krishnan, and E. Rocon, "Adaptive spatial filter based on similarity indices to preserve the neural information on eeg signals during on-line processing," *Sensors*, vol. 17, no. 12, p. 2725, 2017.

[81] P. Nguyen, T. A. Nguyen, and Y. Zeng, "Segmentation of design protocol using eeg," *Ai Edam*, vol. 33, no. 1, pp. 11–23, 2019.

[82] W. A. W. Azlan and Y. F. Low, "Feature extraction of electroencephalogram (eeg) signal-a review," in *2014 IEEE conference on biomedical engineering and sciences (IECBES)*, pp. 801–806, IEEE, 2014.

[83] A. Jain and L. Kumar, "Subject-independent trajectory prediction using pre-movement eeg during grasp and lift task," *Biomedical Signal Processing and Control*, vol. 86, p. 105160, 2023.

[84] S. M. Hosseini and V. Shalchyan, "State-based decoding of continuous hand movements using eeg signals," *IEEE Access*, 2023.

[85] A. Khosla, P. Khandnor, and T. Chand, "A comparative analysis of signal processing and classification methods for different applications based on eeg signals," *Biocybernetics and Biomedical Engineering*, vol. 40, no. 2, pp. 649–690, 2020.

[86] M. Demuru, S. M. La Cava, S. M. Pani, and M. Fraschini, "A comparison between power spectral density and network metrics: an eeg study," *Biomedical Signal Processing and Control*, vol. 57, p. 101760, 2020.

[87] H. Lee, Y. Kwon, Y. Kim, H. Kim, Y. Lee, J. Williamson, S. Fazli, and S. Lee, "EEG dataset and open BMI toolbox for three BCI paradigms: an investigation into BCI illiteracy.," *Giga-Science*, vol. 8, pp. 1–16, 2019.

[88] R. Martín-Clemente, J. Olias, D. B. Thiyam, A. Cichocki, and S. Cruces, "Information theoretic approaches for motor-imagery bci systems: review and experimental comparison," *Entropy*, vol. 20, no. 1, p. 7, 2018.

[89] A. Barachant, S. Bonnet, M. Congedo, and C. Jutten, "Multiclass brain–computer interface classification by riemannian geometry," *IEEE Transactions on Biomedical Engineering*, vol. 59, no. 4, pp. 920–928, 2011.

[90] S. Pahuja, K. Veer, *et al.*, "Recent approaches on classification and feature extraction of eeg signal: A review," *Robotica*, vol. 40, no. 1, pp. 77–101, 2022.

[91] Z. Li, J. E. O'Doherty, T. L. Hanson, M. A. Lebedev, C. S. Henriquez, and M. A. Nicolelis, "Unscented kalman filter for brain-machine interfaces," *PloS one*, vol. 4, no. 7, p. e6243, 2009.

[92] N. Fitzsimmons, M. Lebedev, I. Peikon, and M. A. Nicolelis, "Extracting kinematic parameters for monkey bipedal walking from cortical neuronal ensemble activity," *Frontiers in integrative neuroscience*, vol. 3, p. 501, 2009.

[93] C. F. Blanco-Díaz, C. D. Guerrero-Méndez, M. E. Duarte-González, and S. Jaramillo-Isaza, "Implementation of computational methods to estimate lower limb angle amplitudes during squat," *TecnoLógicas*, vol. 25, no. 53, 2022.

[94] A. Craik, Y. He, and J. L. Contreras-Vidal, "Deep learning for electroencephalogram (eeg) classification tasks: a review," *Journal of neural engineering*, vol. 16, no. 3, p. 031001, 2019.

[95] F. Murtagh, "Multilayer perceptrons for classification and regression," *Neurocomputing*, vol. 2, no. 5-6, pp. 183–197, 1991.

[96] J. Li, Y. Li, and M. Du, "Comparative study of eeg motor imagery classification based on dscnn and elm," *Biomedical Signal Processing and Control*, vol. 84, p. 104750, 2023.

[97] Q. She, J. Zou, Z. Luo, T. Nguyen, R. Li, and Y. Zhang, "Multi-class motor imagery eeg classification using collaborative representation-based semi-supervised extreme learning machine," *Medical & Biological Engineering & Computing*, vol. 58, pp. 2119–2130, 2020.

[98] D. E. Koditschek, "What is robotics? why do we need it and how can we get it?," *Annual Review of Control, Robotics, and Autonomous Systems*, vol. 4, pp. 1–33, 2021.

[99] I. Díaz, J. J. Gil, E. Sánchez, *et al.*, "Lower-limb robotic rehabilitation: literature review and challenges," *Journal of Robotics*, vol. 2011, 2011.

[100] X. Zhang, L. Hui, L. Wei, F. Song, and F. Hu, "A bibliometric analysis of human-machine interaction methodology for electric-powered wheelchairs driving from 1998 to 2020," *International journal of environmental research and public health*, vol. 18, no. 14, p. 7567, 2021.

[101] F. Baronchelli, C. Zucchella, M. Serrao, D. Intiso, and M. Bartolo, "The effect of robotic assisted gait training with lokomat® on balance control after stroke: systematic review and meta-analysis," *Frontiers in Neurology*, vol. 12, p. 661815, 2021.

[102] A. Pennycott and H. Vallery, "Body weight support devices for overground gait and balance training," in *Neurorehabilitation Technology*, pp. 745–756, Springer, 2022.

[103] J. Andrysek, "Lower-limb prosthetic technologies in the developing world: A review of literature from 1994–2010," *Prosthetics and orthotics international*, vol. 34, no. 4, pp. 378–398, 2010.

[104] "Exerpeutic ACTIVcycle 7101 exerpeutic activcycle 7101 owner's manual. available online:." `https://www.manualslib.com/manual/1213854/Exerpeutic-Activcycle-7101.html`. (accessed on May 20, 2023).

[105] M. Callejas-Cuervo, J. C. Alvarez, and D. Álvarez, "Capture and analysis of biomechanical signals with inertial and magnetic sensors as support in physical rehabilitation processes," in *2016 IEEE 13th International Conference on Wearable and Implantable Body Sensor Networks (BSN)*, pp. 119–123, IEEE, 2016.

[106] M. Callejas-Cuervo, R. M. Gutierrez, and A. I. Hernandez, "Joint amplitude mems based measurement platform for low cost and high accessibility telerehabilitation: Elbow case study," *Journal of Bodywork and Movement Therapies*, vol. 21, no. 3, pp. 574–581, 2017.

[107] A. Mathis, P. Mamidanna, K. M. Cury, T. Abe, V. N. Murthy, M. W. Mathis, and M. Bethge, "Deeplabcut: markerless pose estimation of user-defined body parts with deep learning," *Nature neuroscience*, vol. 21, no. 9, pp. 1281–1289, 2018.

[108] L. Storzer, M. Butz, J. Hirschmann, O. Abbasi, M. Gratkowski, D. Saupe, A. Schnitzler, and S. S. Dalal, "Bicycling and walking are associated with different cortical oscillatory dynamics," *Frontiers in human neuroscience*, vol. 10, p. 61, 2016.

[109] Y. Renard, F. Lotte, G. Gibert, M. Congedo, E. Maby, V. Delannoy, O. Bertrand, and A. Lécuyer, "Openvibe: An open-source software platform to design, test, and use brain–computer interfaces in real and virtual environments," *Presence*, vol. 19, no. 1, pp. 35–53, 2010.

[110] C. F. Blanco-Díaz, C. D. Guerrero-Mendez, D. Delisle-Rodriguez, A. F. de Souza, C. Badue, and T. F. Bastos-Filho, "Lower-limb kinematic reconstruction during pedaling tasks from eeg signals using unscented kalman filter," *Computer Methods in Biomechanics and Biomedical Engineering*, pp. 1–11, 2023.

[111] F. Hug and S. Dorel, "Electromyographic analysis of pedaling: A review," *Journal of Electromyography and Kinesiology*, vol. 19, no. 2, pp. 182–198, 2009.

[112] F. Faul, E. Erdfelder, A.-G. Lang, and A. Buchner, "G* power 3: A flexible statistical power analysis program for the social, behavioral, and biomedical sciences," *Behavior research methods*, vol. 39, no. 2, pp. 175–191, 2007.

[113] R. Abiri, S. Borhani, E. W. Sellers, Y. Jiang, and X. Zhao, "A comprehensive review of eeg-based brain–computer interface paradigms," *Journal of Neural Engineering*, vol. 16, p. 011001, jan 2019.

[114] A. Phinyomark, P. Phukpattaranont, and C. Limsakul, "Feature reduction and selection for emg signal classification," *Expert Systems with Applications*, vol. 39, no. 8, pp. 7420–7431, 2012.

[115] D. Delisle-Rodriguez, V. Cardoso, D. Gurve, F. Loterio, M. A. Romero-Laiseca, S. Krishnan, and T. Bastos-Filho, "System based on subject-specific bands to recognize pedaling motor imagery: towards a bci for lower-limb rehabilitation," *Journal of neural engineering*, vol. 16, no. 5, p. 056005, 2019.

[116] W. Lin, C. Li, and S. Sun, "Deep convolutional neural network for emotion recognition using eeg and peripheral physiological signal," in *Image and Graphics* (Y. Zhao, X. Kong, and D. Taubman, eds.), 2017.

[117] R. San-Segundo, M. Gil-Martín, L. F. D'Haro-Enríquez, and J. M. Pardo, "Classification of epileptic eeg recordings using signal transforms and convolutional neural networks," *Computers in biology and medicine*, vol. 109, pp. 148–158, 2019.

[118] D. Delisle-Rodriguez, H. L. de Oliveira Junior, J. C. da Silva, M. L. de Souza, T. Bastos, E. M. Nakamura-Palacios, and A. Frizera-Neto, "Multi-channel eeg-based bci using regression and classification methods for attention training by serious game," *Biomedical Signal Processing and Control*, vol. 85, p. 104937, 2023.

[119] G. Pfurtscheller and C. Neuper, "Motor imagery and direct brain-computer communication," *Proceedings of the IEEE*, vol. 89, no. 7, pp. 1123–1134, 2001.

[120] M. Rodríguez-Ugarte, I. N. Angulo-Sherman, E. Iáñez, M. Ortiz, and J. M. Azorín, "Preliminary study of pedaling motor imagery classification based on eeg signals," in *2017 International Symposium on Wearable Robotics and Rehabilitation (WeRob)*, pp. 1–2, 2017.

[121] D. Liu, W. Chen, K. Lee, R. Chavarriaga, F. Iwane, M. Bouri, Z. Pei, and J. d. R. Millán, "Eeg-based lower-limb movement onset decoding: Continuous classification and asynchronous detection," *IEEE Transactions on Neural Systems and Rehabilitation Engineering*, vol. 26, no. 8, pp. 1626–1635, 2018.

[122] M. Rodríguez-Ugarte, E. Iáñez, M. Ortíz, and J. M. Azorín, "Personalized offline and pseudo-online bci models to detect pedaling intent," *Frontiers in Neuroinformatics*, vol. 11, 2017.

[123] D. Gurve, D. Delisle-Rodriguez, M. Romero-Laiseca, V. Cardoso, F. Loterio, T. Bastos, and S. Krishnan, "Subject-specific eeg channel selection using non-negative matrix factorization for lower-limb motor imagery recognition," *Journal of Neural Engineering*, vol. 17, no. 2, p. 026029, 2020.

[124] V. Quiles, L. Ferrero, E. Iáñez, M. Ortiz, J. M. Cano, and J. M. Azorín, "Detecting the speed change intention from eeg signals: From the offline and pseudo-online analysis to an online closed-loop validation," *Applied Sciences*, vol. 12, no. 1, p. 415, 2022.

[125] C. Wu, S. Qiu, J. Xing, and H. He, "A cnn-based compare network for classification of ssveps in human walking," in *2020 42nd Annual International Conference of the IEEE Engineering in Medicine Biology Society (EMBC)*, pp. 2986–2990, 2020.

[126] A. Presacco, L. W. Forrester, and J. L. Contreras-Vidal, "Decoding intra-limb and inter-limb kinematics during treadmill walking from scalp electroencephalographic (eeg) signals," *IEEE Transactions on Neural Systems and Rehabilitation Engineering*, vol. 20, no. 2, pp. 212–219, 2012.

[127] T. P. Luu, Y. He, S. Brown, S. Nakagome, and J. L. Contreras-Vidal, "Gait adaptation to visual kinematic perturbations using a real-time closed-loop brain–computer interface to a virtual reality avatar," *Journal of neural engineering*, vol. 13, no. 3, p. 036006, 2016.

[128] Y. He, T. P. Luu, K. Nathan, S. Nakagome, and J. L. Contreras-Vidal, "A mobile brain-body imaging dataset recorded during treadmill walking with a brain-computer interface," *Scientific data*, vol. 5, no. 1, pp. 1–10, 2018.